# BIOGEOCHEMICAL CYCLING OF IRON AND PHOSPHORUS UNDER LOW OXYGEN CONDITIONS

**Dissertation**

Zur Erlangung des Doktorgrades Dr. rer. nat. der Mathematisch-Naturwissenschaftlichen Fakultät der Christian-Albrechts-Universität zu Kiel

vorgelegt von
Ulrike Lomnitz

Kiel, Mai 2017

Referent: Prof. Dr. Klaus Wallmann

Koreferent: PD Dr. Mark Schmidt

Tag der mündlichen Prüfung: 14.07.2017

zum Druck genehmigt: 14.07.2017

# Erklärung

Hiermit erkläre ich, dass ich die vorliegende Doktorarbeit selbstständig und ohne Zuhilfenahme unerlaubter Hilfsmittel erstellt habe. Weder diese noch eine ähnliche Arbeit wurde an einer anderen Abteilung oder Hochschule im Rahmen eines Prüfungsverfahrens veröffentlicht oder zur Veröffentlichung vorgelegt. Ferner versichere ich, dass die Arbeit unter Einhaltung der Regeln guter wissenschaftlicher Praxis der Deutschen Forschungsgemeinschaft entstanden ist.

05.05.2017

Ulrike Lomnitz

# Abstract

Benthic release of the key nutrients iron (Fe) and phosphorus (P) is enhanced from sediments that are impinged by oxygen-deficient bottom waters due to its diminished retention capacity for such redox sensitive elements. Suboxic to anoxic and sometimes even euxinic conditions are recently found in open ocean oxygen minimum zones (OMZs, e.g. Eastern Boundary Upwelling Systems) and marginal seas (e.g. the Black Sea and the Baltic Sea). Recent studies showed that OMZs expanded in the last decades and will further spread in the future. Due to the additional release of bioavailable key nutrients from the sediments in such high productivity regions, several feedback mechanisms can evolve. The scenarios range from positive to neutral and negative consequences on the evolution of the ocean's oxygen levels. This controversial issue makes it crucial to investigate the biogeochemical cycling of Fe and P in OMZs.

The study presented in the following aims to shed light on open research questions. Therefore, new data sets of benthic P and Fe release rates from oxygen-deficient waters and geochemical sediment data from the intense Peruvian (lowest $O_2$ ~ 0 µM) and moderate Mauritanian (lowest $O_2$ ~ 35 µM) OMZs are analyzed and discussed. This study revealed the following main findings:

I. The extremely high P release of up to 1.04 ± 0.31 mmol $m^{-2}$ $d^{-1}$ found in the Peruvian OMZ exceeds previously reported values. However, the rain rates of particulate P to the sediments could not maintain the in situ measured P fluxes in the core OMZ. After systematic analysis of all possible P sources, sulfide-oxidizing bacteria were suggested to release the missing P during anoxic or even sulfidic bottom water conditions as prevailing during the sampling campaign. This presupposes that those bacteria recharge their internal P reservoir during periods of less reducing bottom water conditions. In terms of P cycling it could be shown that particulate organic phosphorus was not preferentially mineralized relative to particulate organic carbon in water column particles. Furthermore, the burial efficiencies of particulate organic carbon and total particulate phosphorus were similar indicated by water column particle and surface sediment C/P ratios that were close to the Redfield ratio. Moreover, sediments overlain by low oxygen waters were not depleted in P compared to Redfield, but compared to sediments from oxic sites where the C/P ratios are well below Redfield. The results of this study support the scenario of a positive feedback loop to intensified primary production in the surface water and oxygen respiration during periods of anoxic bottom water conditions and intense benthic P release. However, the deepest station (407 m water depth) along the depth transect showed P uptake into the sediments likely acting as a precursor for the precipitation of CFA

minerals. This process is limiting the positive feedback by long-term trapping of P in the sediments.

II. Intensive field work along a depth transect between 47 and 1108 m at 18°N off Mauritania enabled us to present the first data sets on benthic P and Fe release from that region. The highest P release of 0.2 ± 0.065 mmol $m^{-2}$ $d^{-1}$ was found at 47 m water depth (50 µM $O_2$) and the strongest diffusive Fe flux of 0.03 mmol $m^{-2}$ $d^{-1}$ occurred at 67 m water depth (27 µM $O_2$). The nutrient release was found to be controlled by the rate of organic matter degradation in the surface sediment and varying sediment characteristics rather than the bottom water oxygen concentration. Nutrient fluxes across the sediment water interface off Mauretania are enhanced by bioirrigation and bottom water percolation through permeable sediments induced by bottom water currents interacting with small-scale topography. P mass balance calculations showed a P deficit at 240 m water depth that is likely compensated by downslope transport of P containing particles or lower C/P ratios of the sinking particles compared to the analyzed suspended particles. Ex situ deoxygenation experiments resulted in strongly intensified Fe and P release indicating an enhanced nutrient release from sediments of the Mauritanian OMZ in case of further deoxygenation. However, long-term effects remain speculative.

III. Geochemical analysis of numerous sediment cores revealed widespread iron enrichments beneath the lower boundary of the OMZ along the South American Coast from 3 to 33°S. Fe is mainly captured in silicate minerals such as glauconite. Its formation is favored by slightly reducing, non-sulfidic conditions and low sedimentation rates. Interestingly, the dissolved $Fe^{2+}$ concentrations in the porewaters of the cores with the highest glauconite contents were low which is in contrast to previous hypothesis. Moreover, the widespread formation of authigenic clay minerals containing Fe mobilized from the core OMZ represents an effective long-term sink for bioavailable Fe leading to a negative feedback loop in present times. However, on millennial time scales, persistent vertical expansion of the OMZ could lead to the remobilization of the Fe reversing the negative feedback into a positive feedback.

# Zusammenfassung

Sedimente, die unterhalb von Sauerstoffminimumzonen (SMZ) liegen, begünstigen die benthische Freisetzung von Schlüsselnährstoffen wie gelöstem Eisen ($Fe^{+2}$) und Phosphat ($PO_4^{3-}$). Eine verringerte Rückhaltekapazität der Sedimente für solche redox-sensitiven Elemente führt zu deren Freisetzung im Porenwasser und gegebenenfalls in das darüber liegende Bodenwasser. Heutzutage gibt es sowohl im offenen Ozean (z. B. die Auftriebsgebiete an den östlichen Kontinentalrändern) als auch in Randmeeren (z.B. im Schwarzen Meer und in der Ostsee) sauerstoffverarmte Gebiete mit suboxischen bis anoxischen, teils auch euxinischen Bedingungen in der Wassersäule und im Bodenwasser. Aktuelle Untersuchungen haben gezeigt, dass sich diese Zonen in den letzten Jahren stark ausgedehnt haben und dieser Prozess auch in der Zukunft weiter voranschreiten wird. Der damit verbundene zusätzliche Eintrag von gelösten Nährstoffen in die Wassersäule, die direkt für die Primärproduzenten zur Verfügung stehen, und dessen Folgen werden bezüglich verschiedener Rückkopplungsmechanismen auf das ozeanische Sauerstoffinventar diskutiert. Es ist weitere intensive Forschung zum biogeochemischen Kreislauf von Fe und P in SMZs notwendig, um die Folgen der fortwährenden Sauerstoffverarmung der Ozeane besser abschätzen zu können.

Diese Arbeit trägt durch neue Datensätze von Fe und P Freisetzungsraten, sowie Ergebnissen geochemischer Sedimentanalysen dazu bei, die Kreisläufe von Fe und P in SMZs weiter zu verstehen. In Bezug auf P werden weiterhin Daten eines neuen Ansatzes präsentiert, der auf die Analyse von Partikeln aus der Wassersäule basiert. Die folgende Arbeit beinhaltet die folgenden Hauptergebnisse:

I. Die extrem hohe benthische P Freisetzung in der peruanischen SMZ von bis zu 1.04 ± 0.31 mmol $m^{-2}$ $d^{-1}$ überschreitet bereits publizierte, aber dennoch hohe, Freisetzungsraten in diesem Gebiet. . Allerdings kann die P Freisetzung in der Kernzone der SMZ nicht durch den Eintrag von partikulärem P aus der Wassersäule generiert werden. Nach der systematischen Untersuchung aller möglichen P-Quellen, sind Sulfid-oxidierende Schwefelbakterien als mögliche Quelle für den fehlenden P Eintrag in Betracht zu ziehen. Diese Organismen metabolisieren intern gespeicherte Polyphosphate zur Energiegewinnung während anoxischer oder sulfidischer Bedingungen, wie sie zur Zeit der Probenahme im Bodenwasser vorherrschten, und geben dabei Phosphat ins umliegende Poren- und Bodenwasser ab. Dafür müssen die Organismen ihre internen Speicherkapazitäten für Polyphosphat während weniger reduzierender Bedingungen im Bodenwasser erneuern. Weiterhin zeigen die Ergebnisse der Untersuchung, dass keine präferentielle Mineralisierung von partikulärem Phosphor im Vergleich zu partikulärem Kohlenstoff in den

Wassersäulenpartikeln stattfindet. Außerdem deuten Redfield ähnliche Verhältnisse von Kohlenstoff und Phosphor (C/P Verhältnisse) in den Wassersäulenpartikeln und den Oberflächensedimenten darauf hin, dass beide Elemente mit der gleichen Effizienz im Sediment begraben werden und die Sedimente im Vergleich zu Kohlenstoff nicht an P verarmt sind. Dies steht im Kontrast zu Sedimenten, die von oxischem Bodenwasser überlagert sind, deren C/P Verhältnisse deutlich unterhalb des Redfield Verhältnisses liegen. Die Ergebnisse dieser Studie unterstreichen eine positive Rückkopplung der P Freisetzung auf die Ausdehnung der SMZ. Der erhöhte Eintrag von bioverfügbarem P könnte die Primärproduktion im Oberflächenwasser der SMZ weiter antreiben und so zur verstärkten Sauerstoffzehrung führen. Dies würde zur weiteren Intensivierung und Ausdehnung der SMZ führen. Allerdings konnte während der Messkampagne auch eine sedimentäre P Aufnahme in ca. 400 m Wassertiefe festgestellt werden. Solch eine Aufnahme könnte als Voraussetzung für die Bildung von Kalzium-Fluor-Apatiten fungieren und damit die positive Rückkopplung der P-Freisetzung längerfristig limitieren.

II. In der zweiten Studie dieser Arbeit werden die Ergebnisse von intensiver Feldarbeit entlang des 18°N Tiefentransekts zwischen 47 und 1108 m Wassertiefe gezeigt. Der Datensatz umfasst die ersten Fe und P Freisetzungsraten aus der SMZ von Mauretanien. Die größte P Freisetzung von $0.2 \pm 0.065$ mmol $m^{-2}$ $d^{-1}$ wurde in 47 m Wassertiefe gemessen, wobei die Sauerstoffkonzentration im Bodenwasser bei ca. 50 µM lag. Die stärkste Fe Fluss von 0.03 mmol $m^{-2}$ $d^{-1}$ wurde in 67 m Wassertiefe bei einer Sauerstoffkonzentration von 27 µM im Bodenwasser festgestellt. Die Freisetzung der Nährstoffe Fe und P ist vor Mauretanien vor allem durch die Intensität des Abbaus von organischem Material im Oberflächensediment gesteuert und weniger durch die Sauerstoffkonzentration des Bodenwassers beeinflusst. Weiterhin begünstigen Bodenwasserströmungen und kleinskalige topographische Veränderungen den Durchfluss von Bodenwasser durch die permeablen Sedimente und erhöhen dadurch den Nährstofffluss vom Porenwasser in das darüber liegende Bodenwasser. Außerdem ist Bioirrigation ein wichtiger Faktor für die Überwindung der Sediment-Wasser-Grenzschicht von redox-sensitiven Elementen. Die Berechnungen einer P Massenbilanz haben ein P Defizit in 240 m Wassertiefe ergeben, was wahrscheinlich durch den hangabwärts Transport von P-reichen Partikeln ausgeglichen wird oder aber durch absinkende Partikel mit niedrigeren C/P Verhältnissen als die von den analysierten suspendierten Partikeln kompensiert wird. Weiterhin haben Experimente zur Sauerstoffverarmung ergeben, dass sich der Nährstofffluss in das Bodenwasser stark erhöht, wenn die Sauerstoffkonzentration im Bodenwasser erniedrigt wird. Solche Experimente geben einen ersten Hinweis auf die

möglichen Folgen von weiterer Sauerstoffverarmung auf die benthische Nährstofffreisetzung in der Region, lassen aber Abschätzungen über die Langfristigkeit der Ergebnisse offen.

III. Die geochemische Aufbereitung und Analyse zahlreicher Sedimentkerne ergab, dass ausgedehnte sedimentäre Eisenanreicherungen unterhalb der unteren Grenzschicht der SMZ entlang des südamerikanischen Kontinents von 3 bis 33°S vorkommen. Das Fe ist vor allem in Silikatmineralen wie Glaukonit gebunden. Zum bevorzugten Bildungsmilieu gehören leicht reduzierende, keinesfalls sulfidische, Bedingungen und niedrige Sedimentationsraten. Die Daten dieser Studie zeigen, dass die Porenwasserkonzentrationen von gelöstem Fe vergleichsweise niedrig waren, wo die größten Glaukonitanteile im Sediment bestimmt wurden. Dies steht im Kontrast zu vorausgegangen Studien bezüglich der Bildungsbedingungen. Ferner repräsentiert solch eine weiträumig ausgedehnte Anreichung von Fe, das aus dem Kern der SMZ mobilisiert wurde, eine sehr effektive Langzeitsenke für reaktives, bioverfügbares Fe. Dieser Prozess induziert eine negative Rückkoppelung für den Fe Kreislauf in dem heutigen Gebiet. Auf längeren Zeitskalen könnte eine vertikale Ausdehnung der SMZ allerdings zur erneuten Mobilisierung des Fe Inventars führen und damit die negative Rückkoppelung in eine positive umwandeln.

# Contents

# 1 Introduction

The research focus of this study is to investigate benthic phosphorus and iron cycling in oxygen deficient waters. In the following chapter, general aspects about oxygen minimum zones and cycles of phosphorus and the iron will be introduced.

## 1.1 Oxygen Minimum Zones (OMZs)

Oxygen is a key element for earth's life. In the oceans, oxygen is produced by photosynthesis of phytoplankton in the photic zone. It is mixed into the deep ocean by circulations and is exchanged with the atmosphere. Bacteria consume large quantities of oxygen in the water column and the sediments during organic matter remineralization. In high productive areas such as upwelling regions, oxygen decline can lead to hypoxic or even anoxic waters. Those areas are named Oxygen Minimum Zones (OMZs) with $O_2$ < 20 µM. They occur mainly in eastern regions of the Pacific Ocean, the South Atlantic Ocean and the Northern Indian Ocean (Fig. 1.1, Kamykowski and Zentara, 1990; Helly and Levin, 2004; Paulmier & Ruiz-Pino, 2009). The total volume of the OMZs represent approximately 1% of the total ocean water volume. However, recent studies propose an expansion of oxygen deficient water in the future (Stramma et al., 2008, Schmitdko et al., 2017).

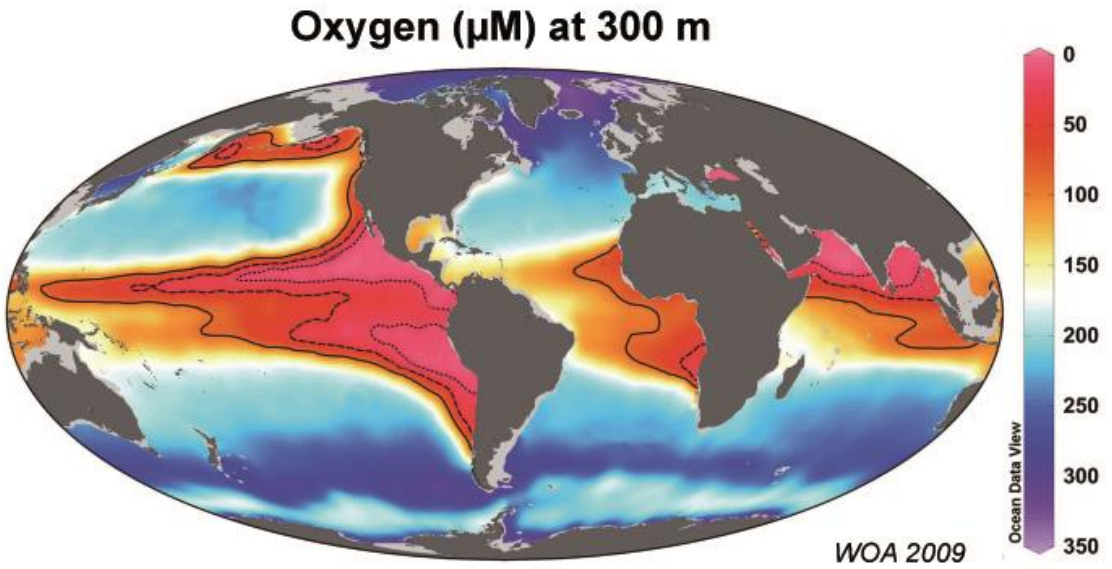


**Fig. 1.1** Oxygen minimum zones of the world's oceans. The pink to red colored areas show the oxygen-deficient water masses at 300 m water depth.

OMZs are associated with wind-driven coastal upwelling areas that are most prominent at the eastern margins of the Pacific and Atlantic Ocean. Intense alongshore trade winds blow towards the equator with seasonally variable strength. Due to the earth's rotation and the friction between the wind and the surface water, water is transported in Coriolis directed deviation to the open

ocean. This process is known as Ekman transport (Ekman, 1905). The surface water is replaced by deeper water masses with low temperatures and low oxygen concentrations as well as high nutrient contents and $CO_2$ concentrations. The subsurface water masses cause an enormous nutrient supply to the surface waters that strongly enhances the organic matter production. The mineralization of organic matter, associated with the consumption of dissolved oxygen in intermediate water depths (100-1000 m), leads to low oxygen concentrations (Ulloa and Pantoja, 2009). Consequently, OMZs develop due to a combination of special circulation pattern and biogeochemical processes (Wyrtki, 1962). Additionally sluggish ventilation and oxygen-poor source waters further intensify the propagation of oxygen-depleted waters.

The layers within an OMZ are differentiated by their oxygen concentrations in suboxic and anoxic zones. An oceanic area is termed OMZ when oxygen concentrations drop below 20 µM (Kamykowski and Zentara, 1990; Ulloa and Pantoja, 2009; Fuenzalida et al., 2009). This denotes the transition from oxic to suboxic conditions. The suboxic zone comprises the transition zone of aerobic respiration to nitrogen reduction. The oxygen concentrations range between 20 and 0.7 µM (Helly and Levin, 2004; Paulmier and Ruiz-Pino, 2009). Conditions denoted as anoxic refer to oxygen concentrations ($O_2$) = 0 µM (Oguz et al., 2000; Paulmier and Ruiz-Pino, 2009; Ulloa and Pantoja, 2009). These conditions are defined as the shift from the nitrate to the sulfate reduction zone. The upper boundary of an OMZ is the oxycline. It is characterized by an oxygen concentration gradient that is ~5 times higher than the downward gradient in classical oxygenated waters (Paulmier et al., 2006; Paulmier and Ruiz-Pino, 2009).

Due to high primary production rates in the surface water, the rain rate of organic matter to the OMZ seabed is higher than in other oceanic regions. Furthermore, the limited bioturbation leads to more or less undisturbed sediments. Therefore, sediments of OMZs often represent a high-resolution sediment record to reconstruct paleoceanographic settings and paleoclimate conditions (Tribovillard et al., 2006). They are also predestinated to investigate biogeochemical cycles of redox-sensitive elements, the preservation of organic matter, the adaption of animals to life-threatening conditions as well as the diversity and evolution of marine biota (Elrod et al., 2004, Helly and Levin, 2004, Ingall and Jahnke, 1994, Wallmann, 2010). Furthermore, OMZs are of great socio-economic importance because they provide about 10 – 20 % of the global fish catch.

## 1.2 The Phosphorus cycle

Phosphorus (P), the eleventh most abundant element in the earth crust, is a key element for life. It is part of DNA and RNA and is used for energy transfer in ATP. Further on, P is a main component in cell membranes and in bones (Ruttenberg, 2013). P cannot be fixed from the atmosphere in contrast to nitrogen and is thus considered to be a limiting macronutrient for primary production over geological time scales (Ingall & Jahnke, 1994; Föllmi, 1996; McManus

et al., 1997; Delaney, 1998; Benitez-Nelson, 2000; Benitez-Nelson et al., 2004; Filippelli, 2002; Paytan & McLaughlin, 2007; Tsandev et al, 2012). Variations in the geologic time scale P cycle are coincident with changes in chemical weathering rates, sea-level fluctuations, MOR spreading rates, glaciations and oceanic circulation (Compton et al., 2000).

The regulation of the marine primary production on long time scales by the availability of P induces a close coupling with the global marine carbon cycle, the sequestration of atmospheric carbon dioxide in organic matter, and the atmospheric $pCO_2$ level (Compton et al., 2000; Paytan & McLaughlin, 2007). A number of mass balance approaches and estimates of fluxes were published previously, e.g. Ruttenberg, 1993; Delaney, 1998; Compton et al., 2000; Slomp and Van Cappellen, 2007; Wallmann, 2003 and 2010. However, key processes such as the P delivery and transformation in the water column and final burial in the sediments are still not very well understood (Compton et al., 2000; Benitez-Nelson, 2000). Moreover, the natural P cycle is overprinted by anthropogenic P input with unknown long term consequences. The riverine flux of dissolved phosphate was drastically increased by mankind during the last decades. In contrast, the particulate phosphate flux has been reduced by river dams (Wallmann, 2010 and references therein). Besides, increasing atmospheric $CO_2$ concentrations cause global warming and lead to declining oceanic oxygen concentrations and thus spreading of oxygen minimum zones (Stramma et al., 2008). As anoxic bottom waters and reducing sediments favor the release of phosphate, benthic phosphate fluxes are thought to increase at continental margins (Wallmann, 2010). Due to its overall impact on life, it is of great importance to improve our still incomplete knowledge on the marine P cycle.

### 1.2.1 Phosphorus sources

The main P source to the oceans is riverine input of P eroded from bedrocks in the hinterland by continental weathering (Fig. 1.2). Riverine P is delivered to the oceans by particulate inorganic and organic P (PIP and POP) and dissolved inorganic and organic P (DIP and DOP). Dissolved P comprises organic, inorganic and macromolecular colloidal P. Particulate P consists of living and dead plankton as well as precipitates of P minerals, particle adsorbed P and amorphous P (Payton and McLaughlin, 2007). Dissolved and particulate P include organic and inorganic compounds such as P-esters, P-diesters, phosphonates and orthophosphate, pyrophosphate, polyphosphate and P containing minerals (Payton and McLaughlin, 2007). Due to the high particle reactivity of P, the largest flux of more than 90% appears to be the particulate P flux (Compton et al., 2000, Payton and McLaughlin, 2007), but flux estimations have large uncertainties (Ruttenberg, 2013). P is mainly bound in the phosphorus-bearing mineral apatite ($Ca_{10}(PO_4)_2(OH, F, Cl)_2$) or adsorbed to Fe and Al (oxyhydr)oxides. The crustal material contains on average 0.1 % $P_2O_4$ (Benitez-Nelson, 2000).

Most of the P entering the costal ocean is rapidly removed via sedimentation and flocculation of humic-Fe complexes and is therefore not directly involved in the biological cycle (Benitez-Nelson, 2000; Paytan & McLaughlin, 2007, Ruttenberg, 2013). However, P adsorbed to clay minerals or to Fe/Al (oxyhydr)oxides in freshwater can be dissolved from the particle surface and be released to the sea water when salinity increases or in anoxic water conditions. Dissolved orthophosphate is directly bioavailable for photosynthetic organisms. The remineralization of organic matter and thus, the regeneration of nutrients usually follows the Redfield ratio expressed as C:N:P = 106:16:1 (Redfield, 1963). However, with increasing water depth the C:P and the N:P ratio in dissolved organic matter (DOM) increases (Payton and McLaughlin. 2007 and references therein). That indicates a preferential regeneration of phosphorus towards carbon and nitrogen from DOM. Thus, it is assumed that DOP cycling is more effective than the cycling of dissolved carbon and nitrogen (Payton and McLaughlin. 2007 and references therein).

A minor part of P input to the oceans is present as DOP which becomes bioavailable by enzymatic hydrolytic production of orthophosphate (Ruttenberg, 2013 and references therein). On average, about 10 - 30% is delivered as DOP to the oceans (Paytan & McLaughlin, 2007). Approximately 25% of the DOP is available for marine biota, the remaining fraction is trapped in shallow marine sediments (Paytan & McLaughlin, 2007). In total, only 10 - 30% of the riverine supplied P to the oceans is reactive (bioavailable) P and 75% of the reactive P reaches the open ocean (Payton and McLaughlin, 2007).

The atmospheric P supply is associated to aeolian dust particles (Payton and McLaughlin, 2007). The impact of atmospheric P sources increases with distance from the coast where other P sources, e.g. riverine input, become less important. Thus, aeolian P provides an important P source to open ocean and non-upwelling regions, but is in the overall budget relatively unimportant (Compton et al., 2000 and references therein, Ruttenberg, 2013). Atmospheric P is equally composed of organic and inorganic compounds whereas the inorganic P is mainly associated with Fe (oxyhydr)oxides or other elements, e.g. Al, Mg, or Ca. Roughly 20 % of the total aeolian P delivery is reactive P and therefore bioavailable (Compton et al., 2000 and references therein; Benitez-Nelson, 2000). The degree of solubility for aeolian dust is dependent on the source, the particle size, the sea surface meteorological conditions and the biology (Benitez-Nelson, 2000). In total, aeolian P flux accounts for less than 1% of the annual primary production, but short and intense bursts could strongly enhance biological production on short time scales, e.g. in high nutrient low chlorophyll (HNLC) regions (Benitez-Nelson, 2000 and references therein).

Human mining activities, deforestation, increased cultivation and waste deposal enhanced the riverine P flux to the oceans in short time periods by 2 to 3 times of the pre-agricultural level

(Ruttenberg, 2013 and references therein). Despite several studies on atmospheric P fluxes more research is needed to improve our knowledge on P fractions which are maybe also soluble in sea water and bacteria that are able to hydrolyze organic bound P (Benitez-Nelson, 2000). Until those mechanisms are better understood the atmospheric P flux could be highly underestimated.
A further, poorly investigated, P source is submarine groundwater seepage (Ruttenberg, 2013 and references therein). These sources are thought to be irrelevant on global scales, but may have a strong temporal and / or regional impact (Föllmi, 1996; Slomp and VanCappeln, 2004, Wallmann, 2010).

### 1.2.2 Phosphorus sinks

P is removed from the water column via uptake by organisms and concurrently released to the water column again by organic matter remineralization (Fig. 1.2, Compton et al., 2000). However, the most effective long-term P sink are marine sediments. Removal mechanisms such as organic matter burial, sorption and precipitation with clay and Fe (oxyhyr)oxides, phosphorite burial and hydrothermal vent activity are the most prominent P sinks (Benitez-Nelson, 2000 and references therein).
The burial of bioavailable, reactive P is mainly restricted to continental margins (Wallmann, 2010). P is delivered to the sediments as sinking particulate matter and bound to Fe (oxyhydr)oxides. The largest part of the burial flux comprises reactive P that was previously involved into biological processes. The nonreactive P originating from terrigenous detritus is mostly deposited at shallow water depth on the continental shelf. The reactive P includes organic matter, P bound to Fe (oxyhyr)oxides, loosely sorbed P, P associated to authigenic minerals (Ca-F minerals) and P in fish bones (Benitez-Nelson, 2000; Wallmann, 2010).

The composition of the specific reactive P compounds and their contribution to P deposition in marine sediments is strongly redox dependent. In oxic sediments ($O_2$ > 20 µM) P is primarily bound to Fe (oxyhydr)oxides, whereas reducing conditions (< 20 µM) favor P associated to Ca-F minerals. Furthermore, the reactive organic P burial is sensitive to the sedimentary redox conditions. C:P ratios of particulate organic matter in reducing sediments show extremely high values. In contrast, particulate organic matter in oxic sediments is characterized by C:P ratios that cluster around the Redfield ratio (Wallmann, 2010). This implies that P is more effectively buried in oxic sediments compared to organic carbon then in anoxic deposits (Payton and McLaughlin, 2007 and references therein).

A further important sink for the oceanic P inventory are phosphorites. Ancient delivered phosphorite deposits coincide with organic-rich facies that correlate with high productivity cycles and intense weathering (Föllmi, 1996). Microbial hydrolysis and the release of organic P under

low oxygen conditions lead in some cases to the formation of phosphorites. These authigenic formations, specifically calcium fluorapatite, develop from the reaction of soluble P and calcium ions at the sediment/water interface or in pore waters (Paytan & McLaughlin, 2007). The occurrence is, among others, documented for the highly productive upwelling areas of the Peruvian continental shelf (Veeh and Burnett, 1973; Suess and von Huene, 1988). The removal potential for oceanic P of fine-grained apatite minerals and the subsequent formation of phosphorites is still uncertain, but thought to play an important role (Benitez-Nelson, 2000; Goldhammer et al., 2010).

Another P sink that has to be taken into account is the activity of hydrothermal vents. They act as a P sink when the escaping fluids contain high amounts of reduced Fe that is immediately oxidized to Fe (oxyhyr)oxides in the water column (Benitez-Nelson, 2000). Dissolved P is rapidly adsorbed to the surface of the Fe (oxyhyr)oxides which are immediately scavenged in the sediments. This process is first of all thought to be important at low temperature hydrothermal processes at the seafloor (Benitez-Nelson, 2000 and references therein).

Besides oxidized Fe (oxyhydr)oxides P could also be adsorbed to various other suspended plume particles that sink down to the sediments (Wallmann, 2010).

Furthermore, P removal mechanism is the circulation of seawater through ridge flanks at mid ocean ridges where P is incooperated into the altered crust. The dissolved P removal fluxes at hydrothermal vents and ridge-flank circulation are estimated to be larger than the input flux of dissolved P by rivers (Wallmann, 2010 and references therein).

### 1.2.3 Phosphorus in the water column

Dissolved and particulate P forms in the ocean are affected by continuous transformations because P is a major element involved in biological processes (e.g. nutrient, cellular components, and skeletal components). DIP uptake mainly occurs in the eutrophic zone of the water column where most intensive primary production and thus, photosynthesis takes place. The dissolved inorganic P, mostly hydrogen phosphate ($HPO_4^{2-}$), is taken up by phytoplankton and autotrophic bacteria from the seawater for their metabolic needs (Payton and McLaughlin, 2007). The inorganic P is alternated to organic P which is consumed by zooplankton and again released as dissolved inorganic or organic P. DOP is not directly available for the most species. Thus, DOP is hydrolyzed to orthophosphate by some phytoplankton species by producing enzymes that catalyze the hydrolytic cleavage of organically bound P when DIP is limited (Payton and McLaughlin, 2007 and references therein; Dyhrman et al., 2007). Besides some specialized phytoplankton species, especially heterotrophic bacteria hydrolyze the dissolved organic P and convert it into dissolved inorganic P. The hydrolysis of DOP to DIP is characteristic for the whole water column, in contrast to DIP assimilation. Thus, the regeneration of DOP is a potentially important source

for bioavailable P and thus, oceanic productivity in regions with oligotrophic surface waters (Payton and McLaughlin, 2007).

DIP and DOP concentrations are subject to spatial and temporal variations in coastal waters. Concentration changes are a result of physical (upwelling/relaxation events) and biological (DIP uptake, DOP production and regeneration) processes (Payton and McLaughlin, 2007 and references therein). The general concentration profile of DIP is similar to other essential nutrients. The typical surface water depletion is caused by DIP uptake by organisms and the concentration raises with depth due to the conversion of POP and DOP into DIP. The DIP concentration also rises with increasing age of the water mass. This is caused by persistent accumulation of sinking particulate matter and its regeneration. Therefore, deep water masses of the Pacific Ocean are enriched in DIP in contrast to deep waters of the Atlantic Ocean where deep water formation happens. The DOP depth profile is the mirror image of the DIP profile. DOP is enriched in surface waters and depleted in deeper water masses. The DOP concentration profile is a result of biological uptake and release mechanisms for DOP. Unlike the DIP enrichment in older water masses, DOP concentration is relatively constant at depth. This suggests a long residence time for DOP compounds (Payton and McLaughlin, 2007 and references therein).

The main P shuttle in the water column is particulate organic matter (Fig. 1.2). However, also authigenic P phases and labile and oxide-associated P has to be taken in account (Faul et al., 2005). Still, only a few studies on P in sinking particulate matter in the water column exist, e.g. Benitez-Nelson et al. (2004) and Faul et al. (2005); Lyons et al. (2011) and Sekula-Wood et al. (2012). Here, more research is urgently requested.

P is associated to the organic matter export that is maintained by different pathways. Particulate organic matter rains to the sea floor due to gravitational forcing and the lateral transport of particles. On the other side, dissolved organic material is transported by diffusion and mixing processes to the sea floor. Most of the exported material never reaches the seafloor. Degradation processes in the water column and at the sediment-water interface lead to P release back into the water column. This P belongs to the reactive marine P pool and is bioavailable again (Filippelli, 2008). The remaining fraction reaches the sediments.

### 1.2.4 Phosphorus in marine sediments

The burial of P at the sediment water interface is strongly dependent on the sedimentary redox conditions and the amount of the deposited organic matter (Fig. 1.2). Large fractions of particulate P are remobilized by bacterial degradation or the reduction of Fe (oxyhydr)oxides in surface sediments (Compton et al., 2000). The resulting dissolved phosphate partly diffuses back into the overlaying bottom water either by molecular diffusion or bioirrigation (Colman and Holland, 2000; Wallmann, 2010, Dale et al., 2013). The remaining dissolved P is removed from

the pore water by Ca-P formation or resorption to Fe (oxyhydr)oxides. Ca-P bound P is permanently removed from the oceanic P cycle.

At some sedimentary settings the so called Fe redox pumping of phosphorus occurs in the sediments (Compton et al., 2000). This mechanism describes the adsorption of P to Fe (oxyhydr)oxides in bottom waters and surface sediments. Further on, the adsorbed P is released for Ca- P formation upon reductive dissolution of Fe (oxyhydr)oxides. The reduced Fe diffuses back to the redox boundary and is oxidized again to Fe (oxyhydr)oxides. The cycle restarts and could cause effective scavenging of P in sediments.

In contrast, anoxic sediments have a desorption/release capacity with regard to phosphorus that exceeds the adsorption capacity of oxic sediments (Fig. 1.2, Payton and McLaughlin, 2007). Low bottom water oxygen concentrations limit Fe (oxyhydr)oxide in trapping P. Thus, settings that favor Fe (oxyhyr)oxide burial are not favorable for Ca-P precipitation and vice versa (Tsandev et al., 2012).

The comparison of organic P and C burial revealed a more efficient scavenging in oxic sediments than in anoxic sediments. The C:P ratios of anoxic sediments are higher than the ratios measured at oxic sites. This indicates the preferential P release from organic matter under anoxic conditions (Ingall and Jahnke, 1994).

The preservation potential for P in anoxic sediments generally increases with increasing organic matter flux to the sediments (Tsandev et al., 2012). However, large amounts of dissolved P are released to the bottom water under low-oxygen conditions. Since only 1% of the modern ocean is covered by oxygen deficient waters, the contribution of those areas to the total oceanic P inventory is not highly relevant but, it is thought to change with further expanding OMZs (Wallmann, 2010). The above described positive feedback loop could play an important role for expanding OMZs.

P can be remobilized from the sediments when organic matter is degraded (Fig. 1.2). For this reason pore water P concentration normally rises with sediment depth. Most of the released P precipitates again as Ca-P minerals or is adsorbed onto Fe (oxyhydr)oxides. A minor part is delivered back to the nutrient cycle and to the photic zone in continental shelf areas by upwelling, vertical advection and eddy diffusion from greater water depth.

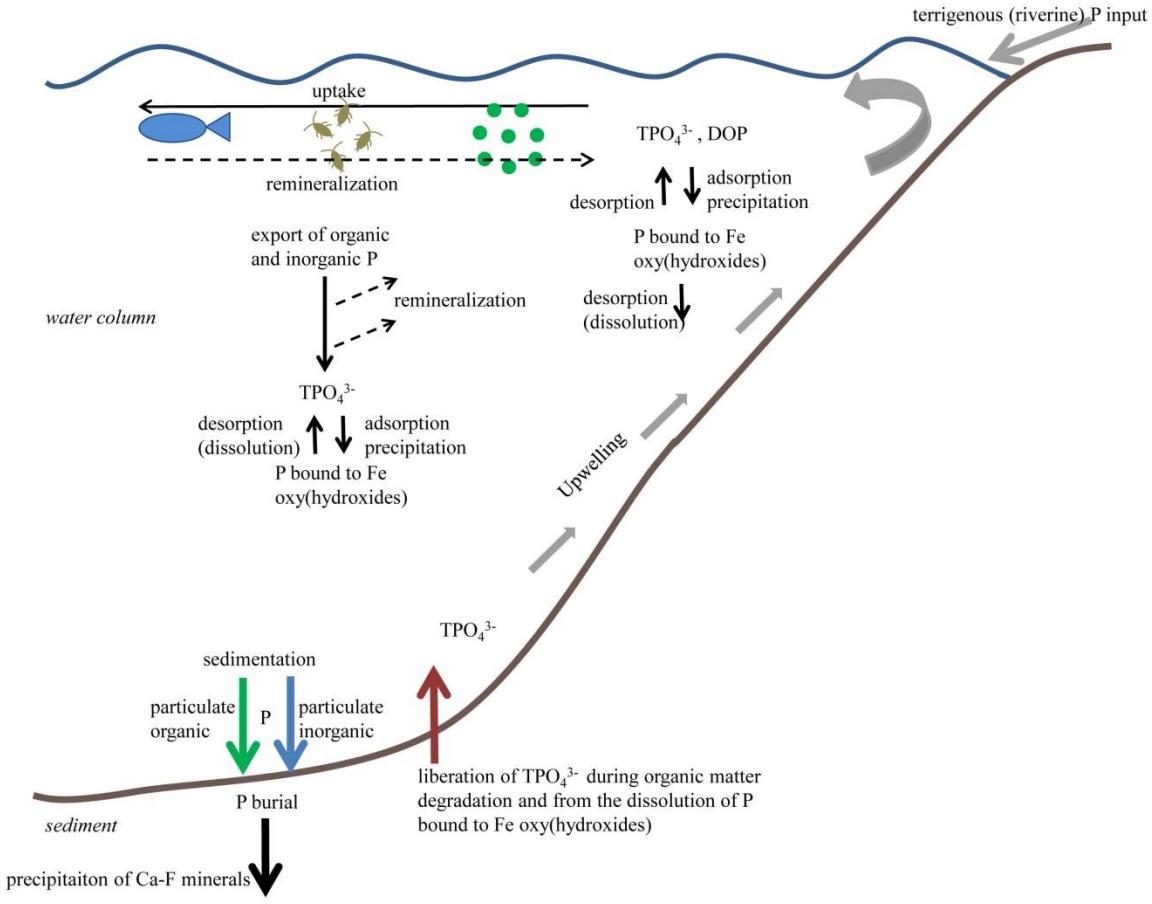


**Fig. 1.2** P cycling in an oxygen-deficient water column (modified after Noffke, 2014).

## 1.3 The Iron cycle

Fe (Fe) is the fourth most abundant element in the earth crust, but its concentration in the ocean is rather low. Therefore, Fe is one of the key player elements of the oceans (Tortell et al., 1999; Haese, 2006). It acts as a limiting nutrient for photosynthetic organisms and thus, essentially controls oceanic primary production (Jickells et al., 2005; Boyd, 2009; Boyd and Ellwood, 2010; Raiswell and Canfield, 2012). The effects of Fe on oceanic primary production in HNLC-areas where examined in detail with Fe enrichment experiments. Those experiments resulted in net primary production enhancement of factors 2 to 4 over short time scales (Martin et al., 1991 and 1994, Coale et al., 1996; Buesseler et al., 2004).

Fe is strongly linked to the efficiency of the 'biological pump' of the ocean. Microorganisms require Fe for cell growth and/or gain energy from $Fe^{3+}$ reduction (Haese, 2006). The 'biological pump' triggers the capacity of the oceanic $CO_2$ uptake and consumption in surface waters and the rate at which carbon is transported and deposited as particulate organic carbon into deep water masses and to the sediments (Tortell et al., 1999). On a global scale, the biological pump affects

the climate relevant atmospheric carbon dioxide concentration (Tortell et al., 1999; Boyd, 2009; Boyd and Ellwood, 2010; Raiswell and Canfield, 2012).

The occurring abiotic reactions are as numerous as the biotic ones. These reactions depend on thermodynamic and kinetic conditions in the sea water and sediments (Haese, 2006). Furthermore, Fe affects other element cycles (phosphate, manganese, and several trace elements) via sorption and desorption and precipitation processes.

### 1.3.1 Iron sources

The Fe sources can be defined by different criteria, e.g. geographically or the amount of Fe input. From the geographical point of view, the coastal and shelf sediments receive most of the Fe from river discharge and by Fe recycling from anoxic sediments. In contrast, Fe is supplied by dust deposition and deep water upwelling to the open ocean (Tortell et al., 1999). Other minor important sources are hydrothermal activity and ice rafted sediments.

Fe is mainly transported as nanoparticulate (oxyhydr)oxides of the minerals ferrihydrite ($5\ Fe_2O_3\ 9H_2O$), goethite (α-FeOOH), lepidocrocite (γ-FeOOH), hematite ($Fe_2O_3$) and schwertmannite (Fe-oxyhyroxysulfate) (Raiswell, 2011). The particles form in soils, sediments and by oxidation with $Fe^{2+}$ in minerals such as carbonates, silicates and aluminosilicates (Raiswell, 2011). Furthermore, the Fe nanoparticulate (oxyhyr)oxides can be formed by transformation of pre-existing nanoparticles (Raiswell, 2011). Marine biota use aqueous Fe species and ferrihydrite, while Fe minerals, e.g. hematite or goethite, are mainly not bioavailable (Raiswell, 2011). The transformation from ferrihydrite to hematite or goethite is temperature and pH dependent but, occurs within a few hundred days (Raiswell, 2011).

**Rivers, Estuaries, Continental Shelf**

The riverine transported Fe amount is estimated to be the largest Fe input to the oceanic shelf regions with an annual mass of ~ $10^{16}$ g Fe (Boyd, 2009). However, Fe nanoparticles rapidly form complexes with abundant particulate organic matter or flocculate due to increasing salinity and ionic strength in estuarine and coastal areas which leads to immediate deposition of most of the stream load Fe (Haese, 2006; Boyd, 2009; Boyd and Ellwood, 2010). Furthermore, a high sediment load of rivers may lead to loss of dissolved Fe via sorption to particle surfaces (Raiswell, 2011). About 70 - 90% of the Fe load of a river is deposited in estuaries and a large portion of the remaining Fe is removed in the continental shelf areas (Raiswell, 2011). The coastal sediments are therefore enriched in Fe whereas the open oceans are often depleted in Fe. The Fe particles change with increasing transport distance and become more and more non-available for marine biota.

At continental shelfs, the Fe recycling potential is comparatively high, as these areas provide dissolved and bioavailable Fe to marine organisms. Especially, OMZs are pronounced regions for strong Fe fluxes from the sediments into the water column.

**Open Ocean**

Fe contributed to open ocean mainly originates from aeolian dust, deposited wet or dry. However, the dust delivered Fe amount is much lower than the riverine input (Jickells et al., 2005, Boyd, 2009, Raiswell, 2011). Windblown dust reaches oceanic areas that are inaccessible for rivers (Raiswell, 2011). It is generated by frequent sandstorms in semi-arid to arid terrestrial areas of low latitude (North Africa and China), combustion products from biomass burning and anthropogenic environmental pollution (Haese, 2006; Boyd, 2009). The particles, commonly < 10 µm in diameter, are uplifted by wind energy and dispersed into the atmosphere where they are transported for thousands of kilometers. The main Fe containing components in atmospheric dust are clay minerals as illite, smectite and chlorite and minor amounts of Fe (oxyhydr)oxides (Raiswell, 2011). Chemical processes within the clouds, e.g. photochemical, influence the Fe solubility and play a key role for bioavailable Fe supply to the surface ocean (Raiswell, 2011). Solid Fe ($Fe^{3+}$) from dust deposition is photochemically reduced to dissolved Fe ($Fe^{2+}$) in surface waters. This reaction causes that about 10% of the total dust induced Fe is dissolved but, partly reoxidized in oxygen containing water masses (Haese, 2006).

As Fe is one of the most abundant elements of the earth crust, also volcanism has to be considered as potential terrestrial Fe source, especially in the Pacific Ocean surrounded by the Circum Pacific Belt. During volcanic eruptions ash particles, also containing Fe, are catapulted into the upper atmosphere and dispersed regionally and globally (Boyd, 2009).

Besides the "new" sources, Fe is also provided by biological and chemical recycling processes ("old sources") in the water column and the sediments.

In the open ocean Fe recycling is mainly driven by organisms. Their uptake and recycling budgets are more or less in balance; this is the so called "ferrous wheel". Biological recycling is a rapidly ongoing process within hours or days and means that the biota changes the oxidation state of Fe when it passes through their acidic gut or due to metabolization. In consequence, Fe is reduced and becomes available for other organisms again (Tortell et al., 1999; Boyd, 2009).

Fe is also chemically recycled. Due to the redox sensitivity of Fe, oxygen minimum zones are predestinated areas of Fe recycling and resupply to the nutrient cycle. The re-suspended Fe form nanoparticles could be transported over long distances to the open ocean. This recycling and transport mechanism is known as "Fe shuttle" (Raiswell, 2011; Scholz et al., 2011).

### 1.3.2 Iron sinks

The main Fe sink are marine sediments. Organic matter, fecal pellets, and inorganic material sinks down to the seafloor and carries biological reworked and inert Fe phases to the sediments. Within the sediments, reduced Fe precipitates to Fe sulfides, Fe carbonates and silicates that are effectively scavenging Fe in the sediments (Boyd, 2009; Taylor and Macquaker, 2011). Dissolved Fe is mainly removed from the sea water by prokaryotic and eukaryotic phytoplankton and heterotrophic bacteria. Furthermore, Fe is taken up by zooplankton and other organisms dissolving Fe in their acidic guts (De Baar and de Jong, 2001). This is also thought to affect Fe-oxide coatings on mineral phases.

### 1.3.3 Iron in the water column

Fe exists in the water column in dissolved or particulate forms and is highly particle reactive. By definition dissolved Fe can be filtered through filter pore sizes of 0.2-0.4 µm whereas particulate Fe is greater than 0.4 µm (Raiswell and Canfield, 2012).

Dissolved Fe is further divided in colloidal/nanoparticulate Fe (0.4-0.02 µm) and soluble/aqueous Fe (<0.02 µm) (Boyd, 2009; Raiswell and Canfield, 2012). The particulate Fe either refers to lithogenic or biogenic Fe. Lithogenic Fe originates from aerosols or re-suspended sediments (Boyd, 2009). The dissolved Fe is bound to 99 % in organic complexes by Fe binding ligands, which are molecules that form coordination bonds to metal ions and have a high binding strength (Boyd, 2009). There are two existing Fe-binding ligands classes. The strong Fe-binding ligand class L1, mainly present in surface waters, and the weaker Fe-binding ligand L2 which is found throughout the whole water column (Raiswell and Canfield, 2012). L1 ligands have a strong affinity to dissolved Fe, like siderophores. Siderophores are typically evolved by prokaryotic organisms to absorb Fe (Raiswell and Canfield, 2012). They are ideal to scavenge dissolved $Fe^{3+}$ under oxygenated conditions due to their high solubility and their reactive sites that can bind the central $Fe^{3+}$ cation (Konhauser et al., 2011).

The aqueous Fe species occur in two valence states at a pH of 8: the thermodynamically stable and minor bioavailable $Fe^{3+}$ (ferric Fe) and the less stable but highly bioavailable $Fe^{2+}$ (ferrous Fe). $Fe^{3+}$ is the dominating form in oxic seawater and occurs as inorganic, particulate phase, e.g. Fe (oxyhydr)oxides, silicates and aluminosilicates and organic complexes (Tortell et al., 1999; Raiswell and Canfield, 2012). The concentration of bioavailable dissolved ferric Fe is with approximately $10^{-10}$ mol per liter extremely low and leads to Fe limitation in the present day oxygenated oceans (Konhauser et al., 2011). $Fe^{2+}$ is the reduced and dissolved Fe species, predominantly occurring and stable under anoxic conditions. The solubility of ferrous Fe is $10^8$ times higher than that of ferric Fe (Boyd, 2009). Under low oxygen concentrations, the inorganic aqueous Fe pool is divided into 76% $Fe^{2+}$ ions and 23% $Fe^{3+}$ complexes (mostly $Fe(OH)_3^0$)

(Raiswell and Canfield, 2012). Due to high oxygen concentrations in the modern atmosphere, the oceans are dominated by ferric Fe, rather than ferrous Fe, limiting the primary production (Boyd, 2009).

Because all organisms require Fe for respiratory pigments, proteins and enzymes, the shape of the dissolved Fe profile in the water column is nutrient like (Tortell, 1999; Haese, 2006; Boyd, 2009; Boyd and Ellwood, 2010). The dissolved Fe is taken up by organisms in the surface water which drops the concentration often down to zero. The organic matter is remineralized in deeper water layers and the Fe concentrations increases again.

Eukaryotic organisms are known to acquire Fe by photochemical reduction and/or by reduction of colloids absorbed to the cell surface (Raiswell and Canfield, 2012 and references therein). They are able to access Fe-siderophore complexes via their membrane transporter systems and can therefore take up Fe from ferryhydrite and natural Fe-bearing organic colloids (Raiswell and Canfield, 2012 and references therein).

Prokaryotic organisms evolved Fe uptake mechanisms for Fe (oxyhydr)oxides. They have the ability to synthesize chelators (siderophores) to complex ferric Fe of mineral Fe and aqueous Fe (Haese, 2006; Raiswell and Canfield, 2012). Siderophores from a complex with ferric Fe and this complex is transported into the cell. Inside the organisms cell the complex is reduced by enzymes and released from the siderophore (Sunda, 2001; Haese, 2006 and references therein).

### 1.3.4 Iron in marine sediments

Fe is transported to the sediments by settling organic matter or inorganic particles. It is mainly accumulated as ferric Fe, in mostly amorphous or poorly crystalline (hydr)oxides and bound to clay minerals (Taylor and Macquaker, 2011). Marine surface sediments undergo diagenesis through the bacterial degradation of organic matter inducing a geochemical zonation according to the potential for dissimilatory bacteria to gain energy from the available electron acceptors (Froehlich et al., 1979; Haese, 2006; Taylor and Macquaker, 2011). The redox potential decreases with increasing sediment depth, depending on the composition and the accumulation rate (Sundby et al., 1992). If the redox potential falls below the stability of Fe (oxyhydr)oxides they are reductively dissolved by microbes.

Fe reduction occurs when oxygen ($O_2$), nitrate ($NO_3^-$), and manganese (Mn (IV)) are consumed as electron acceptors by anaerobe bacteria (Taylor and Macquaker, 2011; Burdige, 1993). The enzymatically reduction pathways resulting in the release of soluble ferrous Fe to the pore waters, are differenced into 5 reactions: the fermentative $Fe^{3+}$ -reduction, sulfur-oxidizing $Fe^{3+}$-reduction, hydrogen-oxidizing $Fe^{3+}$-reduction, organic-acid-oxidizing $Fe^{3+}$-reduction and the aromatic-compound-oxidizing $Fe^{3+}$-reduction (Haese, 2006; Taylor and Macquaker, 2011).

The biogeochemical zonation is well developed when the seafloor receives high amounts of organic matter. If this is the case, Fe reduction is often followed by sulfate reduction which causesthe precipitation of Fe sulfides such as mackinawite that could be further converted into pyrite (Severmann et al., 2006; Raiswell, 2011; Tayler and Macquaker, 2011; Kraal et al., 2012 and references therein; Raiswell and Canfield, 2012). If sulfate reduction is absent (in case of low organic matter supply and/or high sedimentation and/or bioturbation rates), the Fe reduction zone could be very well established reaching up to a meter in thickness (Raiswell, 2011; Raiswell and Canfield, 2012,). This causes high dissolved Fe concentrations in the pore waters from where dissolved Fe migrates to the sediment surface and into the bottom water (Sundby et al., 1986; Pakhomova et al., 2007). The diffusive Fe flux results from high concentration gradients between the sediment pore water and the bottom water. Further mechanisms to recycle $Fe^{2+}$ into the water column occur by physical or biological rework of the sediments (Burdige, 1993; Raiswell, 2011; Taylor and Macquaker, 2011). The dissolved Fe reaching oxygenated water is immediately oxidized to $Fe^{3+}$ and the bottom water becomes saturated in Fe (oxyhydr)oxides. A small portion of the aqueous $Fe^{3+}$ forms complexes with organic ligands whereas the rest precipitates to ferryhydrite. As soon as the complex capacity for $Fe^{3+}$ is exhausted, the remaining Fe is precipitated as nanoparticulate ferryhydrite (Raiswell and Canfield, 2012 and references therein). The ferryhydrite is either scavenged again in continental shelf sediments or remains in suspension and is transported across the shelf to deeper water depths. As freshly precipitated and deposited ferryhydrite is very reactive, it is rapidly reduced within the sediments may starting the recycling process again (Lyons and Severmann, 2006). This is called the oxic Fe shuttle depicting one major pathway of Fe supply to the deep ocean (Taylor and Macquaker, 2011). To examine variations in the dissolved Fe pool of pore waters, Fe isotopes are used (Severmann et al., 2006; Severmann et al, 2010).

The diffusive Fe supply to the bottom water could be enhanced by physical and/or biological resuspension and mixing of pore water and bottom sediments into the oxic water column (Raiswell and Canfield, 2012). Erosion or biological maintained reworking is a process that contributes to the supply of dissolved pore water Fe to the ocean. In sea water it forms nanoparticulate and/or colloidal Fe (oxyhyr)oxides that are may transported from the self to the deep sea (Raiswell and Canfield, 2012 and references therein). Fe (oxyhydr)oxides are pronounced carriers for trace metals and phosphorus. When the solid Fe is dissolved by reduction the adsorbed metals and phosphorus are released to the sediments. Fe enrichment areas could be recognized by the ratios of reactive Fe to total Fe and/or total Fe to Aluminum in contrast to a locally validated detrital background ratio. Fe enrichments in sediments often coincidence with pyrite formation, as mentioned before. The degree of pyritization (DOP) is therefore used to

determine the availability of reducible ferric Fe compared to sulfide Fe. The DOP is expressed by the ratio of pyrite-bound $Fe^{2+}$ to pyrite-bound plus HCL-soluble $Fe^{3+}$ (Raiswell et al., 1988; Taylor and Macquaker, 2011). DOP values close to one indicate euxinic conditions, whereas values lower than 0.8 represent normal open marine conditions (Taylor and Macquaker, 2011). The DOP should always be used together with other chemical proxies as high DOP values were found at settings where oxygen is present.

## 1.4 Iron and Phosphorus in OMZs

The early diagenesis of Fe is of great importance for the behavior of numerous trace metals, organic compounds and phosphorus (Haese, 2006). In contrast to Fe, P is not an electron acceptor used for organic matter degradation. Therefore, the removal of P is limited to adsorption onto particle surfaces or the precipitation of in situ-formed minerals, e.g. Ca-F minerals, or it is re-incorporated into new biomass. P is effectively adsorbed by Fe (oxyhydr)oxides in oxygenated waters which directly links the cycles of both elements in the marine environment (Fig. 1.3). In sediments of continental margins and the deep-sea, Fe (oxyhyr)oxides are preserved together with Fe-bound P. The Fe-bound P of those sediments accounts for up to 30% of the total phosphorus within the sediments (Raiswell and Canfield, 2012 and references therein). On a global scale Fe-bound P accounts for ~ 20% of the total phosphorus removed in sediments (Raiswell and Canfield, 2012 and references therein). Oxygen minimum zones are exceptional areas for studying the interactions and reactions of the Fe and P cycles. $Fe^{2+}$ and $TPO_4^{3-}$ are released into the pore water and the bottom water under oxygen depleted conditions (Fig. 1.3). P release is thought to be also enhanced through reductive dissolution by hydrogen sulfide (Noffke et al., 2012 and references therein). Therefore, OMZs are important sources for bioavailable Fe and P. There are various feedback mechanisms which are not sufficiently understood and where further research is requested. A positive feedback-loop could develop from the Fe and P supply from areas with bottom water anoxia affecting and enhancing the surface water productivity. This could lead to increased surface water productivity, whereas the oxygen demand rises. As a consequence it is thought that oxygen minimum zones could further spread in the future (Van Cappellen and Ingall, 1994; Wallmann, 2003; Slomp and Van Cappellen, 2007; Stramma, et al., 2008; Wallmann, 2010). In turn, a negative feedback can evolve from the precipitation of Ca-F minerals and reactive Fe trapping at the lower boundary in present oxygen deficient waters diminishing the benthic P and release (Schulz and Schulz, 2005, Arning et al., 2009 a, Golhammer et al., 2010, Cosmides et al., 2013). However, also a balance of Ca-F mineral formation and enhanced P release from OMZs is suggested (Delaney et al., 1998, Anderson et al., 2001, Roth et al., 2014). The various feedback mechanisms proposed in the literature emphasize the need for further research on Fe and P cycling in presently expanding OMZs.

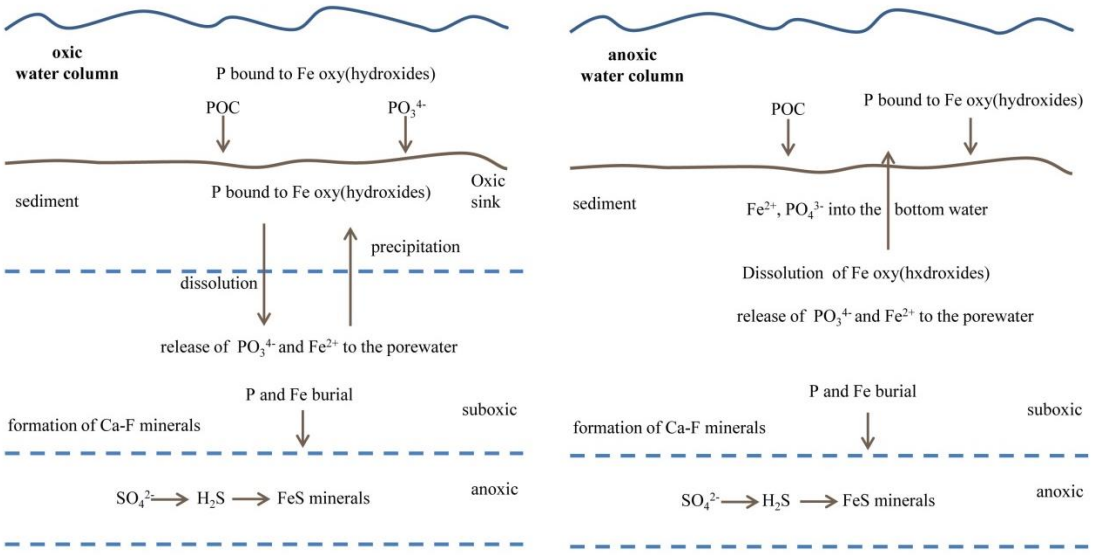


**Fig. 1.3** Interactions of Fe and P in oxic and anoxic environments.

## 1.5 State of the art – Fe and P in the Peruvian OMZ

The release of dissolved Fe and P into the overlying bottom water previously reported from a depth transect at 11°S is larger than at any other open ocean continental margin (Elrod et al., 2004; Pakhomova et al., 2007; Severmann et al., 2010, Scholz et al., 2011; Noffke et al., 2012). However, benthic release of these nutrients is strongly influenced by short time variabilities of the water column. More recent measurements from a 12°S depth transect for example confirm extremely high P release, but Fe release was drastically reduced on the shallow shelf and in the core OMZ (Scholz et al., 2016, this study). Due to the presence of hydrogen sulphide in the water column and surface sediment at the shallow shelf sites, Fe-sulfide minerals precipitated in the surface sediments and inhibited Fe release. Such transient sulfide plumes as previously reported by Schunck et al. (2013) and short oxygenation events induced by costal trapped waves and Kelvin waves as well as El Niño and La Niña (Gutiérrez et al., 2008) events have a great effect on the biogeochemical nutrient cycling. Fe (oxyhydr)oxides are deposited during those events and are immediately reduced and dissolved when bottom water oxygen concentration drops down again (Noffke et al., 2012).

The geochemical composition of the sediments is a mirror for the reported Fe release. Within the OMZ, reactive Fe is depleted compared to the lithogenic background due to the continuous reduction of Fe (oxyhydr) oxides. In the transition area to more oxygenated waters at the lower boundary of the OMZ, sediments are enriched in Fe compared to the lithogenic background due the precipitation of Fe (oxyhydr)oxides induced by nitrate-dependent Fe oxidation and rising oxygen levels (Scholz et al., 2011, Scholz et al., 2016). This observation suggests that a

considerable fraction of the benthic Fe is transported downslope and accumulates at the lower rim of the OMZ rather than being upwelled to the surface ocean or advected out of the OMZ. Further evidence comes from mass balance calculations that combined mass accumulation rates and benthic Fe release with excess Fe concentrations and sedimentary Fe isotope ($^{54,56}$Fe) data (Schloz et al., 2014a). The accumulated reactive Fe was found to transform into silicate-bound Fe during early diagenesis and burial in the sediments at 11°S (Scholz et al., 2014b). Iron precipitated in silicate clay minerals is effectively trapped below the OMZ and removed from the nutrient cycle.
The $TPO_4$ fluxes are not distributed like the dissolved Fe fluxes indicating different control mechanisms (Noffke et al., 2012). Phosphate fluxes could be generated by different sedimentary sources such as organic matter, Fe bound P and fish debris (Noffke et al., 2012 and references therein). The measured fluxes where highest on the shelf and the upper slope at 11°S. Further downslope (below 500-600 m water depth) the fluxes decrease rapidly with increasing bottom water oxygen concentration. Again, the measured fluxes are clearly elevated compared to other oxygen depleted regions (McManus et al, 1997; Hartnett and Devol, 2003; Woulds et al, 2009). The high $TPO_4$ fluxes, observed on the shelf and in the core of the OMZ, could not be explained by organic matter degradation where P is preferentially released over organic carbon (Noffke et al., 2014). The results of a mass balance approach suggest that the P release is driven by authigenic Ca-P minerals rather than from organic and terrigenous P input (Noffke, 2014). Furthermore, the mass balance approach revealed that about 80% of the P supplied to the OMZ is recycled through the surface sediments back into the water column (Noffke, 2014). Therefore, sediments overlain by oxygen deficient bottom water provide an important source for bioavailable P and highlight the importance of further examining the elemental cycling in OMZs.

## 1.6 Focus of research in this study

This study addresses open questions concerning benthic P and Fe cycling in oxygen deficient waters. The research areas are the Peruvian OMZ and the Mauritanian Upwelling.

The main research questions are:

1. What are the P sources to maintain benthic P release in the Peruvian OMZ?

The focus of the first part of this study is the identification of P sources for benthic P release in the core of the Peruvian OMZ. A mass balance including the rain rate of organic and inorganic P from the water column, the P release from the sediments and the P burial is presented. In addition, the fate of P cycling is highlighted in detail by new analysis approaches for water column particles and sediments.

2. What is the magnitude of benthic P and Fe release in suboxic waters off Mauritania and how could the nutrient release evolve in the case of further deoxygenation?

In the second part of this study, the first P and Fe fluxes and geochemical water column and sediment data from the Mauritanian Upwelling are presented. The controlling parameters on the nutrient release are deciphered and compared to results from the Peruvian OMZ. Furthermore, deoxygenation experiments emphasize the potential for enhanced nutrient release in case of progressive oxygen loss in the Mauritanian Upwelling.

3. Are iron enrichments found at the lower boundary of the OMZ at 11°S a widespread feature off South America and in which mineral phases is the iron trapped?

The third part aims to map iron enrichments at the lower boundary of the OMZ off South America. Furthermore, Fe specifications and mineral compositions are derived in order to characterize the sedimentary Fe sink and its reactivity.

## 1.7 References

Anderson, B. S., J. W. Hunt, B. M. Phillips, R. Fairey, H. M. Puckett, M. Stephenson, K. Taberski, J. Newman, and R. S. Tjeerdema (2001), Influence of sample manipulation on contaminant flux and toxicity at the sediment–water interface, Marine Environmental Research, 51(3), 191-211.

Arning, E. T., D. Birgel, B. Brunner, and J. Peckmann (2009), Bacterial formation of phosphatic laminites off Peru, Geobiology, 7(3), 295-307.

Benitez-Nelson, C. R., L. O'Neill, L. C. Kolowith, P. Pellechia, and R. Thunell (2004), Phosphonates and particulate organic phosphorus cycling in an anoxic marine basin, Limnol. Ocean., 49(5), 1593-1604.

Benitez-Nelson, C. R., L. P. O'Neill Madden, R. M. Styles, R. C. Thunell, and Y. Astor (2007), Inorganic and organic sinking particulate phosphorus fluxes across the oxic/anoxic water column of Cariaco Basin, Venezuela, Marine Chemistry, 105(1–2), 90-100.

Boyd, P. W. (2009), Ocean iron cycle, in Surface Ocean—Lower Atmosphere Processes, edited, pp. 161-179, AGU, Washington, DC.

Boyd, P. W., and M. J. Ellwood (2010), The biogeochemical cycle of iron in the ocean, Nature Geosci, 3(10), 675-682.

Buesseler, K. O., J. E. Andrews, S. M. Pike, and M. A. Charette (2004), The Effects of Iron Fertilization on Carbon Sequestration in the Southern Ocean, Science, 304(5669), 414-417.

Burdige, D. J. (1993), The biogeochemistry of manganese and iron reduction in marine sediments, Earth-Science Reviews, 35(3), 249-284.

Coale, K. H., et al. (1996), A massive phytoplankton bloom induced by an ecosystem-scale iron fertilization experiment in the equatorial Pacific Ocean, Nature, 383(6600), 495-501.

Colman, A. S., and H. D. Holland (2000), The global diagenetic flux of phosphorus from marine sediments to the oceans: redox sensitivity and the control of atmospheric oxygen levels, in Marine Authigenesis: From Global to Microbial, edited, pp. 53-75, SEPM (Society for Sedimentary Geology).

Compton, J., D. Mallinson, C. Glenn, G. Filipelli, K. Föllmi, G. Shields, and Y. Zanin (2000), Variations in the global phosphorus cycle, in Marine authigenesis: from global to microbial, edited by C. Glenn, P.-L. L. and L. J., pp. 21-33, SEPM (Society for Sedimentary Geology)

Cosmidis, J., K. Benzerara, N. Menguy, and E. Arning (2013), Microscopy evidence of bacterial microfossils in phosphorite crusts of the Peruvian shelf: Implications for phosphogenesis mechanisms, Chemical Geology, 359, 10-22.

Dale, A. W., V. J. Bertics, T. Treude, S. Sommer, and K. Wallmann (2013), Modeling benthic–pelagic nutrient exchange processes and porewater distributions in a seasonally hypoxic sediment: evidence for massive phosphate release by *Beggiatoa*?, Biogeosciences, 10(2), 629-651.

de Baar, H. J. W., and J. T. M. de Jong (2001), Distributions, sources and sinks of iron in seawater, in The biogeochemistry of iron in seawater, edited by T. D. and H. A., pp. 123-253, IUPAC Series on Analytical and Physical Chemistry of Environmental Systems, Chichester.

Delaney, M. L. (1998), Phosphorus accumulation in marine sediments and the oceanic phosphorus cycle, Global Biogeochemical Cycles, 12(4), 563-572.

Dyhrman, S. T., J. W. Ammerman, and B. A. S. Van Mooy (2007), Microbes and the marine phosphorus cycle, Oceanography, 20(2).

Ekman, W. (1905), On the Influence of the Earth's Rotation on Ocean-Currents, Arkic För Matematik, Astronomi och Physik, 2(11), 1-51.

Elrod, V. A., W. M. Berelson, K. H. Coale, and K. S. Johnson (2004), The flux of iron from continental shelf sediments: A missing source for global budgets, Geophysical Research Letters, 31(12).

Faul, K. L., A. Paytan, and M. L. Delaney (2005), Phosphorus distribution in sinking oceanic particulate matter, Marine Chemistry, 97(3–4), 307-333.

Filippelli, G. M. (2002), The global phosphorus cycle, in Phosphates: Geochemical, Geobiological, and Materials Importance, edited by M. Kohn, J. Rakovan and J. Hughes, pp. 391-425, Reviews in Mineralogy&Geochemistry.

Filippelli, G. M. (2008), The Global Phosphorus Cycle: Past, Present, and Future, Elements, 4(2), 89-95.

Föllmi, K. B. (1996), The phosphorus cycle, phosphogenesis and marine phosphate-rich deposits, Earth-Science Reviews, 40(1–2), 55-124.

Froelich, P. N., G. P. Klinkhammer, M. L. Bender, N. A. Luedtke, G. R. Heath, D. Cullen, P. Dauphin, D. Hammond, B. Hartman, and V. Maynard (1979), Early oxidation of organic matter in

pelagic sediments of the eastern equatorial Atlantic: suboxic diagenesis, Geochimica et Cosmochimica Acta, 43(7), 1075-1090.

Fuenzalida, R., W. Schneider, J. Garcés-Vargas, L. Bravo, and C. Lange (2009), Vertical and horizontal extension of the oxygen minimum zone in the eastern South Pacific Ocean, Deep Sea Research Part II: Topical Studies in Oceanography, 56(16), 992-1003.

Goldhammer, T., V. Bruchert, T. G. Ferdelman, and M. Zabel (2010), Microbial sequestration of phosphorus in anoxic upwelling sediments, Nature Geoscience, 3(8), 557-561.

Haese, R. R. (2006), The Biogeochemistry of Iron, in Marine Geochemistry (2nd edition), edited by H. D. Schulz and M. Zabel, pp. 241-270, Springer-Verlag Heidelberg, New York.

Hartnett, H. E., and A. H. Devol (2003), Role of a strong oxygen-deficient zone in the preservation and degradation of organic matter: a carbon budget for the continental margins of northwest Mexico and Washington State, Geochimica et Cosmochimica Acta, 67(2), 247-264.

Helly, J. J., and L. A. Levin (2004), Global distribution of naturally occurring marine hypoxia on continental margins, Deep Sea Research Part I: Oceanographic Research Papers, 51(9), 1159-1168.

Ingall, E., and R. Jahnke (1994), Evidence for enhanced phosphorus regeneration from marine sediments overlain by oxygen depleted waters, Geochimica et Cosmochimica Acta, 58(11), 2571-2575.

Jickells, T. D., An, Z.S., Andersen, K. K., Baker, A. R., Bergametti, G., Brooks, N., Cao, J. J., Boyd, P. W., Duce, R. A., Hunter, K. A., Kawahata, H., Kubilay, N., LaRoche, J., Liss, P. S., Mahowald, N., Prosperso, J. M., Ridgwell, A. J., Tegen, I., and Torres, R. (2005), Global Iron Connections Between Desert Dust, Ocean Biogeochemistry, and Climate, Science, 308(5718), 67-71.

Kamykowski, D., and S.-J. Zentara (1990), Hypoxia in the world ocean as recorded in the historical data set, Deep Sea Research Part A. Oceanographic Research Papers, 37(12), 1861-1874.

Konhauser, K. O., A. Kappler, and E. E. Roden (2011), Iron in microbial metabolisms, Elements, 7(2), 89-93.

Kraal, P., C. P. Slomp, D. C. Reed, G.-J. Reichart, and S. W. Poulton (2012), Sedimentary phosphorus and iron cycling in and below the oxygen minimum zone of the northern Arabian Sea, Biogeosciences, 9(7), 2603-2624.

Lyons, G., C. R. Benitez-Nelson, and R. C. Thunell (2011), Phosphorus composition of sinking particles in the Guaymas Basin, Gulf of California, Limnology and Oceanography, 56(3), 1093-1105.

Martin, J. H., R. M. Gordon, and S. E. Fitzwater (1991), The case for iron, Limnol. Oceanogr., 36(8), 1793-1802.

Martin, J. H., et al. (1994), Testing the iron hypothesis in ecosystems of the equatorial Pacific Ocean, Nature, 371(6493), 123-129.

McManus, J., W. M. Berelson, K. H. Coale, K. S. Johnson, and T. E. Kilgore (1997), Phosphorus regeneration in continental margin sediments, Geochimica et Cosmochimica Acta, 61(14), 2891-2907.

Noffke A., Hensen C., Sommer S., S. F., Bohlen L., Mosch T., Graco M., and Wallmann K. (2012), Title Benthic iron and phosphorus fluxes across the Peruvian oxygen minimum zone, Limnology and Oceanography, 57(3), 851-867.

Noffke A.: Phosphorus cycling in anoxic sediments, PhD dissertation, University of Kiel, 2014.

Oguz, T., H. W. Ducklow, and P. Malanotte-Rizzoli (2000), Modeling distinct vertical biogeochemical structure of the Black Sea: Dynamical coupling of the oxic, suboxic, and anoxic layers, Global Biogeochem. Cycles, 14(4), 1331-1352.

Pakhomova, S. V., P. O. J. Hall, M. Y. Kononets, A. G. Rozanov, A. Tengberg, and A. V. Vershinin (2007), Fluxes of iron and manganese across the sediment–water interface under various redox conditions, Marine Chemistry, 107(3), 319-331.

Paulmier, A., and D. Ruiz-Pino (2009), Oxygen minimum zones (OMZs) in the modern ocean, Progress In Oceanography, 80(3–4), 113-128.

Paulmier, A., D. Ruiz-Pino, V. Garçon, and L. Farías (2006), Maintaining of the Eastern South Pacific Oxygen Minimum Zone (OMZ) off Chile, Geophys. Res. Lett., 33(20), L20601.

Paytan, A., and K. McLaughlin (2007), The Oceanic Phosphorus Cycle, Chemical Reviews, 107(2), 563-576.

Raiswell, R. (2011), Iron Transport from the Continents to the Open Ocean: The Aging–Rejuvenation Cycle, Elements, 7(2), 101-106.

Raiswell, R., and D. E. Canfield (2012), The iron biogeochemical cycle Past and Present, Geochemical Perspectives, 1(1), 1-232.

Raiswell, R., F. Buckley, R. A. Berner, and T. F. Anderson (1988), The degree of pyritization of iron as a paleoenvironmental indicator of bottom-water oxygenation, Journal of Sedimentary Research, 58, 812-819.

Redfield, A. C., B. H. Ketchum, and F. A. Richards (1963), The influence of organisms on the composition of seawater, in The Sea, edited by N. M. Hill, pp. 26-77, Academic Press, London.

Roth, R., S. P. Ritz, and F. Joos (2014), Burial-nutrient feedbacks amplify the sensitivity of atmospheric carbon dioxide to changes in organic matter remineralisation, Earth Syst. Dynam., 5(2), 321-343.

Ruttenberg, K. C. (1992), Development of a swquential extraction method for different forms of phosphorus in marine sediments, Limnol. Ocean., 37(7), 1460-1482.

Ruttenberg, K. C. (2014), 10.13 - The Global Phosphorus Cycle, in Treatise on Geochemistry (Second Edition), edited by H. D. H. K. Turekian, pp. 499-558, Elsevier, Oxford.

Ruttenberg, K. C., and R. A. Berner (1993), Authigenic apatite formation and burial in sediments from non-upwelling, continental margin environments, Geochimica et Cosmochimica Acta, 57(5), 991-1007.

Scholz, F., C. Hensen, A. Noffke, A. Rohde, V. Liebetrau, and K. Wallmann (2011), Early diagenesis of redox-sensitive trace metals in the Peru upwelling area – response to ENSO-related oxygen fluctuations in the water column, Geochimica et Cosmochimica Acta, 75(22), 7257-7276.

Scholz, F., J. McManus, A. C. Mix, C. Hensen, and R. R. Schneider (2014a), The impact of ocean deoxygenation on iron release from continental margin sediments, Nature Geosci, 7(6), 433-437.

Scholz, F., S. Severmann, J. McManus, A. Noffke, U. Lomnitz, and C. Hensen (2014b), On the isotope composition of reactive iron in marine sediments: Redox shuttle versus early diagenesis, Chemical Geology, 389(0), 48-59.

Scholz, F., et al. (2016), Nitrate-dependent iron oxidation limits iron transport in anoxic ocean regions, Earth and Planetary Science Letters, 454, 272-281.

Schulz, H. N., and H. D. Schulz (2005), Large Sulfur Bacteria and the Formation of Phosphorite, Science, 307(5708), 416-418.

Sekula-Wood, E., C. R. Benitez-Nelson, M. A. Bennett, and R. Thunell (2012), Magnitude and composition of sinking particulate phosphorus fluxes in Santa Barbara Basin, California, Global Biogeochemical Cycles, 26(2), GB2023.

Severmann, S., C. M. Johnson, B. L. Beard, and J. McManus (2006), The effect of early diagenesis on the Fe isotope compositions of porewaters and authigenic minerals in continental margin sediments, Geochimica et Cosmochimica Acta, 70(8), 2006-2022.

Severmann, S., J. McManus, W. M. Berelson, and D. E. Hammond (2010), The continental shelf benthic iron flux and its isotope composition, Geochimica et Cosmochimica Acta, 74(14), 3984-4004.

Slomp, C. P., and P. Van Cappellen (2004), Nutrient inputs to the coastal ocean through submarine groundwater discharge: controls and potential impact, Journal of Hydrology, 295(1–4), 64-86.

Slomp, C. P., and P. Van Cappellen (2007), The global marine phosphorus cycle: sensitivity to oceanic circulation, Biogeosciences, 4(2), 155-171.

Steenbergh, A. K., P. L. E. Bodelier, H. L. Hoogveld, C. P. Slomp, and H. J. Laanbroek (2001), Phosphatases relieve carbon limitation of microbial activity in Baltic Sea sediments along a redox-gradient, Limnol. Oceanogr., 56(6), 2018-2026.

Stramma, L., G. C. Johnson, J. Sprintall, and V. Mohrholz (2008), Expanding Oxygen-Minimum Zones in the Tropical Oceans, Science, 320(5876), 655-658.

Suess, E., and R. von Huene (1988), Ocean Drilling Program Leg 112, Peru continental margin: Part 2, Sedimentary history and diagenesis in a coastal upwelling environment, Geology, 16(10), 939-943.

Sunda, W. G. (2001), Bioavailability and Bioaccumulation of Iron in the Sea, in The biogeochemistry of iron in seawater, edited by T. D. and H. A., pp. 41-84, IUPAC Series on Analytical and Physical Chemistry of Environmental Systems, Chichester.

Sundby, B., L. G. Anderson, P. O. J. Hall, Å. Iverfeldt, M. M. R. van der Loeff, and S. F. G. Westerlund (1986), The effect of oxygen on release and uptake of cobalt, manganese, iron and phosphate at the sediment-water interface, Geochimica et Cosmochimica Acta, 50(6), 1281-1288.

Taylor, K. G., and J. H. S. Macquaker (2011), Iron Minerals in Marine Sediments Record Chemical Environments, Elements, 7(2), 113-118.

Tortell, P. D., M. T. Maldonado, J. Granger, and N. M. Price (1999), Marine bacteria and biogeochemical cycling of iron in the oceans, FEMS Microbiology Ecology, 29(1), 1-11.

Tribovillard, N., T. J. Algeo, T. Lyons, and A. Riboulleau (2006), Trace metals as paleoredox and paleoproductivity proxies: An update, Chemical Geology, 232(1–2), 12-32.

Tsandev, I., D. C. Reed, and C. P. Slomp (2012), Phosphorus diagenesis in deep-sea sediments: Sensitivity to water column conditions and global scale implications, Chemical Geology, 330–331(0), 127-139.

Ulloa, O., and S. Pantoja (2009), The oxygen minimum zone of the eastern South Pacific, Deep Sea Research Part II: Topical Studies in Oceanography, 56(16), 987-991.

Van Cappellen, P., and E. D. Ingall (1994), Benthic phosphorus regeneration, net primary production, and ocean anoxia: A model of the coupled marine biogeochemical cycles of carbon and phosphorus, Paleoceanography, 9(5), 677-692.

Veeh, H. H., W. C. Burnett, and A. Soutar (1973), Contemporary Phosphorites on the Continental Margin of Peru, Science, 181(4102), 844-845.

Wallmann, K. (2003) Feedbacks between oceanic redox states and marine productivity: A model perspective focused on benthic phosphorus cycling, Global Biogeochemical Cycles, 17(3).

Wallmann, K. (2010) Phosphorus imbalance in the global ocean?, Global Biogeochemical Cycles, 24(4).

Woulds, C., J. H. Andersson, G. L. Cowie, J. J. Middelburg, and L. A. Levin (2009), The short-term fate of organic carbon in marine sediments: Comparing the Pakistan margin to other regions, Deep Sea Research Part II: Topical Studies in Oceanography, 56(6–7), 393-402.

Wyrtki, K. (1962), The oxygen minima in relation to ocean circulation, Deep Sea Research and Oceanographic Abstracts, 9(1–2), 11-23.

# 2 Benthic phosphorus cycling in the Peruvian Oxygen Minimum Zone

**U. Lomnitz[1], S. Sommer[1], A. W. Dale[1], C. R. Löscher[1], A. Noffke[2], K. Wallmann[1] and C. Hensen[1]**

(1){GEOMAR Helmholtz Centre for Ocean Research Kiel, Wischhofstr. 1–3, 24148 Kiel, Germany}

(2){Institut für Seenforschung (ISF) der LUBW, Argenweg 50/1, 88085 Langenargen, Germany}

Correspondence to: U. Lomnitz (ulomnitz@geomar.de)

Published in 2016 in Biogeosciences **13**: 1367-1386

## Abstract

Oxygen minimum zones (OMZs) that impinge on continental margins favor the release of phosphorus (P) from the sediments to the water column, enhancing primary productivity and the maintenance or expansion of low-oxygen waters. A comprehensive field program in the Peruvian OMZ was undertaken to identify the sources of benthic P at six stations, including the analysis of particles from the water column, surface sediments and pore fluids as well as in situ benthic flux measurements. A major fraction of solid phase P was bound as particulate inorganic P (PIP) both in the water column and in sediments. Sedimentary PIP increased with depth in the sediment at the expense of particulate organic P (POP). The ratio of particulate organic carbon (POC) to POP exceeded the Redfield ratio both in the water column (202 ± 29) and in surface sediments (303 ± 77). However, the POC to total particulate P (TPP = POP + PIP) ratio was close to Redfield in the water column (103 ± 9) and in sediment samples (102 ± 15 This suggests that the relative burial efficiencies of POC and TPP are similar under low oxygen conditions and that the sediments underlying the anoxic waters on the Peru margin are not depleted in P compared to Redfield. Benthic fluxes of dissolved P were extremely high (up to 1.04 ± 0.31 mmol $m^{-2}$ $d^{-1}$), however, showing that a lack of oxygen promotes the intensified release of dissolved P from sediments, whilst preserving the POC/TPP burial ratio. Benthic dissolved P fluxes were always higher than the TPP rain rate to the seabed, which is proposed to be caused by transient P release by bacterial mats that had stored P during previous periods when bottom waters were less reducing. At one station located at the lower rim of the OMZ, dissolved P was taken up by the sediments indicating ongoing phosphorite formation. This is further supported by decreasing porewater phosphate concentrations with sediment depth, whereas solid phase P concentrations were comparatively high. At this site, the POC/TPP and POC/PIP ratios dropped from average water-column values (close to Redfield for POC/TPP and POC/PIP ~250) to very low sedimentary ratios of ~ 7 (POC/TPP and POC/PIP), indicative of intensive P enrichment in the sediments.

## 2.1 Introduction

Phosphorus is an essential nutrient; it serves as an energy carrier for all living species and is a limiting macronutrient for marine primary production on geological time scales (Ingall and Jahnke, 1994; Föllmi, 1996; McManus et al., 1997; Filippelli, 2002; Paytan and McLaughlin, 2007; Tsandev et al., 2012; Ruttenberg, 2014). Due to its impact on marine primary production, the oceanic phosphorus inventory modulates the atmospheric $CO_2$ level and Earth's climate (Ganeshram et al., 2002; Wallmann, 2003; Ingall, 2010). Hence, it is crucial to understand feedback mechanisms of the P cycle to make future predictions.

Particulate and dissolved phosphorus in the ocean originate from terrestrial chemical weathering of the P containing mineral group of apatite (Filippelli, 2002). Only around 30% of the P discharged to the oceans is potentially bioavailable (Compton et al., 2000) as dissolved P, inorganic P adsorbed minerals or associated with metal oxides and P bound within particulate organic matter. However, the largest fraction of the fluvial P is trapped in estuaries or buried in continental margin sediments and thereby removed from the P cycle before it reaches the open ocean (Compton et al., 2000). The delivery of P to the sediments in the open ocean is mainly composed of organic and inorganic P associated with the export of organic detritus and other particles from the photic zone. P adsorbed to minerals such as Mn and Fe (oxyhydr)oxides (Föllmi, 1996; Delany, 1998; Faul et al., 2005) are further sources, as well as P input from fish debris that could be particularly important in productive upwelling regions (Suess, 1981; Schenau and DeLange, 2001; Dìaz-Ochoa et al., 2009; Noffke, 2014).

P cycling is strongly affected by redox-dependent processes. P can be scavenged by Fe (oxyhydr)oxides in oxic sediment and released across the sediment-water interface due to the reduction dissolution of Fe (oxyhydr)oxides in anoxic sediments (Sundby et al., 1986; Slomp et al., 1998). Furthermore, recent studies showed that sulfur bacteria found in surface sediments of anoxic environments can internally store and release P under oscillating redox conditions (Ingall and Jahnke, 1997 and references therein). Therefore, these organisms are a key player for the modulation of porewater P concentrations and benthic P release to the water column.

Additionally, hypoxic or anoxic conditions favor the precipitation of P in the form of authigenic carbonate fluorapatie (CFA) (Froelich et al., 1988; Suess and von Huene, 1988; Goldhammer et al., 2010; Ingall, 2010; Schenau and De Lange, 2000). For non-upwelling areas, the required phosphate oversaturation in the porewaters has been attributed to the reductive dissolution of P bearing Fe (oxyhydr)oxides (e.g. Ruttenberg and Berner, 1993, Slomp et al., 1996). In contrast, the CFA formation in sediments of the Namibian upwelling area was linked to microbial P release into the porewaters (Schulz and Schulz, 2005).

The resulting feedback on oceanic primary production and atmospheric $O_2$ and $CO_2$ levels triggered by changes in benthic P sequestration is still unclear. Presently, three opposing have been raised: (1) Intensified phosphate release from the sediments to the water column caused by an expansion of low oxygen waters (Ingall and Jahnke, 1994; Stramma et al., 2008) could stimulate the primary production in the surface waters (Wallmann, 2003). This, in turn, may lead to a more intensified oxygen demand and a positive feedback with benthic P release (Slomp and Van Cappellen, 2007; Wallmann, 2010; Moffit et al., 2015). (2) A negative feedback on P release has been postulated based on observations of CFA mineral precipitation found in the present-day

oxygen depleted upwelling areas (Schulz and Schulz, 2005; Arning et al., 2009a; Arning et al., 2009b; Goldhammer et al., 2010; Cosmidis et al., 2013). Being a major sink for bioavailable P (Delaney, 1998; Ingall, 2010), it has been argued that the expansion of OMZs may increase the CFA precipitation in the sediments and thus mitigate the benthic phosphate release (Ganeshram et al., 2002; Goldhammer et al., 2010; Ingall, 2010). (3) A third scenario suggests that the formation of CFA is in balance with enhanced P release from anoxic sediments, implying that the dissolved oceanic P inventory is largely unaffected by oxygen concentrations (Delaney, 1998; Anderson et al., 2001; Roth et al., 2014). These conflicting scenarios show that there is further need to explore the benthic-pelagic P cycling in oxygen deficient environments in order to enable improved predictions.

In this study, we explore P cycling in the Peruvian OMZ to identify and quantify P sources to the sediment and the return of inorganic dissolved P back to the water column. Our data set comprises samples of particulate matter from the water column as well as porewater, sediment samples and samples of filamentous sulfur bacteria. We present in situ benthic phosphate fluxes, particulate matter C/P ratios for water-column particles and surface sediments and P burial fluxes, and relative abundances of sulfur bacteria for 6 stations along the depth transect across the Peruvian shelf at 12°S. From a mass balance for P cycling in the sediments, we conclude that the benthic P sources and sinks were, in general, imbalanced during our sampling campaign.

## 2.2 Study Area

The study area is located in the center of the Peruvian OMZ at 12°S covering the shallow shelf from ~70 m water depth to mid-slope depths of about at ~400 m (Fig. 2.1). During our sampling campaign in January 2013 neutral or slightly negative El Niño-Southern Oscillation (ENSO) conditions dominated (http://www.cpc.ncep.noaa.gov) and the bottom water oxygen concentrations were below detection limit of the Winkler titration (5 µmol $L^{-1}$) down to ~ 450 m water depth (Fig. 2.1, Table 2.1). Below the OMZ, oxygen concentrations increased to 19 and 53µM at 770 m and 1025 m water depth, respectively. Nitrate concentrations were below 12 µM from 128 to 407 m water depth (Table 2.1). During the measuring period, the bottom water at station I (74 m) was sulfidic and depleted in nitrate (Table 2.1; Sommer et al., 2016).

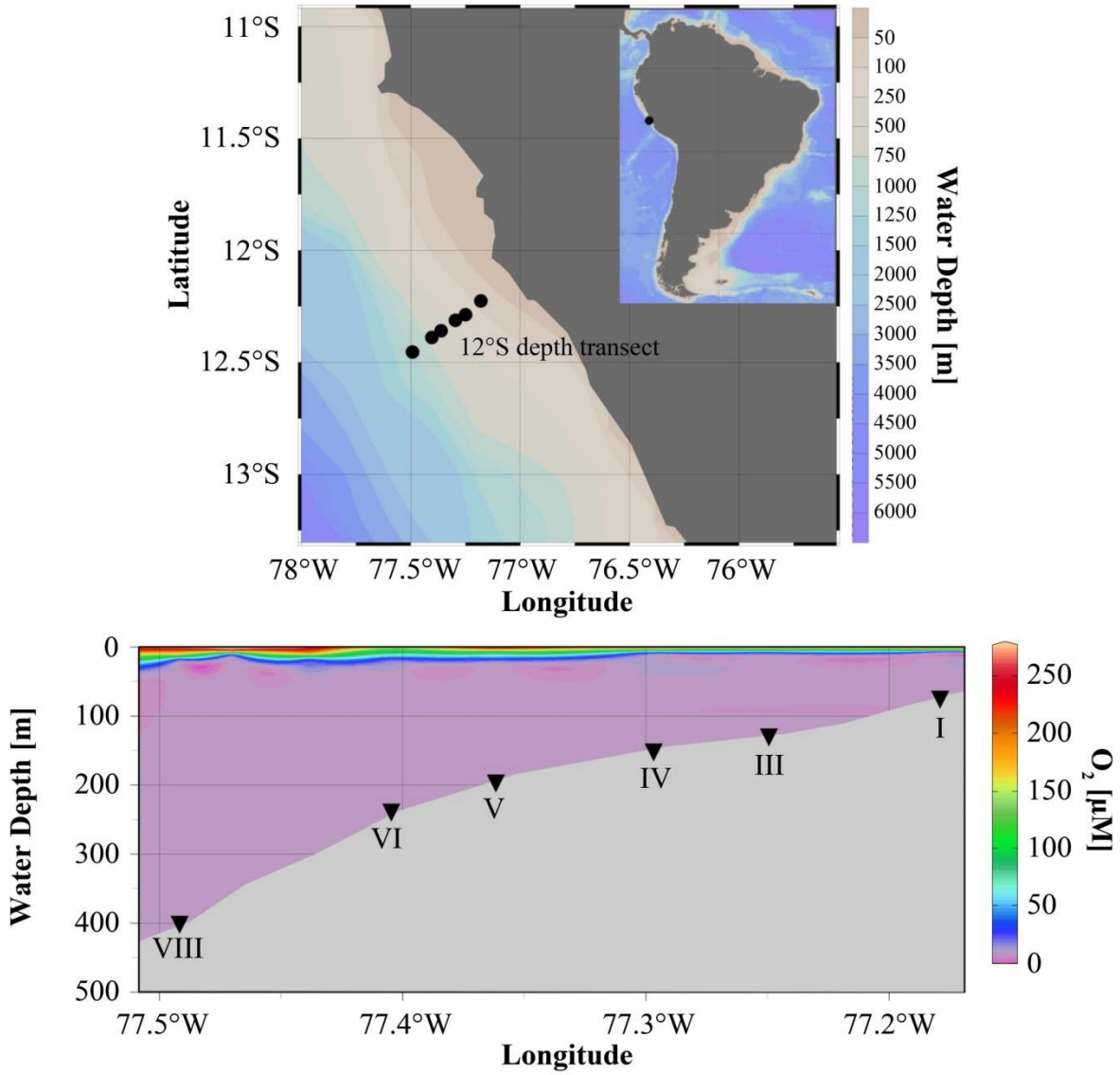


**Fig. 2.1** Study area, sampling stations and $O_2$ concentration in µM along the 12°S transect.

The oxygen deficient waters off Peru belong to one of the world's most prominent OMZ. Southeasterly trade winds that are driven by the Pacific Subtropical Anticyclone engender offshore transport of surface waters and upwelling of subsurface waters from the poleward propagating Peru undercurrent (PUC) (Strub et al., 1998). These water masses are oxygen depleted and rich in nutrients, favoring primary production of up to 3.6 g C $m^{-2}$ $d^{-1}$ in surface waters (Pennington et al., 2006). As a consequence, the intense oxygen consumption induced by the degradation of sinking particulate organic matter and a sluggish ventilation induce the development of a strong OMZ. Based on the definition that the oxycline of an OMZ is at ~22 µM (Fuenzalida et al., 2009), the Peruvian OMZ extends from approximately 50 – 700 m water depth. The greatest upwelling strength is reached during austral winter and spring between 5 and 15°S (Strub et al., 1998). The phases of strong upwelling are followed by high rates of primary

production in austral summer. The coastal area off Peru displays a highly variable hydrographic regime. Especially during positive ENSO periods coastal trapped waves emerging from equatorial Kelvin waves in the equatorial East Pacific occur frequently (Gutiérrez et al., 2008 and references therein; Mosch et al., 2012). Consequently, the thermocline and the oxycline shift downwards by ca. 100 m and bottom-water oxygen concentrations can increase from practically zero to around 100 µM in days to weeks (Gutiérrez et al., 2008; Schunck et al., 2013; Graco et al., 2016). Seasonally, bottom waters of the shelf (75 m) can transition from oxic or hypoxic between austral winter/spring (low primary production) to anoxic throughout the rest of the year (Noffke et al., 2012). Furthermore, porewater uranium (U) profiles at 11°S indicate variable redox conditions at the upper rim of the OMZ (Scholz et al., 2011). The shelf area above 200m water depth is therefore characterized by non-steady state conditions, whereas the oxygen concentrations in the core OMZ (~200-400 m water depth) are predominantly below detection limit throughout the year.

The sediments of the Peruvian OMZ have POC contents ranging from 15-20 wt. % within the OMZ and > 5 wt. % below the OMZ and on the shelf(Dale et al., 2015). The fine-grained, diatomaceous mud lens between 11°S and 15°S accumulates under low PUC bottom-water velocities in 50 to 500 m water depth (Krissek et al., 1980). This favors high sedimentation rates, carbon preservation and burial (Suess et al., 1987; Dale et al., 2015). Further down, at mid-slope depth, a high energy regime favoring erosive settings leads to the formation of phosphorites (Reimers and Suess, 1983; Glenn and Arthur, 1988; Arning et al., 2009b; Mosch et al., 2012). Another interesting observation between 70 and ˜ 300 m of water depth is the occurrence of mat-forming filamentous sulfur bacteria (Mosch et al., 2012). Bacterial mats are not conspicuous below below 300 to 400 m water depth, and instead foraminiferal sands are more common.

**Table 2.1** Station list for the sites of the benthic lander (BIGO), multi-corer (MUC) and CTD deployments including the bottom water concentrations of oxygen ($O_2$), nitrate ($NO_3^-$) and sulfide ($H_2S$) in µM. The station numbers were according to Dale et al., 2015. bdl=below detection limit (5 µM)

| Nr. | Station | Gear | Date (2013) | Longitude (°W) | Latitude (°S) | Water depth (m) | BW $O_2$ (µM) | BW $NO_3^-$ (µM) | BW $H_2S$ (µM) |
|---|---|---|---|---|---|---|---|---|---|
| | 98 | CTD26 | 14.01. | 12°13.504’ | 77°10.799’ | 75 | | | |
| I | 220 | MUC39 | 25.01. | 12°13.531’ | 77°10.061’ | 72 | bdl | - | 33.22 |
| | 110 | BIGO1-2 | 15.01. | 12°13.506’ | 77°10.793’ | 74 | | | |
| | 269 | CTD79 | 29.01. | 12°16.690’ | 77°14.999’ | 128 | | | |
| III | 248 | MUC46 | 27.01. | 12°16.697’ | 77°15.001’ | 129 | bld | 0.02 | - |
| | 165 | BIGO2-4 | 20.01. | 12°16.690’ | 77°14.995’ | 128 | | | |
| | 111 | CTD29 | 15.01. | 12°18.729’ | 77°17.757’ | 145 | | | |
| IV | 36 | MUC10 | 09.01. | 12°18.708’ | 77°17.794 | 145 | bdl | 7.1 | |
| | 57 | BIGO1-1 | 11.01. | 12°18.711’ | 77°17.803’ | 141 | | | |
| | 279 | CTD81 | 30.01. | 12°21.490’ | 77°21.713’ | 195 | | | |
| V | 247 | MUC45 | 27.01. | 12°21.491’ | 77°21.702’ | 195 | bdl | 6.3 | - |
| | 201 | BIGO1-4 | 23.01. | 12°21.502’ | 77°21.712’ | 195 | | | |
| | 92 | CTD24 | 13.01. | 12°23.300’ | 77°24.200’ | 244 | | | |
| VI | 198 | MUC34 | 23.01. | 12°23.300’ | 77°24.228’ | 244 | bdl | 11.9 | - |
| | 74 | BIGO2-2 | 12.01. | 12°23.300’ | 77°24.186’ | 244 | | | |
| | 66 | CTD16 | 12.01. | 12°27.535’ | 77°29.593 | 414 | | | |
| VIII | 107 | MUC23 | 15.01. | 12°27.198’ | 77°29.497’ | 407 | bdl | 12.1 | - |
| | 207 | BIGO2-5 | 24.01. | 12°27.207' | 77°29.517' | 409 | | | |

## 2.3 Methods

Sampling of water-column particulate matter and sediment cores as well as the deployment of the benthic landers BIGO I and II (Biogeochemical Observatories) were conducted along the 12°S depth transect during the RV *Meteor* cruise M92 in January 2013. The geographical position and water-column properties for the main stations are reported in Table 2.1. The data set on in situ phosphate fluxes comprised 10 stations from 74 to 989 m water depth. The water-column particle sampling was performed at 6 stations from 74 to 407 m water depth. These stations are considered as main stations and for consistency the stations are numbered according to the data set published in Dale et al. (2015). Hydrographic parameters and oxygen concentrations were obtained by deploying a CTD/rosette equipped with a Seabird oxygen sensor (detection limit is 5 µM) calibrated by Winkler titration.

### 2.3.1 Water-column particles

Particulate matter was filtered using water from Niskin bottles from the CTD/rosette and analyzed for total particulate phosphorus (TPP), particulate inorganic phosphorus (PIP) and particulate

organic carbon (POC) concentrations. Following Labry et al. (2013), we expect the PIP phase to be comprised of inorganic P phases originating from abiotic particulate P as well as inorganic P from biogenic particulate P. Abiotic PIP comprises detrital P associated to minerals from terrigenous sources. Biotic PIP is composed of orthophosphates, pyrophosphates and polyphosphates within eukaryotic and prokaryotic cells.

Between three and six water depths were sampled per station. The water was filled into 10 L PE containers rinsed beforehand with ultrapure water (MilliQ). The containers were shaken before filtration which was performed within 24 h after sample retrieval. Approximately 2 to 4 L of seawater were filtered through pre-weighed and combusted (450°C, 5h) 0.7 µM Whatman GF/F filter using a seawater vacuum pump and Duran bottle top filters. After filtration, all filters were immediately frozen at -20°C. At the shore-based laboratory the GF/F filters were dried over night at 45°C, and divided into 3 equally sized pieces using a scalpel. The total filtered water volume was divided by three to calculate elemental concentrations on each filter section assuming homogenous coverage of particles on the filters.

### 2.3.2 Total particulate phosphorus (TPP), particulate inorganic phosphorus (PIP) and particulate organic phosphorus (POP)

The determination of TPP and PIP concentrations by combustion and colorimetric methods has been described by Asahi et al. (2014), Aspila et al. (1976), Loh and Bauer (2000) and others. However, the combustion and acid dissolution (HTC/hydrolysis) that has been applied for PIP-determination is limited by the fact that polyphosphates are only partly hydrolysed, but provides the best compromise compared to other methods (Labry et al., 2013). Although polyphosphates are underestimated, it includes intracellular P that is often dominant in plankton and only small amounts of organic P. In the case of TPP we used the Aspila (1976) method without an oxidant (e.g. $MgSO_4$) during combustion, which underestimates the TPP concentration in water-column particles. However, for the sediments, the results following of the Aspila (1976) method were compared total digestions showing an average recovery of the Aspila method of approximately 102%. In two samples we found an overestimation in total digestion of more than 100% and in one sample an underestimation of 32%, possibly due to heterogeneity of the samples caused by very small phosphorite granules.

Filter segments for TPP concentration were combusted at 550°C for 90 min and afterwards soaked with 20 ml 1 N hydrochloric acid (HCl) and shaken for 24 h at room temperature. Then, the solution was filtered and 0.35 ml triple reagent (40 ml 9.8 N sulfuric acid, 12 ml ammonium molybdate and 4 ml potassium antimonyl tartrate solution) and 0.175 ml ascorbic acid and 3 ml 1 N HCl were added to 3.75 ml of the sample solution. Then, 0.3 ml of 12.5 N sodium hydroxide

(NaOH) was added to the solution before colorimetric measurement of phosphate at 880 nm using a Hitachi U-2001 photospectrometer. This was done because test runs with the standard series revealed that the slope of the calibration curve was not steep enough to measure the low phosphate concentrations expected. To resolve this issue, the pH of the solution was slightly increased usingg NaOH. Measurements were accompanied using a standard series consisting of 8 standards ranging from 5 to 100 µM $PO_4^{3-}$, prepared from a Merck phosphate stock solution. We used 0.75 ml of each standard for the standard series and treated each of them in the same manner as described above. The samples were measured undiluted due to low concentrations and the technical detection limit of a 1 cm cuvette. Hence, we used 3.75 ml of the filtered sample solution, added the reagents mentioned above and divided the concentrations by a factor of 5 to adjust the results to those of the standard series. A factor of 0.02 was used to transform the concentration unit to µmol $L^{-1}$. The amount of filtered water (f) refers to 1/3 of the total filtered water volume (f is different for each sample):

$$\text{TPP or PIP } (\mu\text{mol L}^{-1}) = \frac{[PO_4^{3-}] \cdot 0.02}{5 \cdot f}$$

The same procedure was performed for PIP without the combustion step. The POP concentration was calculated by the difference of the measured (as phosphate) TPP and PIP concentrations.

### 2.3.3 Organic carbon concentration

The filter sections for the analysis of POC concentration were fumed with 37 % HCl overnight to remove inorganic carbon, dried and wrapped into tin caps. Samples were measured by flash combustion with a Carlo Erba elemental analyzer (NA1500). The analytical precision and detection limit were 0.04 dry wt. %.The water-column POC concentrations are given in µmol $L^{-1}$.

### 2.3.4 Porewater and solid phase analysis

Sediment cores were recovered using video-guided multiple corers (MUC) equipped with PVC liners with an inner diameter of 10 cm. The porewater and solid phase sub-sampling was performed immediately after recovery in an argon-filled glove bag at in situ seafloor temperature. The bottom water was siphoned with a plastic tube and filtered through cellulose acetate filters. Afterwards, the cores were sectioned into 0.5 cm intervals from 0-5 cm sediment depth and 1 cm intervals afterwards. The sediment samples were filled into centrifuge tubes and the porewater was separated from the sediments by centrifuging for 20 min at ~ 3940 G (centrifuge force). The supernatant porewater was filtered through cellulose acetate filters inside the glove bag. Samples were immediately analyzed for total dissolved phosphate ($TPO_4$) and dissolved ferrous iron ($Fe^{2+}$) after pore water extraction using a Hitachi U-2001 spectrophotometer. The analyses were performed according to the standard techniques described in Grasshoff et al. (1999). A sediment

subsample was taken from each sediment depth and stored refrigerated in pre-weighed air-tight plastic cups to determine the water content, porosity and total organic carbon (TOC) content. The residual sediments were stored frozen at -20°C (sediment and filter samples) and the pore water samples were refrigerated at 4°C for land-based analytics.

The TOC concentration (in µmol $mg^{-1}$) of freeze-dried and ground sediment samples was determined by flash combustion in a Carlo Erba Elemental Analyzer (NA 1500). For POC determination, samples were decalcified with 2.5 N HCl prior to the measurement. Solid phase TPP and PIP concentrations were measured according to the method of Aspila et al. (1976) in a similar manner as described before for the water-column particles. 50 mg of freeze-dried and ground sediment were digested in 1N HCl for a minimum of 24 hours to dissolve the sedimentary PIP phase. Sediment portions analyzed for TPP were combusted at 550°C for 90 min before adding 1 N HCl. The solutions were filtered and the reagents mentioned above were added prior to measurement. We used the sedimentary reference standards SDO-1 (Devonian Ohio Shale, USGS; Govindaraju, 1994) and MESS-3 (Marine Sediment Reference Material, Canadian Research Council) and replicate measurements of samples to ensure measurement accuracy. The standard series applied to the measurements covered a concentration range from 5 to 100 µM.

To determine the terrigenous P input to the sediments, and to calculate the TPP burial flux (for calculation see section 3.6 and Table 2.2), sediments were analyzed using total digestion. About 100 mg of freeze dried and ground sediment was digested in hydrofluoric acid (40%, supra pure), nitric acid (65%, supra pure) and perchloric acid (60%, supra pure). For measurement accuracy the reference standards SDO-1 and MESS-3 as well as methodological blanks were included in the analysis. The aluminum concentration in the digestion solutions was measured using an inductively coupled plasma optical emission spectrometer (ICP-OES, Varian 720 ES). The relative standard deviation (RSD) for (Al) was found to be < 1%.

The XRD data of core 107MUC23 from 407 m water depth were obtained from approximately 1 g of freeze dried and ground sediment in the lab of the University of Bremen.

### 2.3.5 POC in relation to various fractions of P (POC/xP ratios)

The molar POC/xP ratios (where xP = TPP, PIP or POP) of the water column particles at stations I, IV and V were calculated from measurements on two filter samples per water depth. For these samples a minimum and maximum value was calculated. For the other stations III, VI and VIII, only one sample per water depth was available. Here, we assumed an average natural variability calculated from the duplicate measurements of stations I, IV and V for each P species (supplement, Table S2.1). For sediment samples we calculated a standard deviation for each

station. For sediment samples we calculated a standard deviation from repeated measurements of the sediment standards MESS-3 and SDO-1 (supplement, Table S2.1).

### 2.3.6 Benthic lander fluxes

Benthic lander deployments were performed at 10 stations along the 12°S transect (I to X according to Dale et al., 2015). In situ benthic fluxes were obtained using the two BIGOs I and II (BIGO: Biogeochemical Observatory). They were equipped with two circular flux chambers (internal diameter 28.8 cm, area 651.4 $cm^2$) (Sommer et al., 2009). An online video-controlled launch system allowed precise placement of the BIGO at the seafloor directly located beneath the particle sampling stations in the water column and in proximity to the multi-corer stations. After a 4 hour rest period at the seafloor during which surrounding bottom water was periodically flushed into the chamber, the chambers were slowly driven into the sediment. The BIGOs stayed for 28 hours at the seafloor, while 8 water samples per chamber were taken via glass syringes. In order to obtain bottom water background information, additional samples were taken every 8 hours from the ambient bottom water. Phosphate concentrations in the syringe samples were measured on board using an auto analyzer. The standard series covered a concentration range from 0.05 to 3.5 µM. The fluxes were calculated from the slope of linear regression of all 8 data points versus the sampling time (supplement, Fig. S2.1) and corrected for the water volume in the chamber and the dead volume of the 1 m long Vygon tubes connecting the syringes with the flux chambers. The error caused by the dilution from the dead volume of these tubes was calculated from the chloride concentration measured in the syringe samples. Benthic lander $TPO_4$ fluxes for most sites are based on two replicate chamber measurements. The uncertainty given for the $TPO_4$ fluxes is the difference between the minimum and maximum fluxes from the average of the two benthic chambers. At two stations (IV and V), it was only possible to calculate the flux from one chamber. For further details on the benthic flux measurements during the M92 cruise see Dale et al. (2015).

### 2.3.7 Diffusive flux calculations

The diffusive fluxes of $TPO_4$ and $Fe^{2+}$ from the sediment to the bottom water were calculated by applying Fick's First Law of diffusion:

$$F_{TPO4/Fe2+} = - \phi \, D_{SED} \, (\mathrm{d}(C)/\mathrm{d}x) \qquad (1)$$

where the term d($C$)/d$x$ describes the concentration gradient between the bottom water and the first porewater sample of the surface sediment divided by the corresponding sediment depth (0.25 cm or 0.5 cm) and $\phi$ is the porosity of the surface sediment. The diffusion coefficient, $D_{SED}$, for sediments was calculated according:

$$D_{SED} = D_{SW}/\theta^2 \qquad (2)$$

The diffusion coefficients for $TPO_4$ and $Fe^{2+}$ under standard conditions ($D_{SW}$) under standard conditions (298.15 K and 1 bar) were taken from Li and Gregory (1974) and corrected for the in situ temperature and pressure using the Stokes-Einstein equation. The tortuosity ($\theta^2$) was derived from the sediments porosity according to the modified Weissberg formulation (Boudreau, 1996):

$$\theta^2 = 1 - \ln(\phi^2) \qquad (3)$$

Uncertainty in the diffusive flux was calculated at St. I as the difference between the fluxes calculated from two separate sediment cores. For the other stations, only one core was available to calculate the flux.

### 2.3.8 Mass balance of benthic phosphorus cycling

To investigate benthic P cycling quantitatively, a mass balance was developed considering P input, P burial, and P release. The equations for the P mass balance calculations are shown in Table 2.2. Under steady state conditions, the total P rain rate should balance the P buried in the sediments and the benthic $TPO_4$ flux (Eq. 4 in Table 2.2). The rain rates of particulate P delivered to the sediments are differentiated in inorganic P ($RR_{PIP}$) (Eq. 5 in Table 2.2) and organic P ($RR_{POP}$) (Eq. 6, Table 2.2). The rates were calculated using the POC/xP ratio of the water column particles that were taken as close as possible to the seafloor at each station (2-5 m above ground) and the POC rain rate ($RR_{POC}$) (Table 2.4 and supplement, Table S2.1). $RR_{POC}$ for the same stations along the 12°S transect were previously calculated by Dale et al. (2015) as the sum of the measured benthic DIC flux and the POC accumulation rate. The terrigenous P input ($RR_{Pterr}$) (Eq. 7 in Table 2.2) can be estimated by multiplying the solid phase Al concentration of the first sediment sample by the mass accumulation rate (Dale et al., 2015) and a P/Al ratio of 0.02 that characterizes the P/Al ratio of riverine particles originating from the continent (Viers et al., 2009).

The P burial flux ($F_{Pbur}$) (Eq. 8 in Table 2.2) was calculated by multiplying the mass accumulation rate (MAR) and the average solid phase P concentration of the first 11 sediment centimeters ($P_{11}$) (11 cm is due to our sampling resolution). This approach was chosen according to Dale et al. (2015) who also calculated POC accumulation rate for the OMZ stations (i.e. not on the shelf or below the OMZ) using the elemental average concentration of the first 10 cm of sediment. MAR (Eq. 9 in Table 2.2) was calculated from the sedimentation rate ($\omega_{acc}$ in cm $y^{-1}$), dry bulk density ($\rho_{dry}$; in g $cm^{-3}$) and the average porosity of the sediments at the lower core end ($\phi_\infty$). Sedimentation accumulation rates were determined from particle-bound $^{210}Pb_{xs}$ measurements using a modeling approach. A detailed method description and the values used for this work are

published in Dale et al. (2015). The error derived from modeling the sedimentation rate was given as 20 % and propagates to all subsequent calculations where it was used.

**Table 2.2** Equations for the P mass balance calculations. Results are shown in Table 2.4.

| | | |
|---|---|---|
| **Equations for P mass balance calculations** | | |
| **P Input to the sediments (mmol $m^{-2}$ $d^{-1}$)** | | |
| (4) | Total particulate phosphorus rain rate | $RR_{TPP} = RR_{PIP} + RR_{POP} = F_{TPO4} + F_{Pbur}$ |
| (5) | Particulate inorganic phosphorus rain rate | $RR_{PIP} = RR_{POC} / \left(\frac{POC}{PIP}\right)$ |
| (6) | Particulate organic phosphorus rain rate | $RR_{POP} = RR_{POC} / \left(\frac{POC}{POP}\right)$ |
| (7) | Terrigenous P input (P/Al = 0.02, Vier et al., 2009) | $RR_{Pterr} = Al_{(0-1)} * MAR * \frac{P}{Al}$ |
| **P Burial in the sediments (mmol $m^{-2}$ $d^{-1}$ and g $m^{-2}$ $d^{-1}$) at 11 cm** | | |
| (8) | Phosphorus burial flux | $F_{Pbur} = MAR * P_{11}$ |
| (9) | Mass accumulation rate | $MAR = \rho_{dry} * (1 - \phi_{\infty}) * SR$ |
| (10) | TPP burial efficiency | $PBE = MAR * \left(\frac{P_{11}}{RR_{TPP}}\right) * 100\ \%$ |
| **P release from the sediments (mmol $m^{-2}$ $d^{-1}$)** | | |
| Benthic P fluxes ($F_{TPO4}$) and the potential diffusive P fluxes were determined as descried in the methods | | |
| (11) | P release from POP degradation according to Redfield (C/P = 106) | $F_{P(Red)} = F_{DIC}/106$ |
| (12) | True P release from POP | $F_{P(POP)} = F_{DIC} / \left(\frac{POC}{POP}\right)$ |
| (13) | P release from total particulate phosphorus | $F_{P(TPP)} = F_{DIC} / \left(\frac{POC}{TPP}\right)$ |
| (14) | P release from the dissolution of Fe (oxyhydr)oxides (Fe/P = 10, Slomp et al., 1996) | $F_{P(Fe)} = F_{Fe2+} / \left(\frac{Fe}{P}\right)$ |
| (15) | P deficit to outbalance the P budget | $F_{P(deficit)} = RR_{TPP} + RR_{terr} + F_{P(Fe)} - (F_{TPO4} + F_{Pbur})$ |

### 2.3.9 Freeze/thaw experiments

In order to determine the amount of polyphosphate stored in sulfide-oxidizing bacteria, foraminifera and other bacteria we conducted additional sediment experiments at all transect

stations, except station IV. Sediments from MUC corers were sliced into 1 cm thick slices from the surface sediment to 10 cm sediment depth. Before phosphate analysis, sediment slices were repeatedly frozen at -80°C and defrosted in order to burst microbial cells and release the internally stored P to the porewater.

### 2.3.10 Molecular quantification of filamentous bacteria

In order to quantify the abundance of filamentous microbes at the benthic boundary layer, we used a molecular approach. Nucleic acid purification was performed on 0.5 g sediment following established protocols (Bertics et al., 2013). DNA was quality checked on an agarose gel and quantified using a Nanodrop spectrophotometer (Peqlab, Erlangen, Germany). 16S rDNA fragments were taken from a previously generated metagenome from this region (GenBank Bioproject PRJNA280940) and the respective sequence counting's were deposited at GenBank (ID KU312264-KU312267). Sequencing was carried out in the Institute of Clinical Molecular Biology at Kiel University. Sequences were analyzed using a Clustal W alignment tool on Mega 6 (Tamura et al., 2013). A qPCR primer and probe set was established using the Primer Express software (Life Technologies, Carlsbad, USA) with the forward primer 5' AGAAGCACCGGCTAACTCTG-3' , the reverse primer, 5' -CCAGGTAAGGTTCTTCGCGT-3' and the probe 829-Thioploca 5'-GGATTAATTTCCCCCAACAT-3' (Teske et al., 1995). Primers and probes were tested *in silico* on the Silva database and cross amplification was excluded on a variety of 16S rDNA clones. The qPCRs were performed in technical duplicates on a ViiA7 system (Life Technologies, Carlsbad, USA) as previously described (Löscher et al., 2012) using 1x TaqMan PCR buffer (Life Technologies, Carlsbad, USA), 2.5 pmol $\mu L^{-1}$ TaqMan probe, 5 pmol $\mu l^{-1}$ of each primer, 400 ng $\mu l^{-1}$ bovine serum albumin (to avoid PCR inhibition without affecting standard curves or detection limits), 3 µl PCR water, and 5 µl of either standard DNA or environmental sample. A plasmid containing the target sequence was used to generate a standard dilution series for absolute quantification. The melting temperature was set to 50°C. A theoretical detection limit of 4 copies per PCR reaction was calculated. The results of the analysis are given in copies $g^{-1}$ of 16S rDNA sequences of sulfur bacteria that are related to Marithioploca.

## 2.4 Results

### 2.4.1 P composition of water-column particulate matter and surface sediments

**TPP, PIP, POP and POC concentrations**

The TPP concentrations ranged from 0.02 to 0.2 µmol $L^{-1}$ in the water-column particles and from 0.04 to 2.37 µmol $mg^{-1}$ in the surface sediments (supplement, Table S2.1). Overall, the profiles along the transect show no significant trends through the water column (Fig. 2.2A). The highest concentrations occurred in the surface waters around 10 m of water depth. At stations I, V and

VIII (74, 195 and 407 m) the TPP concentrations slightly increased close to the seafloor, whereas at the other stations no such trend was observed (Fig. 2.2A and supplement, Table S2.1). In the sediments the TPP concentrations slightly decreased with sediment depth, except at station VIII (407 m). Here, the highest sedimentary TPP concentrations across the transect were found at 2.25 cm sediment depth (17 µmol $mg^{-1}$). Below that depth the concentrations decreased, but remained high compared to the other stations.

The PIP and POP concentrations (water column and sediments) generally followed the trends of the TPP profiles and contributed roughly equally to TPP. The PIP fraction accounted for 21 to 74 % of TPP in the water-column particles (Fig. 2.3), similar as reported in previous studies (Paytan et al., 2003; Faul et al., 2005; Benitez-Nelson et al., 2007; Lyons et al., 2011; Sekula-Wood et al., 2012). At stations I, VI and VIII (74, 244 and 407 m), the PIP concentrations were larger than POP. The opposite occurred at station V (195 m) where the POP fraction was clearly larger than the PIP fraction throughout the entire water column. In comparison to the water-column particles, the PIP fraction was larger than POP in most samples reaching between 48 to 98% of TPP. However, the strongest deviation between PIP and POP concentrations was found in the sediments of station VIII (407 m) where the PIP concentration was up to a factor of ~ 50 larger than the POP concentration and comprised up to 98% of TPP. XRD data from that station revealed that 7 to 16 wt.% of the sediments consisted of apatite and other P-bearing minerals (data not shown).

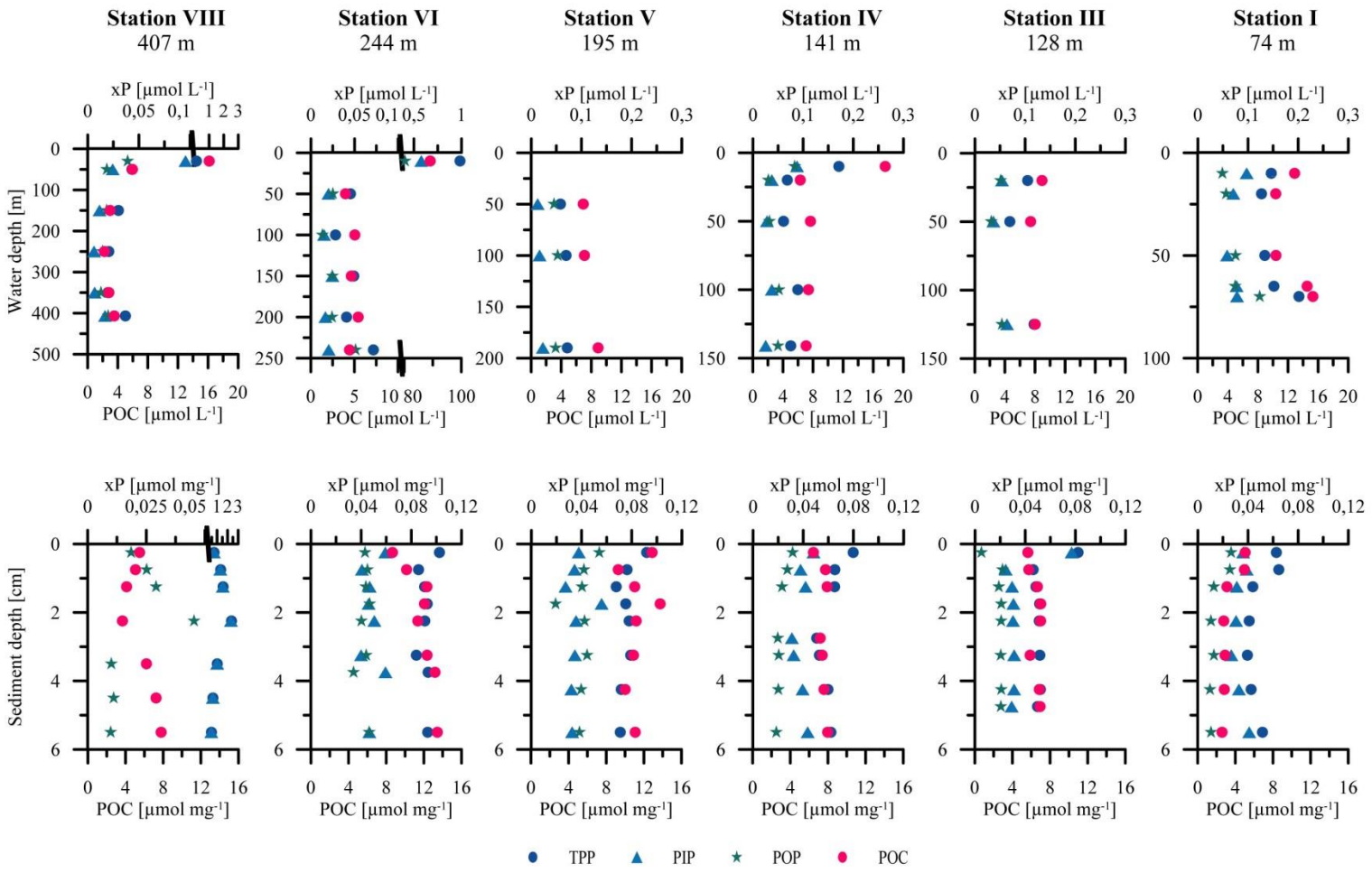


**Fig. 2.2A** Concentration profiles of TPP, PIP, POP and POC of the water-column particles and the surface sediments along the 12°S transect. Water-column particle concentrations (upper panel) are given in µmol $L^{-1}$ and surface sediment concentrations (lower panel) are shown in µmol $mg^{-1}$. Note that the water-column particle concentrations shown for station VI (244 m) at 10 m water depth are ~ 5 times higher than at the other stations.

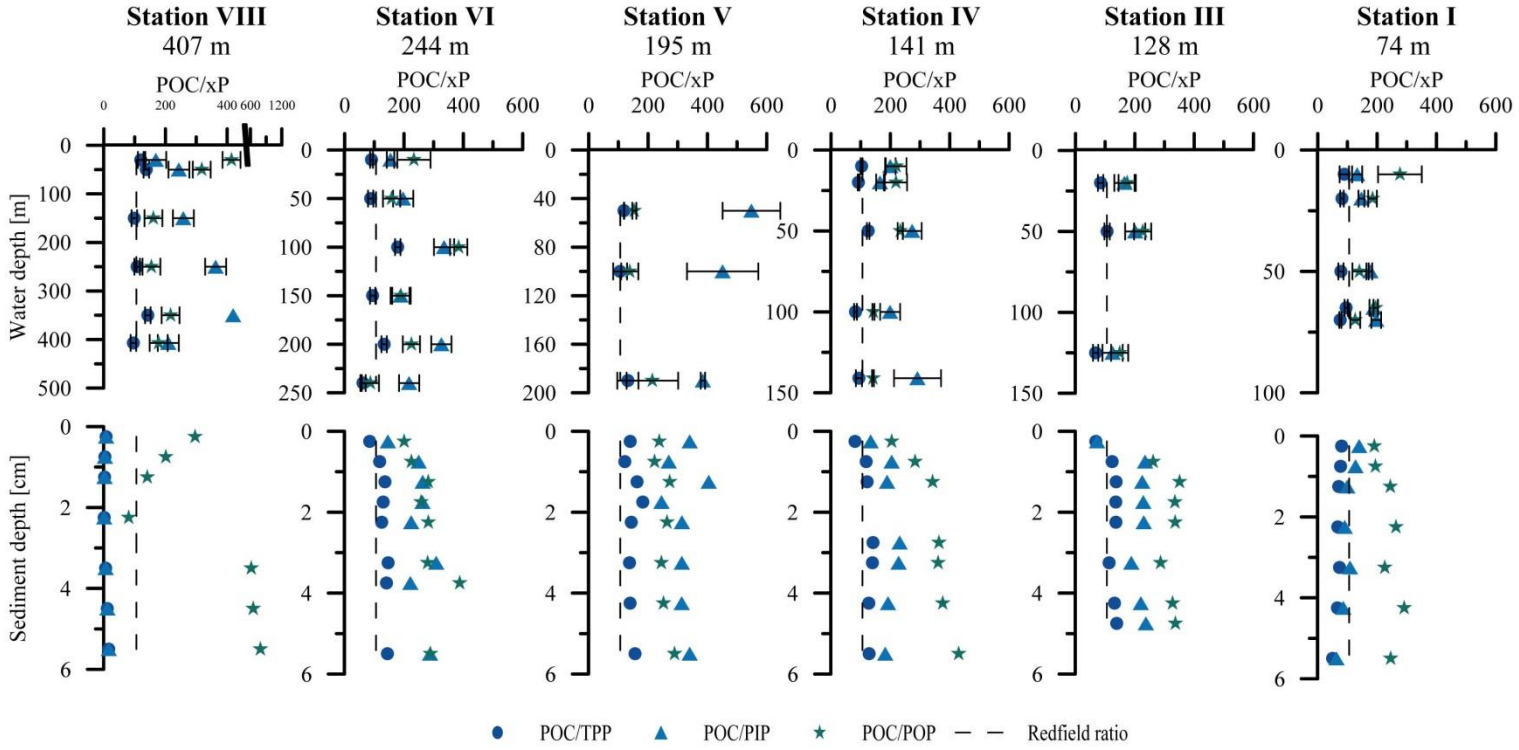


**Fig. 2.2B** Ratios of POC to TPP, PIP and POP (POC/xP) along the 12°S depth transect of water-column particles and surface sediments (0 – 5.5 cm depth) of station I to VIII (74 to 407 m).

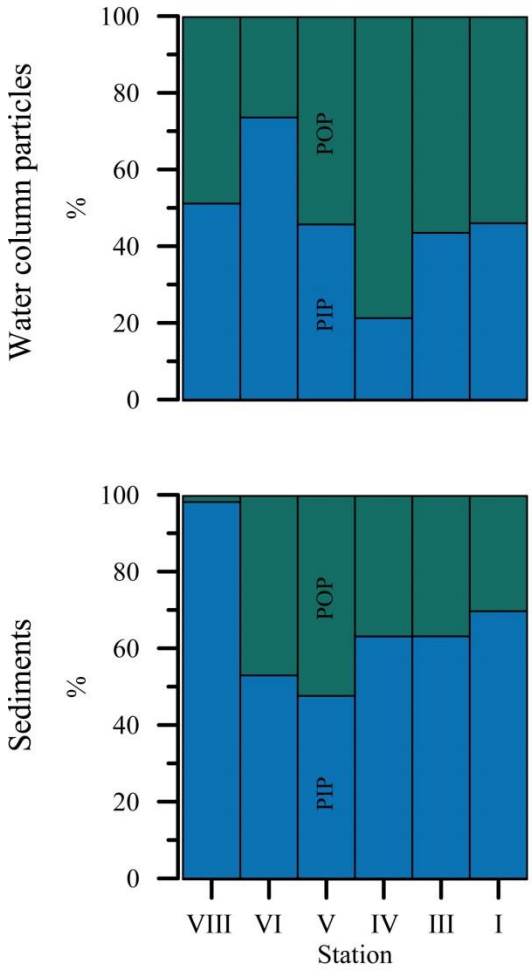


**Fig. 2.3** Average distribution of POP and PIP (%) per station in the water-column particles and in the top 5.5 cm of the sediments.

The particulate organic carbon concentrations ranged from 2.2 to 17.6 µmol $L^{-1}$ in the water-column particles and from 2.8 to 13.4 µmol $mg^{-1}$ in the surface sediments. Within the water column the highest concentrations occurred in the surface water samples, while the concentration measured at station VI (244 m) is about 5 times higher than compared to other samples from the same water depth. Below the surface water concentration peak, the concentrations were on average 7 µmol $L^{-1}$ with distinct depth trends. The sedimentary POC concentrations were on average 7.7 µmol $mg^{-1}$ for the whole transect. Overall, the POC concentrations showed little variability with sediment depth. At station III, VI and VIII (128, 244 and 407 m) the concentrations increased slightly with sediment depth. At station I (74 m) the concentration decreased slightly with sediment depth.

### 2.4.2 Particulate organic carbon to phosphorus (POP, PIP, TPP) ratios

**POC/POP ratios**

The molar POC/POP ratios of the water-column particles and of the surface sediments were consistently higher than the Redfield ratio at all stations (Fig. 2.2B). The average POC/POP ratio of the water-column particles was 202 ± 29. There was no clear trend through the water column, except slightly increasing ratios between the deepest water-column samples and the surface sediment samples. In the surface sediments, the ratios increased within the upper 6 cm with an average POC/POP ratio of 303 ± 77. Station VIII (407 m) is an exception, and here the ratio decreased to 81 within the first ~ 2 cm of sediment and then strongly increased to ≥600.

**POC/PIP ratios**

The average POC/PIP ratio of the water-column particles was 248 ± 34. Similar to the POC/POP ratios, there was no significant trend through the water column. At the majority of the stations, the ratios decreased close to the seabed. The average POC/PIP ratio of the surface sediments was 184 ± 34 and almost invariable with water depth. In the sediments, the ratios showed no significant down-core trend. At station VIII (407 m) the ratio in the sediments showed a dramatic decrease compared to the water column, with an average of 7, similar to the POC/TPP ratios (below).

**POC/TPP ratios**

The POC/TPP ratios of the water-column particles and surface sediments consistently varied around the Redfield ratio. The exceptions are station I (74 m) and the deepest station (Sta. VIII, 407 m). At station I, the sediments showed significantly lower than Redfield ratios with an average of 69 in the surface sediments. The average POC/TPP ratio of the surface sediments at station VIII (407 m) was 7. Between the deepest water-column sample and the first sediment sample, the POC/TPP ratios were rather constant without a consistent trend, again with the exception of station VIII (407 m) where the ratios decreased sharply.

### 2.4.3 In situ benthic chamber fluxes

The benthic lander $TPO_4$ fluxes ($F_{TPO4}$) are presented in Table 2.3 and Fig. 2.4A. Positive fluxes are defined as directed from the sediments into the water column. The highest $TPO_4$ flux along the depth transect of 1.04 ± 0.31 mmol $m^{-2}$ $d^{-1}$ occurred at station I (74 m). Below 74 m water depth, fluxes decreased by at least a factor of 3 to 0.2 – 0.3 mmol $m^2$ $d^{-1}$ at 144 m water depth. Measurements at station V (195 m) showed a slightly increased $TPO_4$ flux of 0.44 ± 0.07 mmol $m^{-2}$ $d^{-1}$, while the fluxes measured at 244 m (St. VI) and 306 m (St. VII) decreased to the before mentioned levels. At 407 m water depth (St. VIII) the $TPO_4$ flux was negative, indicating a phosphate uptake by the sediment. Below the OMZ, the fluxes increased to slightly positive values, but remained low at 0.06 and 0.02 ± 0.02 mmol $m^{-2}$ $d^{-1}$.

**Table 2.3** In situ benthic chamber $TPO_4$ fluxes in mmol $m^{-2}$ $d^{-1}$ along the 12°S transect. The numbers are shown as an average calculated from the minimum and maximum flux determined from two benthic chambers. In the cases where only a single number is displayed, the benthic flux was determined from only one benthic chamber.

| Station | | Water depth (m) | $F_{TPO4}$ (mmol $m^{-2}d^{-1}$) |
|---|---|---|---|
| **I** | **BIGO1_2** | 74 | 1.04 ± 0.31 |
| **II** | **BIGO1_5** | 101 | 0.35 ± 0.01 |
| **III** | **BIGO2_4** | 128 | 0.30 ± 0.05 |
| **IV** | **BIGO1_1** | 141 | 0.23 [a] |
| **V** | **BIGO1_4** | 195 | 0.12 [a] |
| **VI** | **BIGO2_2** | 243 | 0.44 ± 0.07 |
| **VII** | **BIGO2_1** | 306 | 0.26 ± 0.04 |
| **VIII** | **BIGO2_5** | 409 | -0.07 [a] |
| **IX** | **BIGO2_3** | 756 | 0.06 [a] |
| **X** | **BIGO1_3** | 989 | 0.02 ± 0.02 |

[a] only one benthic flux was measured

### 2.4.4 Comparison of benthic chamber $TPO_4$ fluxes and diffusive $TPO_4$ fluxes

The measured benthic chamber $TPO_4$ fluxes and the calculated diffusive $TPO_4$ fluxes showed large discrepancies. The calculated diffusive fluxes were consistently higher than the benthic fluxes (Table 2.4, Fig. 2.4B). In contrast to the in situ measured benthic chamber $TPO_4$ release rates, the calculation of diffusive $TPO_4$ fluxes relies on bottom water and pore water $PO_4^{3-}$ concentrations. A subsurface $PO_4^{3-}$ peak occurred at all stations in the uppermost depth interval at 0-0.25 cm causing a large concentration gradient between the bottom water and the pore water $PO_4^{3-}$ concentrations (Fig. 2.7). Even though the measured benthic $TPO_4$ fluxes exceeded the fluxes that could be generated by TPP degradation by a factor of approximately 6, the diffusive $TPO_4$ fluxes were still higher (Table 2.4). Hence, the diffusive $TPO_4$ flux will be referred to as potential $TPO_4$ flux in the following.

### 2.4.5 TPP burial fluxes and TPP burial efficiency

The P burial fluxes decreased with increasing water depth (Table 2.4). Station I (74 m) showed by far the highest P burial flux with with 0.23 mmol $m^{-2}$ $d^{-1}$. In contrast the P burial efficiency at this station (Eq. 10) was comparatively low reaching only approximately 26 %. At Station VIII (407 m), the TPP burial flux was 13 mmol $m^{-2}$ $d^{-1}$ and the P burial efficiency exceeded 100 % due to the uptake of dissolved P from ambient bottom waters.

### 2.4.6 Molecular analysis and relative abundance of filamentous sulfur bacteria

Molecular analysis indicated the presence of Marithioploca-related bacteria (Salman et al., 2011) in the surface sediments (0-5 cm). Our analysis may, however, underestimate the absolute

abundance of these organisms due to a self-splicing mechanism of the 16S rDNA gene (Salman et al., 2012) and is therefore only indicative for their relative abundance.

The relative abundance of Marithioploca-related bacteria decreased with increasing water depth (Table 2.4). Highest relative abundance with more than 4000 copies $g^{-1}$ sediment was found at station I (74 m), decreasing by more than a factor of 20 to 190 copies $g^{-1}$ sediment at station VIII (407 m).

## 2.5 Discussion

### 2.5.1 POC/xP ratios in water-column particles and sediments

In order to characterize the fate of P in oxygen deficient waters and sediments we determined POC/xP ratios from both environments. Previous studies focused either on the water column or on the sediments (Anderson et al., 2001 and references therein; Benitez-Nelson et al., 2004; Faul et al., 2005; Jilbert et al., 2011; Lyons et al., 2011; Sekula-Wood et al., 2012). The present data set provides a more complete insight into compositional changes and allows us to more rigorously constrain the sedimentary P mass balance compared to earlier studies (Ingall and Jahnke, 1994; Mort et al., 2010; Kraal et al., 2012; Noffke, 2014).).

Both water-column particles and the surface sediments from the Peruvian OMZ displayed POC/POP ratios above Redfield, indicating depletion of organic P relative to organic C. Similar observations have been reported before from this and other regions of the ocean (Loh and Bauer, 2000; Benitez-Nelson et al., 2004; Faul et al., 2005; Franz et al., 2012 and others). Preferential remineralization of P phases from sinking particles should lead to increasing POC/POP ratios with increasing water depth, as observed in oxygenated areas of the ocean (reviewed by Ruttenberg, 2014). However, in the anoxic Cariaco Basin, no such preferential P mineralization was noted (Benitez-Nelson et al., 2004). Our results also showed no clear decrease in the POC/POP ratio in the water column, with the possible exception of St. I and VIII. Higher than Redfield POC/POP ratios were observed at Peru on a previous occasion, and may instead be driven by the C-to-P composition of the diatomaceous phytoplankton communities (Franz et al., 2012) rather than preferential P dissolution or other controls such as the input of terrestrial plant material with high POC/POP ratios.

Preferential POP over POC remineralization in anoxic sediments remains controversial (Ingall and Van Cappellen, 1990; Ingall and Jahnke, 1994; Colman et al., 1997; Anderson et al, 2001; McManus et al, 1997; Ruttenberg, 2003; Jilbert et al, 2011). Our results, however, also showed no clear trend across all stations. At station I, IV and VI (74, 141 and 244m) the POC/POP increased with sediment depth indicating preferential POP over POC remineralization. At station III (128

m) this trend occured only in the upper cm and at station V (195 m) no preferential POP over POC remineralization was found. POC/POP ratios at station VIII (407 m) showed a POP enrichment over the upper 2 cm of the sediment. Below this depth, there was a sudden increase in POC/POP ratios, which is likely due to intense POP remineralization and subsequent authigenic formation of phosphorites (sink-switching, see section 5.2.3).

Another interesting finding pointing to sink-switching can be found in the POC/POP and POC/PIP ratios of the deepest water-column particle sample and the first sediment sample at stations I, IV, VI and VIII (74, 141 and 407 m). Increasing POC/POP and decreasing POC/PIP ratios indicate that POP is converted into PIP while the TPP content of the sediment is conserved (Fig. 2.2A and B). In agreement with similar findings in anoxic sediments (Ruttenberg and Berner, 1993; Faul et al., 2005 and others) we assume that the observed POP to PIP transformation is due to the formation of CFAs. However, our results emphasize that sink-switching is obviously occurring at the interface between bottom waters and sediments.

Interestingly, the water-column POC/TPP ratios were close to Redfield ratio. This could be an effect of surface adsorption of P on phytoplankton as previously described by Sanudo-Wilhelmy et al. (2004). Those authors investigated different species of *Trichodesmium* from the Atlantic Ocean and found that the intracellular P pool was strongly depleted relative to C, whereas the combination of the intracellular plus the surface adsorbed P was close to the Redfield ratio. Although we did not exactly differentiate between internal and external P pools, and considering that additional P sources like terrigenous P are negligible (see section 5.2.1), our results generally support the findings of Sanudo-Wilhelmy et al. (2004). However, future studies are required to substantiate this hypothesis.

Sedimentary POC/TPP ratios were also close to Redfield, except at station I and VIII (74 and 407 m). Thus, on the one hand, the sink switching mechanism operates efficiently under low oxygen conditions and on the other hand, the relative degradation of TPP and POC are not changing from the water column to the sediments (Fig. 2.2B). This is an important finding because at first sight this observation seems to be inconsistent with the long-standing paradigm that low oxygen conditions promote the enhanced release of dissolved P from sediments (Van Cappellen and Ingall, 1996). However, it should be noted that marine sediments covered by oxygenated bottom waters display molar POC/TPP ratios ranging from about 10 to 50 (Baturin, 2007). These ratios are much lower than Redfield because P is retained in sediments via adsorption, authigenic mineral precipitation such as Fe (oxyhydr)oxides and microbial P sequestration (Ingall and Jahnke, 1994), and because POC is more efficiently degraded under aerobic conditions (Hedges et al., 1999, Wallmann, 2010). In contrast, our data set implies that oxygen deficiency causes a shift

of POC/TPP ratios to values closer to Redfield compared to oxygenated regions, which is due to both, the enhanced preservation of POC (Dale et al., 2015) and release of dissolved phosphate under low oxygen conditions. It remains puzzling why the extreme P depletion observed in some black shale sequences (e.g. POC/TPP > 3000, Ingall and Jahnke, 1994) are not found in modern anoxic sediments such as those on the Peru margin.

### 2.5.2 P mass balance

P release rates from sediments underlying oxygen deficient waters are strongly enhanced compared to oxygenated marine settings, especially in the Peruvian OMZ (Noffke et al., 2012 and 2016). Nonetheless, the sources for the enhanced P release are still not completely identified. The widely held view is that POP raining from the water column to the sediments represents the main source for sedimentary P in high productive areas like the Peru upwelling system (Delaney, 1998; Filippelli, 2008). Mass balance approaches that resolve the P regeneration versus burial in oxygen deficient environments by combining sedimentary data and benthic P fluxes are rare (Ingall and Jahnke, 1994; Ingall et al., 2005; Mort et al., 2010; Kraal et al., 2012; Noffke, 2014). These studies are all based on sediment data only, that is, the external P input to the sediments is estimated or ignored. Furthermore, the study areas were often not covered by fully anoxic bottom waters. Noffke (2014) presented an approach that combines measurements of solid phase P speciation, sediment burial fluxes and benthic chamber flux measurements for a mass balance on benthic P cycling in the Peruvian OMZ. Interestingly, the measurements on the solid phase P speciation revealed that organic P accounted for only 18-37% of the total sedimentary P on the shelf and upper slope (Noffke, 2014). Furthermore, it was found that P bound to Fe (oxyhydr)oxides and terrigenous P was of minor importance for the total sedimentary P inventory. However, authigenic Ca-P with a high amount of fish-P accounted for up to 47% of the total P in sediments down to 300 m water depth and for up to 70% in sediments below 300 m water depth. Consequently, Noffke (2014) suggested that authigenic Ca-P phases are an additional major P source besides organic P for benthic P release in the Peruvian OMZ.

Their mass balance approach was solely based on benthic work and has large uncertainties regarding the particulate P input from the water column. Our approach includes the particulate organic and inorganic P input from the water column, benthic P flux measurements and the P burial fluxes and is based on the steady state assumption that the P input has to be sufficient to maintain the benthic P flux and P burial flux. The P mass balance calculations (Table 2.4) illustrate the variability in $TPO_4$ release and burial as well as in the magnitude of particulate organic (Fig. 2.5A) and particulate inorganic P input (Fig. 2.5B) across the transect. Following the general assumption that POP is the major P phase delivered to the sediments (Delaney, 1998;

Filippelli, 2008), we first calculated whether the rain rate of POP ($RR_{POP}$) to the seafloor can account for the measured benthic P fluxes ($F_{TPO4}$) and P burial fluxes ($F_{Pbur}$) (Fig. 2.5A, Table 2.4). However, as already suggested by Noffke et al. (2012 and 2014), the POP fraction is far too small to balance the measured benthic fluxes in the Peruvian OMZ. The POP rain rates calculated along the transect can account for only 25 to 48% of the measured $TPO_4$ fluxes (Fig. 2.5A), suggesting the likely presence of an additional inorganic source of dissolved phosphate (Noffke, 2014). Similar to previous studies (Paytan et al., 2003; Faul et al., 2005; Benitez-Nelson et al., 2007; Lyons et al., 2011; Sekula-Wood et al., 2012), we found that the PIP fraction in water-column particles ranging from 75 to 407 m water depth comprises between 21-74% of TPP (Fig. 2.3). In the sediments, the average PIP fraction rises to 48-98% of TPP (Fig. 2.3). Furthermore, POC and PIP were correlated ($r^2$=0.74) in the water-column particles indicating highly reactive material.

The mass balance approach including the PIP rain rate to the seafloor (Fig. 2.5B) allows the depth transect to be divided into two sections. The transect section I (station I, 74 m and III, 128 m) is characterized by high P input and release rates. The calculations on the P budget show a balance between the particulate P input, the benthic P fluxes and the P burial fluxes within the error margin (± 20%). In transect section II (stations IV, 141 m, V, 195 m and VI, 244 m), the P input decreases drastically (Fig. 2.5B, Table 2.4) whereas the benthic P fluxes are still comparatively high. The distinct mismatch in P input and P output prevails as the particulate P rain rates supported only 37 to 53 % of the measured $TPO_4$ fluxes and calculated burial fluxes. This leads to the question: What drives the excess $TPO_4$ release in the core of the Peruvian OMZ?

**Table 2.4** Measured and calculated parameters for the P mass balance along the 12°S transect. The numbers in front of key parameters correspond to equations in Table 2.2.

| | Transect section I | | Transect section II | | | Phosphorite formation |
|---|---|---|---|---|---|---|
| **12°S** | **Station I** | **Station III** | **Station IV** | **Station V** | **Station VI** | **Station VIII** |
| | **74 m** | **128 m** | **141 m** | **195 m** | **244 m** | **407 m** |
| **Benthic chamber $TPO_4$ flux ($F_{TPO4}$)*** mmol $m^{-2}$ $d^{-1}$ | 1.04 ± 0.31 | 0.3 ± 0.05 | 0.23 - | 0.12 - | 0.44 ± 0.07 | -0.07 - |
| **Potential (diffusive) $TPO_4$ flux (pot. $F_{TPO4}$)** mmol $m^{-2}$ $d^{-1}$ | 1.07 ± 0.23 | 2.0 - | 0.5 - | 1.6 | 1.5 - | |
| **Relative abundance of Marithioploca-related bacteria*** copies $g^{-1}$ (0-5 cm sediment depth) | 4159 | | 1687 | 3072 | | 190 |
| **Benthic chamber DIC flux ($F_{DIC}$)**** mmol $m^{-2}$ $d^{-1}$ | 65.9 ± 21 | 20.4 ± 7 | 8 ± 0.4 | 3.2 ± 1 | 4.7 ± 1 | 2.2 ± 0.3 |
| **POC rain rate ($RR_{POC}$)**** mmol $m^{-2}$ $d^{-1}$ | 79.5 ± 33 | 28.2 ± 12 | 10.5 ± 3 | 12.5 ± 6 | 10.6 ± 4 | 2.7 ± 1 |
| **Sediment accumulation rate ($\omega_{acc}$)**** cm $yr^{-1}$ | 0.45 ± 0.09 | 0.2 ± 0.04 | 0.04 ± 0.008 | 0.1 ± 0.02 | 0.07 ± 0.014 | 0.01 ± 0.002 |
| **Mass accumulation rate (MAR)**** g $m^{-2}$ $yr^{-1}$ | 1800 ± 360 | 600 ± 120 | 128 ± 26 | 320 ± 64 | 182 ± 37 | 44 ± 9 |
| Ratios for particulate matter from the water column (2 to 5 m above the sea floor): | | | | | | |
| **POC/TPP*** | 76 ± 4 | 68 ± 9 | 94 ± 10 | 132 ± 36 | 62 ± 9 | 96 ± 9 |
| **POC/PIP*** | 197 ± 17 | 125 ± 34 | 291 ± 79 | 385 ± 7 | 217 ± 34 | 209 ±34 |
| **POC/POP*** | 126 ± 17 | 149 ± 29 | 142 ± 3 | 214 ± 87 | 87 ± 29 | 178 ±29 |
| **(4) TPP rain rate ($RR_{TPP}$)** mmol $m^{-2}$ $d^{-1}$ | 1.00 ± 0.31 | 0.40 ± 0.09 | 0.11 ±0.02 | 0.09 ± 0.02 | 0.17 ± 0.02 | 0.03 ± 0.01 |
| **(5) PIP rain rate ($RR_{PIP}$)** mmol $m^{-2}$ $d^{-1}$ | 0.39 ± 0.14 | 0.22 ± 0.04 | 0.04 ± 0 | 0.03 ± 0.02 | 0.05 ± 0.01 | 0.01 ± 0.01 |
| **(6) POP rain rate ($RR_{POP}$)** mmol $m^{-2}$ $d^{-1}$ | 0.61 ± 0.18 | 0.18 ± 0.05 | 0.07 ±0.02 | 0.06 ± 0.01 | 0.12 ± 0.01 | 0.01 ± 0.01 |
| **(7) Terrigenous P input ($RR_{Pterr}$)** | 0.10 - | 0.02 - | 0.01 - | 0.02 - | 0.01 - | 0.00 - |
| **(8) Burial flux ($F_{Pbur}$) in 11 cm sediment depth** | 0.23 - | 0.09 - | 0.02 - | 0.08 - | 0.04 - | 0.13 - |

| | | | | | | | | | | | | |
|---|---|---|---|---|---|---|---|---|---|---|---|---|
| mmol $m^{-2}$ $d^{-1}$ | | | | | | | | | | | | |
| **Avg. Al conc. ( 0-1 cm sediment)($Al_{0-1}$)*** mmol $g^{-1}$ | 0.99 | - | 0.70 | - | 1.10 | - | 0.97 | - | 0.72 | - | 0.66 | - |
| **Avg. P conc. (0-11 cm sediment ($P_{11}$)*** mmol $g^{-1}$ | 0.05 | - | 0.05 | - | 0.07 | - | 0.09 | - | 0.08 | - | 1.05 | - |
| **(10) P burial efficiency (PBE) at11 cm sediment depth** % | 26 | ± 8 | 23 | ± 4 | 23 | ± 5 | 92 | ± 20 | 23 | ± 2 | 490 | ± 100 |
| **(11) P release from POP degradation according to Redfield ($F_{P(Red)}$)** mmol $m^{-2}$ $d^{-1}$ | 0.62 | ± 0.2 | 0.19 | ± 0.06 | 0.08 | ± 0.01 | 0.03 | ± 0.01 | 0.04 | ± 0.02 | 0.02 | ± 0 |
| **(12) P release from POP degradation ($F_{P(POP)}$)** mmol $m^{-2}$ $d^{-1}$ | 0.52 | ± 0.16 | 0.14 | ± 0.05 | 0.06 | ± 0.01 | 0.02 | ± 0.01 | 0.05 | ± 0.02 | 0.01 | ± 0 |
| **(13) P release from TPP degradation ($F_{P(TPP)}$)** mmol $m^{-2}$ $d^{-1}$ | 0.87 | ± 0.17 | 0.3 | ± 0.1 | 0.09 | ± 0.01 | 0.02 | ± 0.01 | 0.08 | ± 0.02 | 0.02 | ± 0.01 |
| **Benthic diffusive $TPO_4$ flux (potential P flux)*** | 1.08 | ± 0.23 | 2.0 | - | 0.5 | - | 1.6 | - | 1.5 | - | - | - |
| **Diffusive $Fe^{2+}$ flux ($F_{Fe2+}$)*** | 0.04 | ± 0.02 | 0.01 | | 0.02 | | 0.0 | | 0.03 | | 0.0 | |
| **(14) P release from Fe (oxyhydr)oxides ($F_{P(Fe)}$)** mmol $m^{-2}$ $d^{-1}$ | 0.004 | ± 0.002 | 0.001 | | 0.002 | | 0.0 | | 0.003 | | 0.0 | |
| **(15) P deficit to outbalance the P budget ($F_{P(deficit)}$)** mmol $m^{-2}$ $d^{-1}$ | - | | - | | 0.12 | - | 0.09 | - | 0.3 | - | - | |

* this study, **published data from Dale et al. (2015)

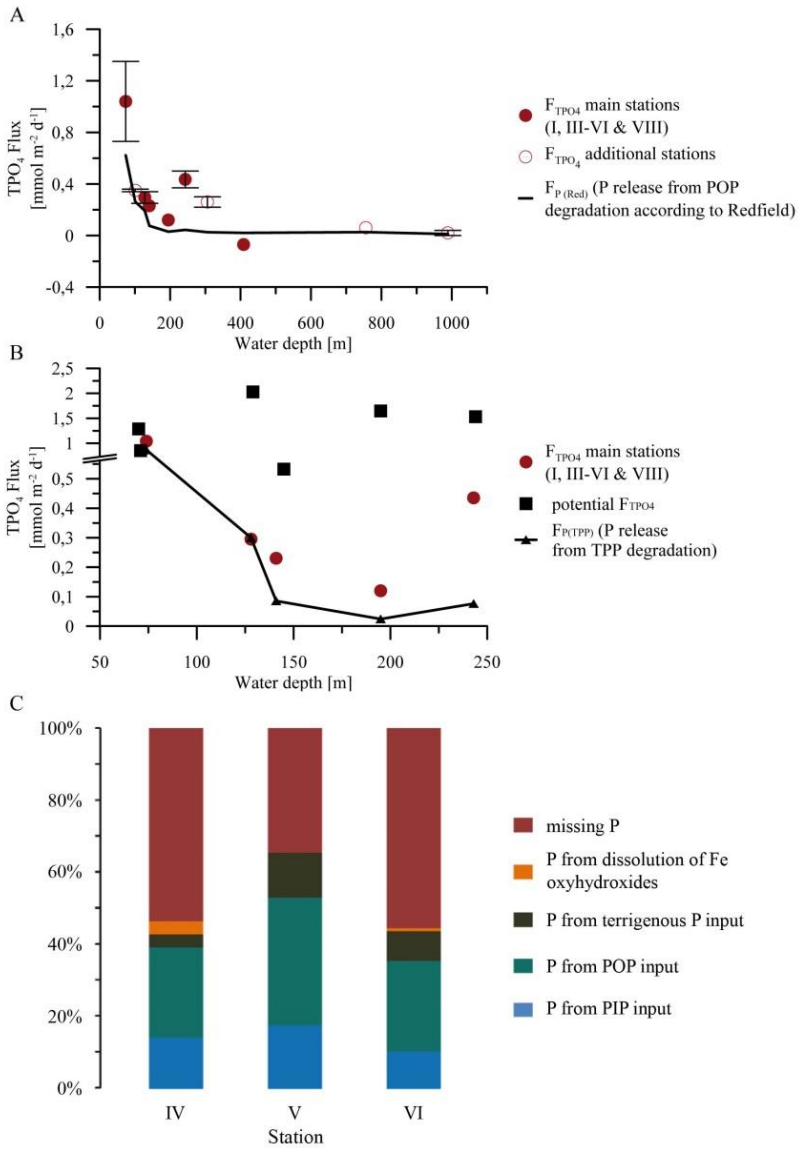


**Fig. 2.4A** Measured benthic $TPO_4$ fluxes (mmol $m^{-2}$ $d^{-1}$) at 12°S. The black line shows the theoretical $TPO_4$ flux generated from organic matter degradation with a Redfield POC/POP ratio of 106. **2.4B** Potential $TPO_4$ fluxes (mmol $m^{-2}$ $d^{-1}$) calculated from porewater profiles compared to the measured benthic $TPO_4$ fluxes (mmol $m^{-2}$ $d^{-1}$) at stations I to VIII (74 to 407 m). The black line with triangles depicts the $TPO_4$ flux that could be generated during degradation of total particulate phosphorus. **2.4C** P percentages of the different P sources and the missing P that is needed to maintain the measured $TPO_4$ release rates and P burial fluxes for stations IV, V and VI (141, 195 and 244 m) of transect section II. The missing P is assumed to be supplied by sulfide-oxidizing Marithioploca-related bacteria (see Discussion).

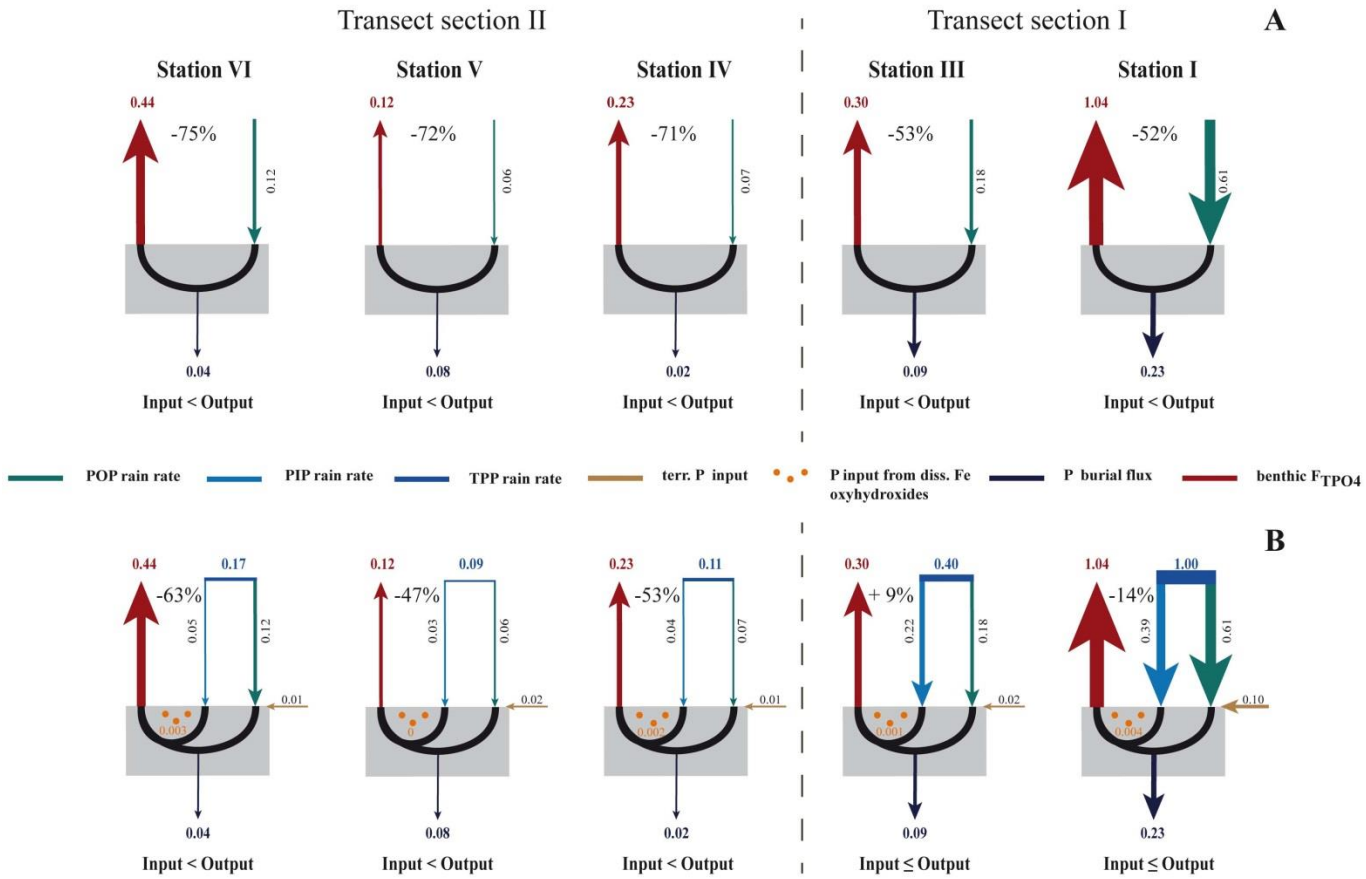


**Fig. 2.5** Mass balance calculations and measured benthic $TPO_4$ fluxes for stations I to VIII (74 to 407 m). All fluxes are in mmol $m^{-2}$ $d^{-1}$. **2.5A** POP rain rates, $TPO_4$ fluxes and P burial rates only. The number in percent denotes missing P needed to sustain the benthic $TPO_4$ fluxes. **2.5B** Mass balance calculations including the POP and PIP rain rates, the terrigenous P input, P release from the reductive dissolution of Fe (oxyhydr)oxides and the benthic $TPO_4$ fluxes into the bottom waters as well as the P burial rates.

**Additional P input**

Besides the particulate matter raining to the sediments, other potential other P sources can be considered. Firstly, riverine transported material from the continent may be an additional source of P to the sediments. Due to fast sinking speed and laterally dominated transport it is possible that this P fraction is at least underrepresented on the filter samples. In order to provide a maximum estimate for the contribution of the terrigenous P input to the sediments, this fraction was calculated using the mass accumulation rate of Al in the first centimeter of sediment and an average molar P/Al-ratio (Table 2.2) of 0.02 for riverine suspended particles (Viers et al., 2009). The resulting terrigenous P flux accounted for 5-19 % of the total P input, which is insufficient to explain the observed discrepancies in the P budget of transect section II (Table 2.4, Fig. 2.4C, 2.5B).

Laterally transported particles enriched in P from the very shallow shelf could be an additional P source (e.g. Jahnke, 1990). However, the particles would need to be strongly enriched in P, which is not the case. In addition, this would have to be reflected in the POC/TPP ratios of the surface sediments in transect section II (Fig. 2.2B). The ratios are not, or only slightly, enriched in TPP compared to the water-column particles, which leadsto the conclusion that lateral transport of P-enriched particles to the sediments is an unlikely candidate for the missing P source.

Another alternative is the existence of an additional PIP phase supplied by fast sinking material (e.g. P containing fish scales; Suess, 1981) that was not sampled during CTD casts, and hence underrepresented on our filter samples. Díaz-Ochoa et al. (2009) showed that fish P can make up to 20% of the total sedimentary P inventory in the shelf sediments of the Peruvian OMZ. Fish P input should be depicted in low sedimentary POC/TPP ratios compared to the water-column particles. Since this difference is not observed it is likely that fish debris can be ruled out for closing the P budget during the sampling campaign. Theoretically, sediments need to be composed of particles having POC/TPP ratios between 11 ± 1 and 25 ± 12 (Table 2.4) to maintain the measured P release rates in transect section II. It seems unlikely that the mismatch in the P mass balance is caused by additional particles deposited at the seabed since their POC/TPP ratio would need to be much lower than any value observed in our data set.

**Non steady state scenarios – internal sedimentary P pools**

Besides an additional P input to the sediments from the water column, episodic dissolution of particulate P within the sediment could contribute to the excess P release (Noffke et al., 2012). This could include P solubilized from Fe (oxyhydr)oxides or the degradation of internally stored polyphosphates within sulfide-oxidizing bacteria. Driving factors could include the temporal variability in bottom-water oxygen and nutrient concentrations induced by the passage of internal

Kelvin waves and/or interannual variability related to El Niño and La Niña (Guitérrez et al., 2008).

It is well recognized that the sedimentary cycles of Fe and P are strongly linked (e.g. Sundby et al., 1986). Fe (oxyhydr)oxides are expected to be important carriers for phosphorus from the water column to the sediments. Following dissolution of solid Fe minerals in the sediments, the adsorbed P is released to the porewaters. However, in the Peruvian OMZ, oxygen concentrations in the water column are generally below detection limit. Consequently, Fe (oxyhydr)oxides are likely already dissolved in the water column and not such an important P source to the sediments. An estimate of phosphate released during the reduction of Fe (oxyhydr)oxides can be calculated from the diffusive $Fe^{2+}$ fluxes and the molar Fe/P ratio typically found in Fe (oxyhydr)oxides. The diffusive $Fe^{2+}$ fluxes were in the range of 0 to 0.03 mmol $m^{-2}$ $d^{-1}$during the M92 cruise (Table 2.4) and the molar Fe/P ratio of Fe (oxyhydr)oxides in sediment is around 10 (Slomp et al., 1996). The calculation of the $TPO_4$ release rates from Fe (oxyhydr)oxides (Eq. 14 in Table 2.2) results in a flux of 0.003 mmol $PO_4^{3-}$ $m^{-2}$ $d^{-1}$ (Table 2.4, Fig. 4C and 5B), which is equivalent to less than 5% of the benthic P flux and burial flux.

An additional internally activated P pool is phosphate released from large sulfur-oxidizing bacteria, e.g. *Beggiatoa* (Sannigrahi and Ingall, 2005; Brock and Schulz-Vogt, 2011). These microorganisms store P in the form of intracellular polyphosphate granules when terminal electron acceptors for sulfide oxidation are available (oxic conditions) and release dissolved P during periods when these oxidants are scarce (anoxic conditions). Hence, it is generally assumed that they strongly affect benthic $TPO_4$ fluxes in a system with frequently changing bottom water redox conditions (Ingall and Jahnke, 1994; Sannigrahi and Ingall, 2005; Schulz and Jørgensen, 2005; Brock and Schulz-Vogt, 2011; Dale et al., 2013).Polyphosphates have been shown to an important P pool in the sediments of highly productive upwelling areas (Kraal et al., 2015). Along the depth transect at Peru, dense mats of sulfur bacteria related to Marithioploca were observed on the sediments during video-launched MUC and benthic lander deployments down to 300 m water depth (Dale et al., 2015). Similar findings extended distributions of microbial mats along a latitudinal transect at 11°S off were also previously described by Mosch et al. (2012) and Gutiérrez et al. (2008). Although, these organisms are not known to store polyphosphates like their close relatives, *Beggiatoa* spp. and *Thiomargarita* spp. (Høgslund et al., 2009; Holmkvist et al., 2010), our findings provide circumstantial indications for P uptake and release by Marithioploca-related bacteria.

Firstly, we found that the relative abundance of copies of Marithioploca-related bacteria per $g^{-1}$ sediment and the measured benthic $TPO_4$ release rates correlate linearly ($r^2$=0.92, Fig. 2.6). This finding supports the suggestion that bacteria exert an important control on benthic P fluxes.

Secondly, a comparison of the in situ measured benthic P fluxes and the diffusive P fluxes calculated from the difference of the $TPO_4$ bottom water concentration and the $TPO_4$ porewater concentration of the surface sediments revealed large differences (Fig. 2.4B). Such a difference could be explained by the lysis of bacterial cells during sample retrieval followed by the release of the internally stored polyphosphate pool into the porewater. Following this argument, the diffusive P fluxes cannot be taken as real fluxes, but as a measure for potential maximum release rates of P by Marithioploca-related bacteria. It should be noted that, the potential fluxes are more than sufficient to compensate for the missing P fraction in transect section II (ranging from 0.5 to 1.6 mmol $m^{-2}$ $d^{-1}$; Table 2.4, Fig. 2.4B).

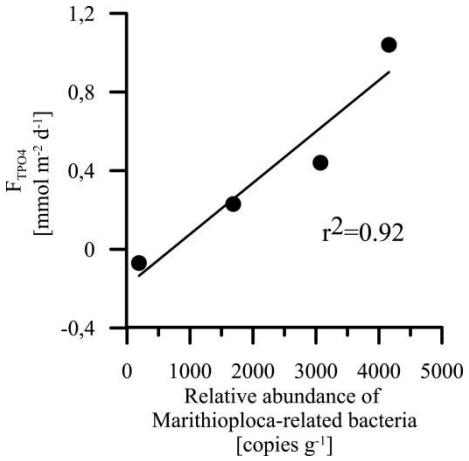


**Fig. 2.6** Measured $TPO_4$ fluxes versus relative abundance of Marithioploca in cells $g^{-1}$ in the upper 5 cm of the sediment. Highest abundance and $TPO_4$ flux was found at station I. The other data points are for the stations IV, VI and VIII (with decreasing abundance and $TPO_4$ flux).

In addition to the established porewater extraction procedure, we carried out freeze/thaw experiments to quantify the amount of P stored in sulfide-oxidizing bacteria (see method section 3.7). The released polyphosphates from the microbial cells after repeated freeze/thaw cycles are rapidly hydrolyzed to orthophosphate under acidic conditions (Jager and Heyns, 1998). Hence, the standard method to determine phosphate in the porewaters using acidic reagents will favor the hydrolysis of polyphosphates enabling us the measure its concentration in the porewaters after conducting the experiments. However, this method cannot exclude P release from other bacteria and, possibly, foraminifera in the sediments. A comparison of the porewater phosphate concentrations and the experiment results shows that the amount of the internal P reservoir is as twice as high as the porewater P concentration in transect section I and more than ten times higher in section II (Fig. 7). These results are coincident with the findings from the mass balance approach, where the largest discrepancies occur in transect section II and are another indication for the bacterial impact on the benthic P release. Interestingly, the highest phosphate concentrations after the freeze/thaw experiments were found at station VIII (407 m) with

abundant foraminifera rather than sulfide-oxidizing bacteria. Hence, we assume that the sulfide-oxidizing bacteria at station IV, V and VI (141, 194 and 244 m) and, potentially, the foraminifera observed at station VIII (407 m) are contributing phosphate to the porewaters. To our knowledge, P storage by foraminifera has not been demonstrated previously and awaits further study.

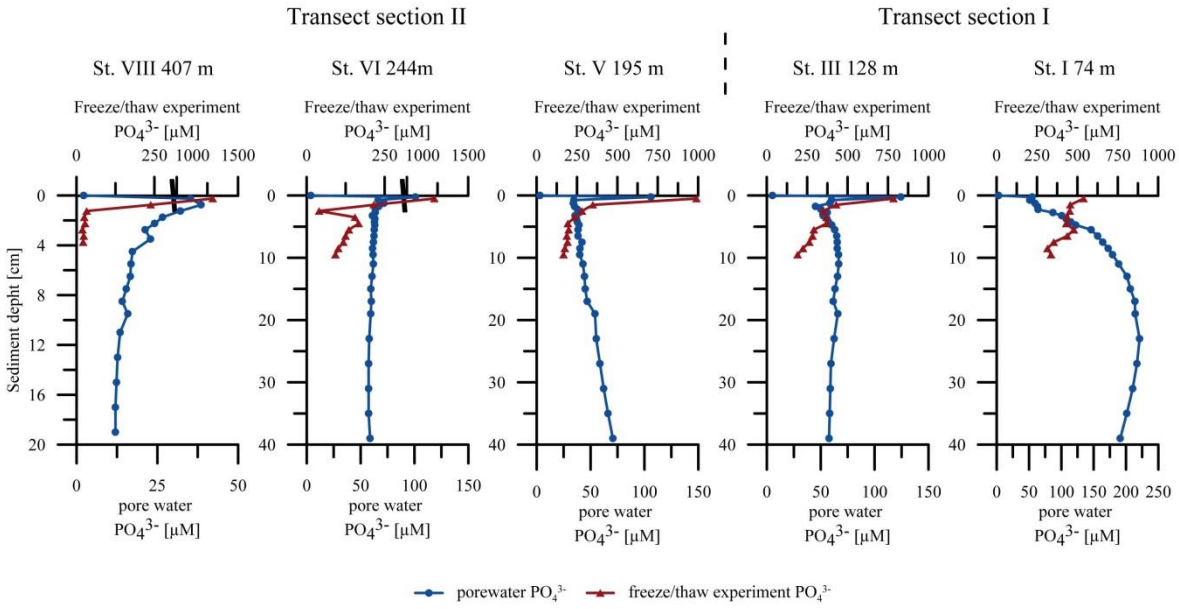


**Fig. 2.7** Comparison of pore water $PO_4^{3-}$ concentrations before (blue) and after the freeze/thaw experiments (red) in µmol $L^{-1}$.

It remains to be shown how these mechanisms play out in detail (e.g. nutrient concentration thresholds, P uptake and release time scales by Marithioploca-related bacteria) and how they impact benthic P release in oxygen and nitrate deficient environments on longer time scales. Summarizing the results of the mass balance, it should be noted, that, even with the relevant data on particulate P rain rates, the benthic P mass balance for the core of the Peruvian OMZ is imbalanced and requires an additional P source to maintain the benthic $TPO_4$ fluxes. We suggest that sulfur bacteria make an important contribution to this missing P source.

**Indications for active phosphorite formation**

In contrast to the stations between 74 and 244 m water depth characterized by P release, data from station VIII at 407 m water depth indicate the uptake of phosphate from the bottom water. To our best knowledge, this is the first time that a downward flux of dissolved phosphate from bottom waters into phosphorite-bearing surface sediments has been documented by in situ benthic flux measurements. Furthermore, the PIP concentrations in the surface sediments of station VIII (Fig. 2.2A) were 10 to 60 times higher compared to the shallower stations where P was released from the sediments. Taken together, these observations indicate that a PIP phase, likely phosphorite, is

precipitating from the porewater phosphate at the time of sampling. This is also reflected in decreasing porewater phosphate concentrations (Fig. 2.7).

Arning et al. (2008) presented investigations on phosphorites recovered from the Peruvian OMZ including a station at 12°S from the same water depth (~ 400 m) close to sampling station VIII. The suboxic bottom waters and low sedimentation rates in that area seem to be favorable for phosphorite formation close to the sediment-water interface (Arning et al., 2009b). Cosmidis et al. (2013) suggested three mechanisms how high porewater phosphate concentrations that are essential for the phosphogenesis can be generated in the sediments: (1) remineralization of organic matter mainly through bacterial sulfate reduction releasing phosphate to the porewaters, (2) reductive dissolution of Fe (oxyhydr)oxides and the release of adsorbed P and (3) synthesis of internally stored polyphosphates by large sulfide-oxidizing bacteria. Using the same mass balance approach as presented before, we calculate a P accumulation rate of 33 ± 4 mmol $m^{-2}$ $yr^{-1}$ at station VIII where most of the P is derived from ambient bottom waters (26 mmol $m^{-2}$ $yr^{-1}$). Hence, our data suggest that the phosphorite nodules at this station contain phosphate that originates predominantly from ambient bottom waters. Additionally, as already mentioned, sediments at station VIII were covered by benthic foraminifera instead of mat-forming sulfur bacteria. The release of phosphate from frozen samples from this site may indicate that these foraminifera are a source for polyphosphates (see section 3.7 and Fig. 2.7). Our observations suggest that benthic foraminifera rather than bacterial mats might facilitate the uptake of bottom water phosphate and the formation of phosphorites at this station. However, this remains an open question and should be addressed in future field campaigns.

The P uptake rate of ~ 26 mmol P $m^{-2}$ $yr^{-1}$ derived from our lander measurements may be compared to previous estimates on phosphorite growth rates in the area. Dating of phosphoric laminites yields a P uptake rate of only 3 mmol P $m^{-2}$ $yr^{-1}$ for a ca. 1 Ma old nodule (Arning et al., 2009a). These different fluxes may be at least partly explained by the methodological difference (present flux measurement vs. long-term average). However, growth rates determined on modern nodules are broadly consistent with our flux measurements (Burnett et al., 1982).

## 2.6 Conclusions

This study aimed to identify the P sources of benthic P release in the Peruvian OMZ. We determined the rain rates of particulate organic phosphorus and particulate inorganic phosphorus as well as benthic P release rates and P burial fluxes.

Our calculations revealed that within the core OMZ particulate phosphorus rain rates cannot account for measured benthic P fluxes and burial fluxes. From systematic analysis of potential P sources, we conclude that periodic P release from sulfur bacteria that store and release P under

oscillation redox conditions could strongly modulate benthic P fluxes, and hence explain for the missing P source. We visited the area during austral summer when oxygen and nitrate levels were depleted by high export production and respiration. It is possible that the Peruvian OMZ was less reducing prior to our sampling period due to lower respiration rates and/or better ventilation. Thus, we propose that the bacterial mats on the Peruvian margin act as phosphorus capacitors being, discharged during austral summer and recharged during other periods of the year when bottom waters are less reducing, as previously proposed in Dale et al. (2013). This hypothesis could be tested by studying the seasonality of benthic fluxes in the Peruvian up-welling system and P dynamics within the bacterial community.

In addition, measurements at one station (407 m water depth) showed clear indications for the uptake of dissolved phosphate by the sediments facilitating phosphorite formation. Our data imply that most of the P accumulating in these authigenic minerals originates from ambient bottom waters. Since this site was marked by a high abundance of benthic foraminifera, we speculate that phosphate uptake and phosphorite formation may be linked to the presence of these organisms. This requires further study.

There was no clear preferential mineralization of POP relative to POC with depth in the water column. POC/TPP ratios in both water-column particles and sediments were close to Redfield at most sites in the Peruvian OMZ. This observation strongly suggests that the relative burial efficiencies of POC and TPP are similar under low oxygen conditions. Importantly, it further shows that the sediments underlying the anoxic waters on the Peru margin are not depleted in P compared to Redfield. Rather, they are depleted relative to sediments underlying oxic waters, which show POC/TPP ratios well below Redfield (Wallmann, 2010). Thus, at Peru, a lack of oxygen promotes the intensified release of dissolved P from sediments, whilst preserving a POC/TPP burial ratio that is similar to Redfield.

Our data support the hypothesis that benthic P release is linked via a positive feedback loop to intensified primary production in the surface water and oxygen demand in the water column during periods where bottom water redox conditions promote the release of P from the sediments. However, this positive feedback is limited by the formation of authigenic inorganic P phases that maintains the long-term average POC/TPP burial ratio close to Redfield.

## Author contribution

UL, AD and SS supported the shipboard work, geochemical analysis and contributed to the manuscript. CH, KW and AN helped with fruitful discussions related to the manuscript and helped with the manuscript preparation. CL carried out the molecular analysis and contributed to the manuscript.

## Acknowledgements

We are very grateful to the crew of RV *Meteor* during cruise M92 for the support of. Our thanks also go to A. Petersen, M. Türk and S. Cherednichenko for their assistance in deploying the landers. For their enthusiastic help and cooperation, we thank B. Domeyer, S. Kriwanek, A. Bleyer, R. Suhrberg, S. Trinkler and V. Thoenissen for biogeochemical analyses on board and in the home laboratory. Furthermore, we appreciate Christopher Voigt from the University of Bremen for carrying out XRD analysis. This work is a contribution of the Sonderforschungsbereich 754 "Climate – Biogeochemistry Interactions in the Tropical Ocean" (www.sfb754.de) which is supported by the Deutsche Forschungsgemeinschaft.

## 2.7 References

Anderson, L. D., Delaney, M. L., and Faul, K. L.: Carbon to phosphorus ratios in sediments: Implications for nutrient cycling, Global Biogeochemical Cycles, 15(1), 65-79, 2001.

Arning, E. T., Birgel, D., Schulz-Vogt, H. N., Holmkvist, L., Jørgensen, B. B., Larson, A., and Peckmann, J.: Lipid Biomarker Patterns of Phosphogenic Sediments from Upwelling Regions, Geomicrobiology Journal, 25(2), 69-82, 2008.

Arning, E. T., Birgel, D., Brunner, B., and Peckmann, J.: Bacterial formation of phosphatic laminites off Peru, Geobiology, 7(3), 295-307, 2009a.

Arning, E. T., Lückge, A., Breuer, C., Gussone, N., Birgel, D., and Peckmann, J.: Genesis of phosphorite crusts off Peru, Marine Geology, 262(1–4), 68-81, 2009b.

Asahi, T., Ichimi, K., Yamaguchi, H., and Tada, K.: Horizontal distribution of particulate matter and its characterization using phosphorus as an indicator in surface coastal water, Harima-Nada, the Seto Inland Sea, Japan, Journal of Oceanography, 70(3), 277-287, 2014.

Aspila, K. I., Agemian, H., and Chau, A. S. Y.: A semi-automated Method for the Determination of Inorganic, Organic and Total Phosphate in Sediments, Analyst, 101, 187-197, 1976.

Baturin, G. N.: Issue of the relationship between primary productivity of organic carbon in ocean and phosphate accumulation (Holocene– Late Jurassic), Lithol. Miner. Resour., 42(4), 318–348, 2007, doi:10.1134/ S0024490207040025.

Benitez-Nelson, C. R.: The biogeochemical cycling of phosphorus in marine systems, Earth-Science Reviews, 51(1–4), 109-135, 2000.

Benitez-Nelson, C. R., O'Neill, L., Kolowith, L. C., Pellechia, P., and Thunell, R.: Phosphonates and particulate organic phosphorus cycling in an anoxic marine basin, Limnol. Ocean., 49(5), 1593-1604, 2004.

Benitez-Nelson, C. R., O'Neill Madden, L. P., Styles, R. M., Thunell, R. C., and Astor, Y.: Inorganic and organic sinking particulate phosphorus fluxes across the oxic/anoxic water column of Cariaco Basin, Venezuela, Marine Chemistry, 105(1–2), 90-100, 2007.

Bertics, V. J., Löscher, C. R., Salonen, I., Dale, A. W., Gier, J., Schmitz, R. A., and Treude, T.: Occurrence of benthic microbial nitrogen fixation coupled to sulfate reduction in the seasonally hypoxic Eckernförde Bay. Baltic Sea. Biogeosciences. 10, 1243-1258, 2013.

Boudreau, B. P.: The diffusive tortuosity of fine-grained unlithified sediments. Geochim. Cosmochim. Acta 60, 3139–3142, 1996.

Brock, J., and Schulz-Vogt, H. N.: Sulfide induces phosphate release from polyphosphate in cultures of a marine Beggiatoa strain, ISME J, 5(3), 497-506, 2011.

Burnett, W. C., Beers, M. J., and Roe, K. K.: Growth Rates of Phosphate Nodules from the Continental Margin Off Peru, Science, 215(4540), 1616-1618, 1982.

Colman, A. S., Mackenzie, F. T., and Holland, H. D.: Redox Stabilization of the Atmosphere and Oceans and Marine Productivity. Science 275, 406-408. 1997.

Compton, J., Mallinson, D., Glenn, C., Filippelli, G., Föllmi, K., Shields, G., and Zanin, Y.: Variations in the global phosphorus cycle, in Marine authigenesis: from global to microbial, SEPM (Society for Sedimentary Geology), 21-33, 2000.

Cosmidis, J., Benzerara, K., Menguy, N., and Arning, E.: Microscopy evidence of bacterial microfossils in phosphorite crusts of the Peruvian shelf: Implications for phosphogenesis mechanisms, Chemical Geology, 359, 10-22, 2013.

Dale, A., Bertics, W., V. J., Treude, T., Sommer, S., and Wallmann, K.: Modeling benthic–pelagic nutrient exchange processes and porewater distributions in a seasonally hypoxic sediment: evidence for massive phosphate release by *Beggiatoa*? Biogeosciences 10, 629-651, 2013.

Dale, A. W., Sommer, S., Lomnitz, U., Montes, I., Treude, T., Liebetrau, V., Gier, J., Hensen, C., Dengler, M., Stolpovsky, K., Bryant, L. D., and Wallmann, K.: Organic carbon production, mineralisation and preservation on the Peruvian margin, Biogeosciences, 12(5), 1537-1559, 2015.

Delaney, M. L.: Phosphorus accumulation in marine sediments and the oceanic phosphorus cycle, Global Biogeochemical Cycles, 12(4), 563-572, 1998.

Díaz-Ochoa, J. A., Lange, C. B., Pantoja, S., De Lange, G. J., Gutierrez, D., Munoz, P., and Salamanca M.: Fish scales in sediments from off Callao, central Peru, Deep-Sea Res. Part II-Top. Stud. Oceanogr., 56(16), 1113-1124, 2009.

Faul, K. L., Paytan, A., and Delaney, M. L.: Phosphorus distribution in sinking oceanic particulate matter, Marine Chemistry, 97(3–4), 307-333, 2005.

Filippelli, G. M.: The global phosphorus cycle, in Phosphates: Geochemical, Geobiological, and Materials Importance, edited by M. Kohn, J. Rakovan and J. Hughes, pp. 391-425, Reviews in Mineralogy&Geochemistry, 2002.

Filippelli, G. M.:The Global Phosphorus Cycle: Past, Present, and Future, Elements, 4(2), 89-95, 2008.

Föllmi, K. B.: The phosphorus cycle, phosphogenesis and marine phosphate-rich deposits, Earth-Science Reviews, 40(1–2), 55-124, 1996.

Franz, J., Krahmann, G., Lavik, G., Grasse, P., Dittmar, T., and Riebesell, U.: Dynamics and stoichiometry of nutrients and phytoplankton in waters influenced by the oxygen minimum zone in the eastern tropical Pacific, Deep Sea Research Part I: Oceanographic Research Papers, 62(0), 20-31, 2012.

Froelich, P. N., Arthur, M. A., Burnett, W. C., Deakin, M., Hensley, V., Jahnke, R., Kaul, L., Kim, K. H., Roe, K., Soutar, A., Vathakanon, C.: Early diagenesis of organic matter in Peru continental margin sediments: Phosphorite precipitation, Marine Geology, 80(3–4), 309-343, 1988.

Fuenzalida, R., Schneider, W., Garcés-Vargas, J., Bravo, L., and Lange, C.: Vertical and horizontal extension of the oxygen minimum zone in the eastern South Pacific Ocean, Deep Sea Research Part II: Topical Studies in Oceanography, 56(16), 992-1003, 2009.

Ganeshram, R. S., Pedersen, T. F., Calvert, S., and Francois, R.: Reduced nitrogen fixation in the glacial ocean inferred from changes in marine nitrogen and phosphorus inventories, Nature, 415(6868), 156-159, 2002.

Glenn, C. R., and Arthur, M. A.: Petrology and major element geochemistry of Peru margin phosphorites and associated diagenetic minerals: Authigenesis in modern organic-rich sediments, Marine Geology, 80(3–4), 231-267, 1988.

Goldhammer, T., Bruchert, V., Ferdelman, T. G., and Zabel, M.: Microbial sequestration of phosphorus in anoxic upwelling sediments, Nature Geosci, 3(8), 557-561, 2010.

Govindaraju K.: Compilation of working values and sample description for 383 geostandards. Geostandard Newslett. 18, 1–158, 1994.

Graco, M., Purca, S., Dewitte, B., Morón, O., Ledesma, J., Flores, G., Castro, C., and Gutiérrez, D.: The OMZ and nutrients features as a signature of interannual and low frequency variability off the peruvian upwelling system, Biogeosciences Discuss., 2016, 1-36, 2016.

Grasshoff, K., Erhardt, M., Kremling, K.: Methods of seawater analysis, 3rd ed. Wiley-VCH (1999).

Gutiérrez, D., Enríquez, E., Purca, S., Quipúzcoa, L., Marquina, R., Flores, G., and Graco, M.: Oxygenation episodes on the continental shelf of central Peru: Remote forcing and benthic ecosystem response, Progress in Oceanography, 79(2–4), 177-189, 2008.

Hedges, J. I., Hu, F. S., Devol, A. H., Hartnett H. E., Tsamakis, E. and Keil, R. G.: Sedimentary organic matter preservation: A test for selective degradation under oxic conditions. American Journal of Science 299, 529-555. 1999.

Høgslund, S., Revsbech, N. P., Kuenen, J. G., Jorgensen, B. B., Gallardo, V. A., Vossenberg, J. v. d., Nielsen, J. L., Holmkvist, L., Arning, E. T., and Nielsen, L. P.: Physiology and behaviour of marine Thioploca, ISME J, 3(6), 647-657, 2009.

Holmkvist, L., Arning, E. T., Küster-Heins, K., Vandieken, V., Peckmann, J., Zabel, M., and Jørgensen, B. B.: Phosphate geochemistry, mineralization processes, and Thioploca distribution in shelf sediments off central Chile, Marine Geology, 277(1–4), 61-72, 2010.

Ingall, E. D., and Van Cappellen P.: Relation between sedimentation rate and burial of organic phosphorus and organic carbon in marine sediments, Geochimica et Cosmochimica Acta, 54(2), 373-386, 1990.

Ingall, E., and Jahnke R.: Evidence for enhanced phosphorus regeneration from marine sediments overlain by oxygen depleted waters, Geochimica et Cosmochimica Acta, 58(11), 2571-2575, 1994.

Ingall, E., and R. Jahnke: Influence of water-column anoxia on the elemental fractionation of carbon and phosphorus during sediment diagenesis, Marine Geology, 139(1–4), 219-229, 1997.

Ingall, E., Kolowith, L., Lyons, T., and Hurtgen, M.: Sediment carbon, nitrogen and phosphorus cycling in an anoxic fjord, Effingham Inlet, British Columbia, American Journal of Science, 305(3), 240-258, 2005.

Ingall, E. D.: Biogeochemistry: Phosphorus burial, Nature Geosci, 3(8), 521-522, 2010.

de Jager, H.-J., and Heyns, A. M.: Kinetics of Acid-Catalyzed Hydrolysis of a Polyphosphate in Water, The Journal of Physical Chemistry A, 102(17), 2838-2841, 1998.

Jahnke, R. A.: Early diagenesis and recycling of biogenic debris at the seafloor, Santa Monica Basin, California, Journal of Marine Research, 48(2), 413-436, 1990.

Jilbert, T., Slomp, C. P., Gustafsson, B. G., and Boer W.: Beyond the Fe-P-redox connection: preferential regeneration of phosphorus from organic matter as a key control on Baltic Sea nutrient cycles, Biogeosciences, 8(6), 1699-1720, 2011.

Kraal, P., Slomp, C. P., Reed, D. C, Reichart, G.-J., and Poulton, S. W.: Sedimentary phosphorus and iron cycling in and below the oxygen minimum zone of the northern Arabian Sea, Biogeosciences, 9(7), 2603-2624, 2012.

Kraal, P., Bostick, B. C., Behrends, T., Reichart, G.-J., and Slomp, C. P.: Characterization of phosphorus species in sediments from the Arabian Sea oxygen minimum zone: Combining sequential extractions and X-ray spectroscopy, Marine Chemistry, 168(0), 1-8, 2015.

Krissek, L. A., Scheidegger, K. F., and Kulm, L. D.: Surface sediments of the Peru-Chile continental margin and the Nazca plate, Geological Society of America Bulletin, 91(6), 321-331, 1980.

Li, Y.-H. and Gregory, S.: Diffusion of ions in sea water andin deep-sea sediments. Geochim. Cosmochim. Acta 38, 703–714, 1974.

Loh, A. N., and Bauer, J. E.: Distribution, partitioning and fluxes of dissolved and particulate organic C, N and P in the eastern North Pacific and Southern Oceans, Deep Sea Research Part I: Oceanographic Research Papers, 47(12), 2287-2316, 2000.

Löscher, C. R., Kock, A., Könneke, M., LaRoche, J., Bange, H. W., and Schmitz, R. A.: Production of oceanic nitrous oxide by ammonia-oxidizing archaea. Biogeosciences. 9. 2419-2429, 2012.

Lyons, G., Benitez-Nelson, C. R., and Thunell, R. C.: Phosphorus composition of sinking particles in the Guaymas Basin, Gulf of California, Limnology and Oceanography, 56(3), 1093-1105, 2011.

McManus, J., Berelson, W. M., Coale, K. H., Johnson, K. S., and Kilgore, T. E.: Phosphorus regeneration in continental margin sediments, Geochimica et Cosmochimica Acta, 61(14), 2891-2907, 1997.

Moffitt, S. E., Moffitt, R. A., Sauthoff, W., Davis, C. V., Hewett, K., and Hill T. M.: Paleoceanographic Insights on Recent Oxygen Minimum Zone Expansion: Lessons for Modern Oceanography, PLoS ONE, 10(1), 2015.

Mort, H. P., Slomp, C. P., Gustafsson, B. G., and Andersen, T. J.: Phosphorus recycling and burial in Baltic Sea sediments with contrasting redox conditions, Geochimica et Cosmochimica Acta, 74(4), 1350-1362, 2010.

Mosch, T., Sommer, S., Dengler, M., Noffke, A., Bohlen, L., Pfannkuche, O., Liebetrau, V., and Wallmann, K.: Factors influencing the distribution of epibenthic megafauna across the Peruvian oxygen minimum zone, Deep Sea Research Part I: Oceanographic Research Papers, 68(0), 123-135, 2012.

Noffke A., Hensen, C., Sommer, S., Scholz, F., Bohlen L., Mosch, T., Graco M., and Wallmann K.: Benthic iron and phosphorus fluxes across the Peruvian oxygen minimum zone, Limnology and Oceanography, 57(3), 851-867, 2012.

Noffke A.: Phosphorus cycling in anoxic sediments, PhD dissertation, University of Kiel, 2014.

Noffke, A., Sommer, S., Dale, A.W., Hall, P.O.J., and Pfannkuche, O.: Benthic nutrient fluxes in the Eastern Gotland Basin (Baltic Sea) with particular focus on microbial mat ecosystems, Journal of Marine Systems, 2016, doi: 10.1016/j.jmarsys.2016.01.007.

Paytan, A., Cade-Menun, B. J., McLaughlin, K., and Faul, K. L.: Selective phosphorus regeneration of sinking marine particles: evidence from 31P-NMR, Marine Chemistry, 82(1–2), 55-70, 2003.

Paytan, A., and McLaughlin, K.: The Oceanic Phosphorus Cycle, Chemical Reviews, 107(2), 563-576, 2007.

Pennington, J. T., Mahoney, K. L., Kuwahara, V. S., Kolber, D. D., Calienes, R., and Chavez, F. P.: Primary production in the eastern tropical Pacific: A review, Progress in Oceanography, 69(2–4), 285-317, 2006.

Redfield, A. C., Ketchum, B. H., and Richards, F. A.: The influence of organisms on the composition of seawater, in The Sea, Academic Press, London, 26-77, 1963.

Reimers, C. E., and Suess, E.: Spatial and temporal patterns of organic matter accumulation on the Peru continental margin, in Coastal Upwelling: Part B. Sedimentary Record of Ancient Coastal Upwelling, edited by E. Suess and J. Thiede, pp. 311-346, Plenum Press, New York, 1983.

Roth, R., S. P. Ritz, S. P. and Joos, F.: Burial-nutrient feedbacks amplify the sensitivity of atmospheric carbon dioxide to changes in organic matter remineralisation. Earth Syst. Dynam., 5, 321-343, 2014.

Ruttenberg, K. C., and Berner, R. A.: Authigenic apatite formation and burial in sediments from non-upwelling, continental margin environments, Geochimica et Cosmochimica Acta, 57(5), 991-1007, 1993.

Ruttenberg, K. C.: The Global Phosphorus Cycle, In: Treatise on Geochemistry, Turekian K.K. and Holland D.J., (eds), Elsevier, 585–643, 2003.

Ruttenberg, K. C.: The Global Phosphorus Cycle. In Treatise on Geochemistry, H. D. Holland and K. K. Turekian (eds), Elsevier, 499-558, 2014.

Salman, V., Amann R., Girnth A.-C., Polerecky L., Bailey J. V., Høgslund S., Jessen G., Pantoja S., and Schulz-Vogt H. N.: A single-cell sequencing approach to the classification of large, vacuolated sulfur bacteria, Systematic and Applied Microbiology, 34(4), 243-259, 2011.

Salman, V., Amann, R, Shub, D. A., Schulz-Vogt, H. N.: Multiple self-splicing introns in the 16S rRNA genes of giant sulfur bacteria, PNAS, 109(11), 4203-4208, 2012, doi:10.1073/pnas.1120192109.

Sannigrahi, P., and Ingall, E.: Polyphosphates as a source of enhanced P fluxes in marine sediments overlain by anoxic waters: Evidence from 31P NMR, Geochemical Transactions, 6(3), 52, 2005.

Sanudo-Wilhelmy, S. A., Tovar-Sanchez, A., Fu, F.-X., Capone, D. G., Carpenter, E. J., and Hutchins, D. A.: The impact of surface-adsorbed phosphorus on phytoplankton Redfield stoichiometry, Nature, 432(7019), 897-901, 2004.

Schenau, S. J., and De Lange, G. J.: A novel chemical method to quantify fish debris in marine sediments, Limnology and Oceanography, 45(4), 963-971, 2000.

Schenau, S. J., and De Lange, G. J.: Phosphorus regeneration vs. burial in sediments of the Arabian Sea, Marine Chemistry, 75(3), 201-217, 2001.

Scholz, F., Hensen, C., Noffke, A., Rohde, A., Liebetrau, V., and Wallmann, K.: Early diagenesis of redox-sensitive trace metals in the Peru upwelling area – response to ENSO-related oxygen fluctuations in the water column, Geochimica et Cosmochimica Acta, 75(22), 7257-7276, 2011.

Schulz, H. N., and Jørgensen, B. B.: Thiomargarita, In Krieg, N. R., J. T. Staley, and D. J. Brenner (ed), Bergey's Manual of Determinative Bacteriology, Vol. 2, part B, Springer-Verlag, Berlin, Heidelberg, New York, 2005.

Schulz, H. N., and Schulz, H. D.: Large Sulfur Bacteria and the Formation of Phosphorite, Science, 307(5708), 416-418, 2005.

Schunck, H., Lavik, G., Desai, D. K., Großkopf, T., Kalvelage, T., Löscher, C. R., Paulmier, A., Contreras, S., Siegel, H., Holtappels, M., Rosenstiel, P., Schilhabel, M. B., Graco, M., Schmitz, R. A., Kuypers, M. M. M., and LaRoche, J.: Giant Hydrogen Sulfide Plume in the Oxygen Minimum Zone off Peru Supports Chemolithoautotrophy, PLoS ONE 8(8), 2013.

Sekula-Wood, E., Benitez-Nelson, C. R., Bennett, M. A., and Thunell R.: Magnitude and composition of sinking particulate phosphorus fluxes in Santa Barbara Basin, California, Global Biogeochemical Cycles, 26(2), GB2023, 2012.

Slomp, C. P., Van der Gaast, S. J., and Van Raaphorst, W.: Phosphorus binding by poorly crystalline iron oxides in North Sea sediments, Marine Chemistry, 52(1), 55-73, 1996.

Slomp, C. P., Malschaert, J. F. P., and Van Raaphorst, W.: The role of adsorption in sediment-water exchange of phosphate in North Sea continental margin sediments, Limnol. Ocean., 43(5), 832-846, 1998.

Slomp, C. P., and Van Cappellen, P.: The global marine phosphorus cycle: sensitivity to oceanic circulation, Biogeosciences, 4(2), 155-171, 2007.

Sommer, S., Linke, P., Pfannkuche, O., Schleicher, T., v. Deimling, S., Reitz, A., Haeckel, M., and Hensen, C.: Seabed methane emissions and the habitat of frenulate tubeworms on the Captain Arutyunov mud volcano (Gulf of Cadiz), Marine Ecology Progress Series, 382, 69-86, 2009.

Sommer, S., Gier, J., Treude, T., Lomnitz, U., Dengler, M., Cardich, J. and Dale, A.: Depletion of oxygen, nitrate and nitrite in the Peruvian oxygen minimum zone cause an imbalance of benthic nitrogen fluxes. Deep-Sea Research Part I, 113-122, 2016.

Stramma, L., Johnson, G. C., Sprintall, J., and Mohrholz, V.: Expanding Oxygen-Minimum Zones in the Tropical Oceans, Science, 320(5876), 655-658, 2008.

Strub, P. T., Mesias, J. M., Montecino, V., Ontecino, R., and Salinas S.: Coastal ocean circulation of western South. America, in The Sea, edited by A. R. R. a. K. H. Brink, pp. 273–313, Wiley, 1998.

Suess, E.: Phosphate regeneration from sediments of the Peru continental margin by dissolution of fish debris, Geochimica et Cosmochimica Acta, 45(4), 577-588, 1981.

Suess, E., Kulm, L. D., and Killingley, J. S.: Coastal upwelling and a history of organic rich mudstone deposition off Peru., in Marine Petroleum Source rocks, edited by J. Brooks and A. J. Fleet, pp. 1129-1145, Geological Society Spec, 1987.

Suess, E., and von Huene, R.: Ocean Drilling Program Leg 112, Peru continental margin: Part 2, Sedimentary history and diagenesis in a coastal upwelling environment, Geology, 16(10), 939-943, 1988.

Sundby, B., Anderson, L. G., Hall, P. O. J., Iverfeldt, Å., van der Loeff, M. M. R., and Westerlund, S. F. G.: The effect of oxygen on release and uptake of cobalt, manganese, iron and phosphate at the sediment-water interface, Geochimica et Cosmochimica Acta, 50(6), 1281-1288, 1986.

Tamura K., Stecher, G., Peterson, D., Filipski, A. and Kumar, S.: MEGA6, Molecular Evolutionary Genetics Analysis Version 6.0. Molecular Biology and Evolution 30: 2725-2729, 2013.

Teske, A., Ramsing, N. B., Küver, J., and Fossing, H.: Phylogeny of Thioploca and Related Filamentous Sulfide-Oxidizing Bacteria, Systematic and Applied Microbiology, 18(4), 517-526, 1995.

Tsandev, I., Reed, D. C., and Slomp, C. P.: Phosphorus diagenesis in deep-sea sediments: Sensitivity to water column conditions and global scale implications, Chemical Geology, 330–331(0), 127-139, 2012.

Van Cappellen, P., and Ingall, E. D.: Redox Stabilization of the Atmosphere and Oceans by Phosphorus-Limited Marine Productivity, Science, 271(5248), 493-496, 1996.

Viers, J., Dupré, B., and Gaillardet, J.: Chemical composition of suspended sediments in World Rivers: New insights from a new database, Science of The Total Environment, 407(2), 853-868, 2009.

Wallmann, K.: Feedbacks between oceanic redox states and marine productivity: A model perspective focused on benthic phosphorus cycling, Global Biogeochemical Cycles, 17(3), 2003.

Wallmann, K.: Phosphorus imbalance in the global ocean?, Global Biogeochemical Cycles, 24(4), 2010.

# 3 Benthic phosphate and iron fluxes in the Mauritanian upwelling

U. Lomnitz[1], C. Hensen[1], A. W. Dale[1], F. Scholz[1], D. Clemens[1], S. Sommer[1], A. Noffke[2] and K. Wallmann[1]

[1]GEOMAR Helmholtz-Centre for Ocean Research Kiel, Wischhofstr. 1-3, 24148 Kiel

[2]Institut für Seenforschung (ISF) der LUBW, Argenweg 50/1, 88085 Langenargen, Germany

Correspondence to: Ulrike Lomnitz (ulomnitz@geomar.de)

In preparation for submission

## Abstract

Benthic fluxes of total dissolved phosphate ($TPO_4^{3-}$, named P release in following) and dissolved iron ($Fe^{2+}$, named Fe release in the following) were determined at 9 stations along a depth transect between 47 and 1108 m water depth at 18°N off Mauritania (NW Africa). Bottom water $O_2$ concentrations were always ≥ 25 µM, and fluxes were always directed from the sediments into the bottom water. The highest benthic $PO_4^{3-}$ release of 0.2 ± 0.07 mmol $m^2$ $d^{-1}$, measured using incubation chambers in situ, was found at 47 m water depth (50 µM $O_2$). The highest diffusive $Fe^{2+}$ flux of 0.03 mmol $m^2$ $d^{-1}$, determined from porewater $Fe^{2+}$ concentrations, occurred at 67 m water depth (27 µM $O_2$). $PO_4^{3-}$ release rates decreased concurrently with dissolved inorganic carbon (DIC) flux and water depth. A difference of up to one order of magnitude between benthic chamber and diffusive $TPO_4^{3-}$ fluxes indicated that the total P release was strongly enhanced by bioirrigation. Bioirrigation, combined with possible stabilization of dissolved Fe by organic ligands, may have favored the observed flux of Fe to the water column under oxygenated bottom waters between 47 and 236 m and at 786 m water depth. However, the reductive Fe loss was lower than the detrital Fe supply as indicated by constant Fe/Al ratios along the depth transect. These trends are similar to those measured in 2011, generally indicating comparable release rates during the upwelling season. Furthermore, oxygen manipulation experiments on sediment cores ex situ showed an increase of the nutrient release (e.g. $PO_4^{3-}$, $Fe^{2+}$, $NH_4$) after 7 days of anoxic bottom water conditions. The fluxes were enhanced by a factor of 1.4 for P and of 7.3 for Fe compared to the natural measured release and reached values as high as those measured in the anoxic oxygen minimum zone off Peru. This observation indicates that future deoxygenation may enhance sedimentary P and Fe release off Mauritania.

## 3.1 Introduction

Phosphorus (P) and iron (Fe) are limiting nutrients for oceanic primary production (Broecker, 1982; Martin, 1990). P mainly derives from chemical weathering of apatite on land and is discharged to the oceans by riverine transport (Ruttenberg, 2014). However, only about 10-30% of the total delivered P is reactive and potentially bioavailable. About 75% of this fraction reaches the ocean, with the remaining 25% scavenged by sedimentation or flocculation in estuaries and coastal waters (Paytan & McLaughlin, 2007).

Continental margins receive Fe mainly from weathered continental rocks by river discharge. In contrast, the open ocean is supplied by Fe (oxyhydr)oxides from dust deposition whereas only a small fraction of 1-10% is dissolved and bioavailable (Jickells and Spokes, 2001) making Fe a key limiting nutrient in about 30 to 40% of the world oceans (Boyd and Ellwood, 2010). However, also the benthic release of Fe represents a much larger source for the water column (Dale et al., 2015, Emerson, 2016).

The release of redox-sensitive nutrients is enhanced in oceanic oxygen deficient areas such as the eastern boundary upwelling systems (EBUS), e.g. off Peru, Namibia, Oregon and North West Africa (Sundby et al., 1986, McManus et al., 1997, Severmann et al., 2010, Noffke et al., 2012). Although, EBUEs cover only 1% of the world's oceans, they contribute about 10-15 % to the total marine primary production and are therefore important areas for fisheries (Carr, 2002, Behrenfeld and Falkowski, 1997, Cropper et al., 2014 and references therein).

Off Mauritania, seasonal upwelling of cold nutrient-rich waters favors high surface primary production rates of up to 1.7 g C $m^{-2}$ $d^{-1}$ (Carr, 2002). Degradation of the organic detritus leads to strong oxygen consumption and minimum oxygen concentrations of about 30 µM below the surface mixed layer. Oxygen depletion enhances phosphate and iron release from sediments and potentially fuels surface water primary production in a positive feedback loop (Ingall and Jahnke, 1997, Wallmann, 2010, Dale et al., 2015). Recent studies on ocean deoxygenation found a siginificant oxygen loss in the past decades and predict an ongoing decline in the future (Stramma et al., 2008, Schmidtko et al., 2017). Hence, it is crucial to understand the mechanisms behind nutrient release from sediments and how this process may affect surface ocean primary production.

A decisive step into this direction is the measurement of natural benthic nutrient fluxes in oxygen-depleted upwelling areas. Here we present a new comprehensive data set on P and Fe release fluxes for the Mauritanian upwelling along a depth transect at 18°N ranging from 47 to 1108 m water depth (Fig. 3.1A, Table 3.1). We aim to identify the P and Fe sources as well as the processes controlling the magnitude of the fluxes. Furthermore, the data set is accompanied by P and Fe flux measurements conducted during a previous cruise to the same study area, enabling us to compare the flux magnitudes and their temporal variability. In addition, we conducted ex situ oxygen manipulation experiments in order to estimate the potential for enhanced nutrient release under scenarios of further decreasing oxygen levels. In the last part of this study we compare the P and Fe release rates with data from the Peruvian OMZ and discuss reasons for the different magnitudes of the fluxes in these areas.

## 3.2 Study Area

The Mauritanian margin at 18°N lies within the Canary Upwelling System (11-35°N). Strong oxygen consumption takes place in the study area as a result of seasonal upwelling occurring from boreal winter to spring, leading to high primary production rates (0.3 to 2.3 g C $m^{-2}$ $d^{-1}$, Morel et al., 1996). The seasonality of the upwelling is driven by the migration of the Inter Tropical Convergence Zone (ITCZ) (Mittelstaedt, 1983). The upwelled South Atlantic Central Water (SACW) has a low salinity and is enriched in inorganic nutrients (Stramma et al., 2009). Trade winds export large quantities of Saharan dust into the waters off Mauritania, which is reflected by

high solid phase Fe concentrations in the sediments (Mittelstaedt, 1983, Baker et al., 2006, Ohnemus & Lam, 2015).

The margin and offshore waters are characterized by a moderate oxygen minimum zone (OMZ) between ~50 and 500 m water depth (Oschlies et al., 2008, Schmidtko et al., 2017). The lowest bottom water oxygen concentrations of ~30 µM occur between 200 and 600 m water depth (Fig. 3.1B, Table 3.1). The oxygen concentration in the wider Western Tropical North Atlantic is apparently decreasing at a rate of 0.5 µmol $kg^{-1}$ $yr^{-1}$ (Stramma et al., 2008). The region is an important fishery whose future may be under threat by the ongoing deoxygenation (Pauly and Christensen, 1995).

The sediments in the study area are characterized by variable lithology. At water depths <100 m, sand accounts for up to 70 dry wt. % of the total particulate material. Between 170 and 255 m water depth, the sand and mud fractions are nearly equal, whereas the sand fraction increases at ~ 425 m water depth to 66 wt. %. In deeper waters (~ 780 – 1120 m) mud dominates the sediments and the sand content decreases to ~ 7 wt. % (Dale et al., 2014 and references there in). Sokoll et al. (2016) characterized sediments down to ~ 480 m as permeable with strong advective transport component in the porewater and at the sediment-water interface. Geochemically, the sediments are carbonate-rich and contain considerable amounts of biogenic silica and quartz (Hartmann et al. 1976). The particulate organic carbon content (POC) ranges between 1 – 3 % dry weight (Dale et al., 2014). The seafloor is densely covered by traces of burrow-dwelling macrofauna indicating that bioirrigation is likely an important process of solute exchange (Dale et al., 2014, Kirstensen et al., 2012).

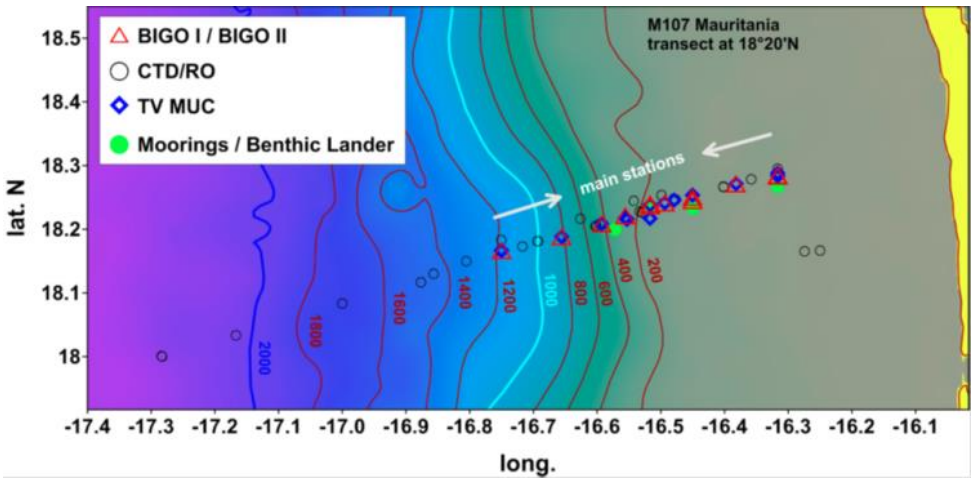


**Fig. 3.1A** Study area off Mauritania showing the 18°N depth transect and the deployed devices at each station during the M107 cruise.

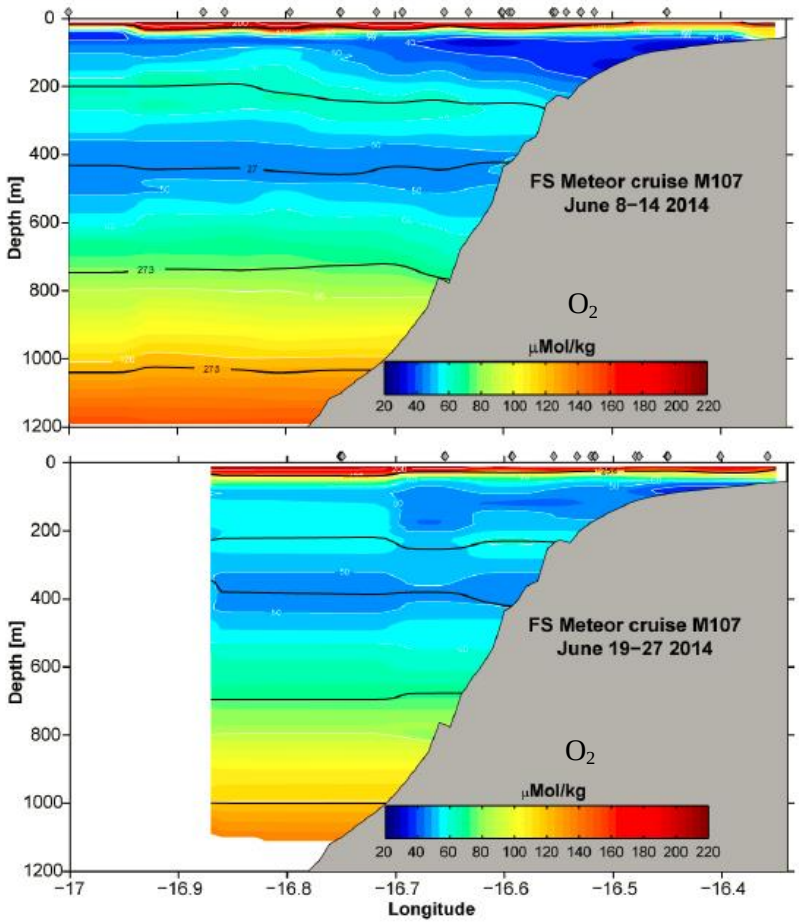


**Fig. 3.1B** Cross section across the 18°N depth transect showing $O_2$ concentrations (µmol $kg^{-1}$) from 06/8-14/2015 (second panel) and from 06/19-27/2015 (third panel) and the station locations across 18°N.

**Table 3.1** Station list including geographic coordinates, sampling date, water depths and bottom water oxygen concentration for all sites along the 18°N depth transect from cruise M 107 and MSM17/4.

| No. | Station | Gear | Lat. N | Long. W | Date | Water depth (m) | Bottom water $O_2$ (µM) |
|---|---|---|---|---|---|---|---|
| **M107** | | | | | | | |
| I | 658 | MUC13 | 18°17.299' | 16°18.994' | 23.06.14 | 47 | 50 |
| | 665 | BIGO2-4 | 18°17.100' | 16°18.997' | 23.06.14 | 47 | |
| II | 686 | MUC19 | 18°16.287' | 16°22.910 | 25.06.14 | 66 | 27 |
| | 688 | BIGO2-5 | 18°16.286 | 16°22.932' | 25.06.14 | 67 | |
| III | 628 | MUC10 | 18°15.197' | 16°27.002' | 21.06.14 | 90 | 25 |
| | 630 | BIGO1-3 | 18°15.006' | 16°27.010' | 21.06.14 | 91 | |
| IV | 672 | MUC17 | 18°14.483' | 16°29.634' | 24.06.14 | 129 | 35 |
| | | BIGO1-4 | 18°14.485' | 16°29.635' | 24.06.14 | 129 | |
| V | 697 | MUC20 | 18°14.299' | 16°30.995' | 26.06.14 | 169 | 42 |
| | 617 | BIGO2-3 | 18°14.397' | 16°31.000' | 20.06.14 | 171 | |
| VI | 612 | MUC8 | 18°12.945' | 16°33.153' | 20.06.14 | 236 | 53 |
| | 598 | BIGO1-2 | 18°13.286' | 16°33.334' | 15.06.14 | 236 | |
| | 583 | MUC7A | 18°12.998' | 16°33.197' | | 237 | |
| | 583 | MUC7B | 18°12.998' | 16°33.197' | 14.06.14 | 237 | 50 |
| | 583 | MUC7C | 18°12.998' | 16°33.197' | | 237 | |
| VII | 554 | MUC5 | 18°12.504' | 16°35.583' | 12.06.14 | 412 | 46 |
| | 557 | BIGO2-2 | 18°12.504' | 16°35.585' | 12.06.14 | 412 | |
| VIII | 534 | MUC3 | 18°11.288' | 16°39.328' | 10.06.14 | 786 | 72 |
| | 547 | BIGO1-1 | 18°11.31' | 16°39.335' | 11.06.14 | 787 | |
| IX | 527 | BIGO2-1 | 18°10' | 16°44.99' | 09.06.14 | 1096 | 132 |
| | 669 | MUC15 | 18°10.001' | 16°44.997' | 24.06.14 | 1099 | |
| | 524 | MUC1 | 18°09.991' | 16°45.023' | 09.06.14 | 1108 | |
| **MSM17/4** | | | | | | | |
| | 485 | BIGO 1-4 | 18°17.30' | 16°19.01' | 28.03.11 | 53 | 56 |
| | 463 | MUC35 | 18°17.30' | 16°19.01' | 25.03.11 | 52 | |
| | 409 | BIGO1-2 | 18°15.20' | 16°27.00' | 20.03.11 | 98 | 59 |
| | 406 | MUC25 | 18°15.23' | 16°27.00' | 20.03.11 | 98 | |
| | 560 | MUC52 | 18°14.31' | 16°27.03' | 17.04.11 | 98 | |
| | 539 | BIGO2-4 | 18°14.30' | 16°31.01' | 04.04.11 | 174 | 57 |
| | 536 | MUC50 | 18°14.30' | 16°31.01' | 04.04.11 | 174 | |
| | 466 | BIGO2-1 | 18°13.10' | 16°33.30' | 21.03.11 | 241 | 57 |
| | 421 | MUC28 | 18°13.05' | 16°33.30' | 21.03.11 | 241 | |
| | 584 | MUC53 | 18°12.90' | 16°33.30' | 08.04.11 | 255 | |
| | 453 | BIGO1-3 | 18°12.54' | 16°35.65' | 24.03.11 | 425 | 53 |
| | 448 | MUC31 | 18°12.56' | 16°35.60' | 24.04.11 | 417 | |
| | 530 | BIGO1-5 | 18°11.29' | 16°39.32' | 03.04.11 | 789 | |
| | 506 | MUC44 | 18°11.31' | 16°39.32' | 31.03.11 | 786 | |
| | 466 | BIGO2-2 | 18°10.00' | 16°45.00' | 25.03.11 | 1113 | 139 |
| | 483 | MUC36 | 18°10.00' | 16°45.00' | 28.03.11 | 1108 | |

## 3.3 Methods

The stations were chosen for comparability according to a previous R/V Maria S. Merian cruise (MSM17-4) in March/April 2011. To enhance the data base in shallow waters, 3 additional stations were sampled during the more recent R/V Meteor (M 107) cruise in May/June 2014. The stations for the multiple-corer (MUC) and benthic lander deployments were chosen in close vicinity to each other. Additionally, water column particles were sampled at two stations in 47 and 236 m water depth using a CTD/Rosette equipped with Niskin bottles. The bottom water oxygen concentrations were manipulated in ex situ experiments using MUCs from 236 m water depth.

### 3.3.1 Porewater and solid phase analysis

Sediment cores were retrieved using a video-guided multiple-corer (MUC). After retrieval, all cores were immediately transferred to a cool room (12°C, mean bottom water temperature across the depth transect) and processed within 1-2 hours. The porewater was extracted using rhizons for the sandy shelf and upper slope sediments (water depth < 400 m) (St. I – VI). The first 0.5 ml of porewater extruded through the rhizons was discarded. Porewater extraction using this method required up to 30 minutes, yielding about 10 ml of porewater at each depth interval. For muddier sediments below 400 m (St. VII – IX), the cores were sectioned in an argon filled glove bag at a depth resolution of 0.5 or 1 cm at the surface to 2 cm at depth. The porewater was separated by centrifugation at 4000 rpm for 20 min, and then filtered through 0.2 µm cellulose-acetate filters under argon. Additional sediment sub-samples were taken at each sediment depth interval and stored refrigerated in pre-weighed, air-tight plastic cups for the determination of water content, porosity, total organic carbon (TOC) and solid phase constituents in onshore laboratory. Porewater samples were stored refrigerated at 4 °C.

The TOC concentration of freeze-dried and ground sediment samples was determined by flash combustion in a Carlo Erba Elemental Analyzer (NA 1500). Samples were decalcified with 2.5 N HCl prior to analysis.

Elemental analysis was conducted on one core from each water depth. About 100 mg of freeze-dried and ground sediment were digested in hydrofluoric acid (40 %, supra pure), nitric acid (65 %, sub-boiled distilled), and perchloric acid (60 %, supra pure). For measurement accuracy, the reference standards SDO-1 and MESS-3 as well as methodological blanks were included in the analysis. The Fe and Al concentrations in the digestion solutions were measured using an inductively coupled plasma optical emission spectrometer (ICP-OES, Varian 720 ES). The relative standard deviation (RSD) for [Al] and [Fe] was found to be < 1 %.

### 3.3.2 In situ TPO43- flux measurements

Benthic chamber in situ $TPO_4^{3-}$ fluxes were obtained using two BIGOs I and II (BIGO: Biogeochemical Observatory) at 9 stations along a depth transect at 18°20' N in water depths of 47, 67, 91, 130, 171, 236, 412, 787 and 1096 m (Table 3.3). The two circular flux chambers attached to each BIGO had an internal diameter of 28.8 cm and a total area of 651.4 $cm^2$ (Sommer et al., 2009). The system was equipped with an online video-controlled launch system for precise placement at the seafloor in proximity to the multiple-corer stations. After deployment at the sea floor, the surrounding bottom water was periodically flushed into the chambers for 4 hours. Afterwards, the chambers were driven into the sediments at ~ 30 cm $h^{-1}$ and closed after the water inside the chamber was replaced once more with ambient bottom water to flush out solutes that might have been released from the sediment during chamber insertion. Over the incubation period, 8 sequential water samples were removed with glass syringes (volume ~ 47 ml). To monitor the ambient bottom water, 4 additional glass syringes were filled. Phosphate concentrations in the syringe samples were measured on board using an auto analyzer. The standard series covered a concentration range from 0.05 to 3.5 µM. The fluxes were calculated from the slope of the linear regression of all eight data points vs. the sampling time (supplement, Fig. S3.1) and corrected for the water volume in the chamber and the dead volume of the 1m long Vygon tubes connecting the syringes with the flux chambers. The error caused by the dilution from the dead volume of distilled water in these tubes was corrected by against the chloride concentration measured in the syringe samples versus ambient sea water. Benthic chamber $TPO_4^{3-}$ fluxes for most sites are reported based on two replicate chamber measurements. The uncertainty given for the $TPO_4^{3-}$ fluxes is the difference between the minimum and maximum fluxes from the average of the two benthic chambers.

### 3.3.3 Diffusive Fe2+ flux calculation

The Fe release was estimated from pore water profiles by Fick's 1st Law of diffusion, because no significant temporal change in Fe concentrations could be detected in the benthic chambers:

$$(1)\ diffusive\ Fe^{2+}flux = -\phi D_{Sed}\frac{d[C]}{dx}.$$

$\phi$ is the porosity of the surface sediment sample and $D_{Sed}$ is the diffusion coefficient at the sediment-water interface. The term d[C]/dx denotes the concentration difference between the bottom water and the uppermost porewater sample divided by the depth below the seafloor (1 cm at St. II, III, IV and VI, 0.5 cm elsewhere). $D_{SW}$ was taken from Boudreau (1997) and corrected for the in situ temperature (from CTD measurements) at each station and for salinity and pressure using by the Stokes Einstein relationship (Li and Gregory, 1974). The resulting diffusion coefficient was adjusted to account for sediment porosity (Boudreau, 1997).

$$(2) \qquad D_{Sed} = \frac{D_{SW}}{1 - \ln(\phi^2)}$$

Diffusive $TPO_4^{3-}$ fluxes were also determined in this way.

### 3.3.4 Water column particle sampling and analysis

Suspended and sinking particles were sampled by filtration (0.7 µm Whatman GF/F) of 4 to 12 L of water that was retrieved from Niskin bottles attached to a CTD/Rosette at 47 and 236 m water depth. The particles were analyzed for total particulate phosphorus (TPP), particulate inorganic phosphorus (PIP) and particulate organic carbon (POC) according to the method described in Lomnitz et al. (2016). TPP and PIP were determined using standard combustion and colorimetric methods (Aspila, 1976). Measurements were made using eight standards ranging from 5 to 100 µM $PO_4^{3-}$, prepared from a Merck phosphate stock solution.

POC was determined by flash combustion with a Carlo Erba elemental analyzer (NA 1500) with an analytical precision and detection limit of 0.04 wt. %

### 3.3.5 Ex situ O2 manipulation experiments

We conducted an ex situ experiment to test the effect of anoxia on the P and Fe release from the sediments at 237 m water depth in undisturbed sediment cores . Beforehand, the MUC liners were prepared with calibrated oxygen sensitive spots for non-invasive $O_2$ measurements during the entire experiment. Three replicate sediment cores (A, B, and C) were transferred to the cold room (10 – 12°C, i.e. in situ temperature) and allowed to stand (while stirred) for 24h before the experiment was started.

Core A and B were kept oxic for approximately 20 h before the oxygen concentration was lowered by pumping argon gas into the overlying bottom waters. The anoxic phase of core A and B was maintained for at least 9.5 days before core A was sliced for porewater analyses and solid phase sampling. Core B was then oxygenated again and kept under oxic conditions for approximately 3 days. Core C was a control core maintained at an oxygen concentration similar to the in situ bottom water concentration. The enclosed waterbody was ventilated with air or argon to regulate the oxygen concentrations. During the experimental period (14.5 d), water samples were taken every 4 h. After each sampling, the water volume equivalent to the sample volume of ~ 20 ml was refilled with bottom water from reservoir bags.

Measurements of $NO_3^-$, $NO_2^-$, $NH_4^+$ and $PO_4^{3-}$ in the water samples were performed on board once a day using a QuAAtro autoanalyzer (Seal Analytical) with a precision of ±0.1 µmol $l^{-1}$, ±0.1 µmol $l^{-1}$, ±0.2 µmol $l^{-1}$ and ±0.24 µmol $l^{-1}$, respectively. For ferrous iron concentration analysis, subsamples of 0.5 to 1 ml were complexed with Ferrozin and determined photometrically

(Stookey, 1970). Sample cups where flushed with Argon after filling to minimize oxidation artefacts.

## 3.4 Results

### 3.4.1 Porewater $Fe^{2+}$ and $PO_4^{3-}$ profiles

Porewater $PO_4^{3-}$ profile shapes are very similar to those of $Fe^{2+}$ (Fig. 3.2). The concentration peaks coincide or are slightly shifted below the $Fe^{2+}$ maxima. At water depths between 47 and 169 m, the concentrations varied around 10 to 15 µM and remain more or less constant to the core end. Below 169 m water depth, concentrations rose up to 30 µM and the concentration maxima were shifted down-core.

### 3.4.2 Solid phase Fe, P and Al

The average solid phase Fe, P and Al concentrations increase with water depth along the depth transect (Fig. 3.3, supplement Table S3.1). Concentration peaks of Fe and P occur inversely correlated to the concentration peaks found in porewater profiles of both solutes. The profiles show no depth trend with increasing sediment depth along the depth transect. The average Fe/Al ratio for all analysed samples is 0.55 whereas the ratio is enhanced at St. III to VI and slightly depleted at St. I (Fig. 3.4). The lithogenic background Fe/Al ratio is between 0.4 and 0.8 (Scheuvens et al., 2013) with the main Fe input from Saharan dust and soils.

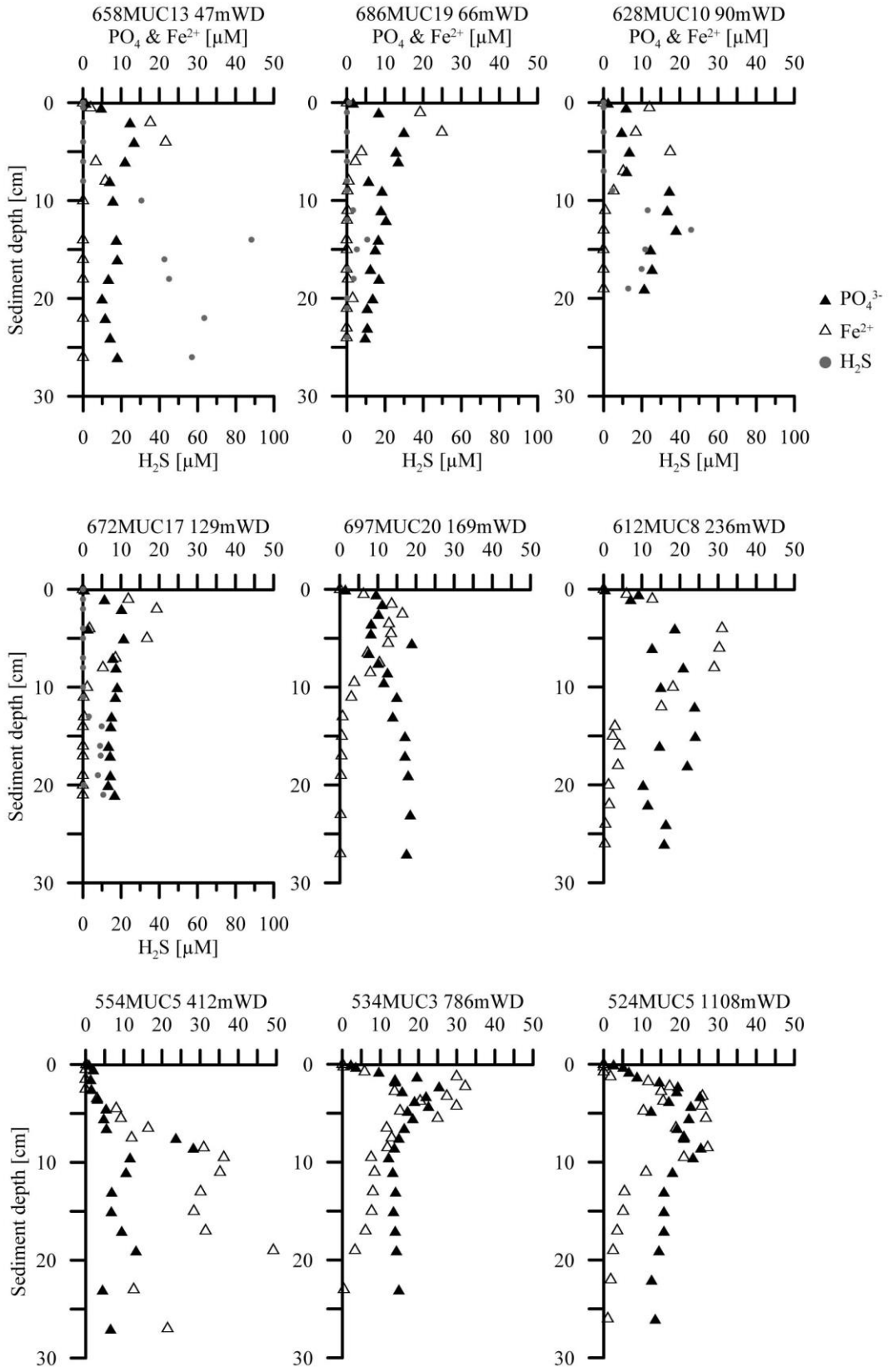


**Fig. 3.2** Porewater profiles of dissolved $PO_4^{3-}$ (closed triangles), $Fe^{2+}$ (open triangles) and $H_2S$ (solid grey circles) in µM for all stations along the 18°N depth transect. The first data point of each solute indicates the bottom water concentration obtained from the overlying water in the multiple-corers (MUCs). $H_2S$ was only measured at station I to IV.

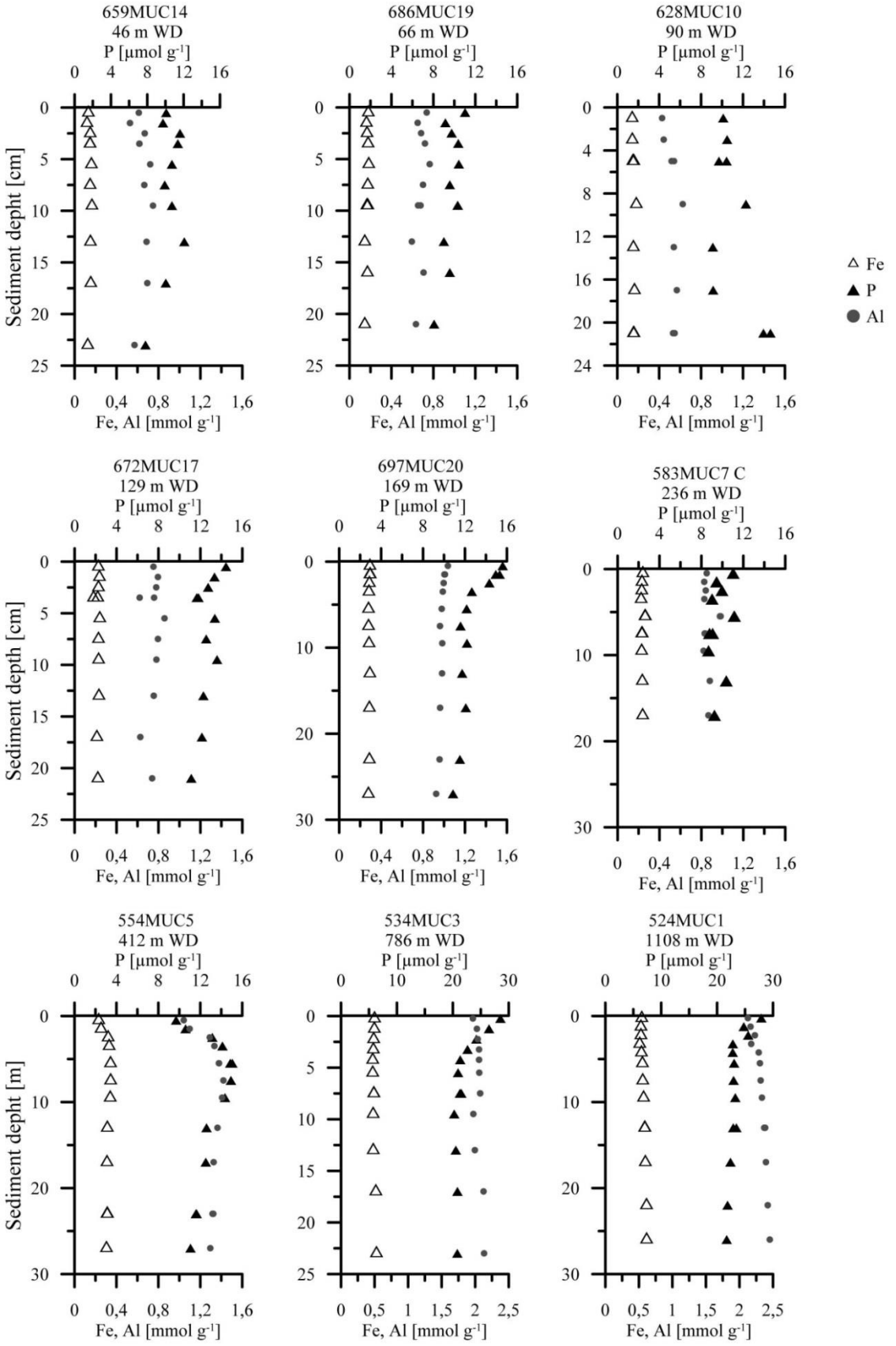


**Fig. 3.3** Solid phase P (µmol $g^{-1}$), Fe and Al (mmol $g^{-1}$) concentration profiles of multiple-cores retrieved along the 18°N depth transect. Note the change in scales at the two deepest stations.

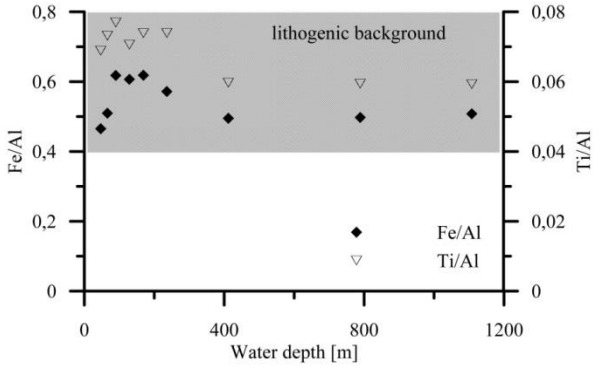


**Fig. 3.4** Mean Fe/Al and Ti/Al ratios against water depth. The grey shaded area indicates the lithogenic background ratio for Fe/Al. Ti/Al indicate grain size changes along the depth transect.

### 3.4.3 Sedimentary particulate organic carbon (POC) content

The particulate organic carbon (POC) content of the sediments increases along the depth transect (supplement, Table S3.1). Lowest values of 0.7 wt. % occur at St. II and III (66 and 90 m water depth). The other stations are in a range between 0.9 and 1.3 wt. %, whereas a sharp increase occurs at ~ 1000 m water depth. Here, the POC content increases to 2.6-2.9 wt. %.

Sedimentary POC/TPP ratios are below Redfield, in the surface sediments (Table 3.2). With exception of station I, the ratios slightly increase with sediment depth as well as with increasing water depth. The mean POC/TPP ratio of all sediment samples is 76.

**Table 3.2** POC/TPP, POC/PIP and POC/POP ratios for water column particles, collected at St. I and VI, and surface sediments of all stations along the depth transect. The error given for the water column particle ratios was determined from two filter samples taken in each sampling depth.

| **Station** | **Water depth** | **Sampling depth (m or cm)** | **POC/TPP** | **POC/PIP** | **POC/POP** |
|---|---|---|---|---|---|
| **Water column particles** | | | | | |
| 645 CTD 46 | 46 | 10 | 98 ±1 | 160 ± 14 | 264 ± 44 |
| 645 CTD 46 | 46 | 20 | 87 ± 7 | 138 ± 36 | 693 ± 546 |
| **645 CTD 46** | **46** | **BW** | **103 ± 8** | **208 ± 38** | **235 ± 79** |
| Sediments | | | | | |
| | | 0.5 | 91 | 117 | 408 |
| | | 1.5 | 106 | 121 | 872 |
| | | 2.5 | 55 | 73 | 227 |
| 659 MUC 14 | 47 | 3.5 | 56 | 60 | 1009 |
| | | 5.5 | 91 | 112 | 492 |
| | | 7.5 | 85 | 106 | 427 |
| | | 9.5 | 67 | 88 | 291 |
| | | 0.5 | 62 | 82 | 243 |
| | | 1.5 | 54 | 80 | 171 |
| 686 MUC 19 | 66 | 2.5 | 64 | 83 | 285 |
| | | 3.5 | 71 | 92 | 321 |
| | | 5.5 | 72 | 97 | 280 |

| | | | | | |
|---|---|---|---|---|---|
| | | 7.5 | 72 | 99 | 269 |
| | | 9.5 | 75 | 97 | 336 |
| 628 MUC 10 | 90 | 1 | 42 | 55 | 185 |
| | | 3 | 52 | 66 | 251 |
| | | 7 | 67 | 90 | 267 |
| | | 9 | 80 | 88 | 840 |
| 697 MUC 20 | 169 | 0.5 | 73 | 97 | 292 |
| | | 1.5 | 78 | 97 | 413 |
| | | 3.5 | 79 | 111 | 272 |
| | | 5.5 | 77 | 106 | 278 |
| | | 7.5 | 76 | 102 | 293 |
| | | 8 | 87 | 114 | 364 |
| 583 MUC 7C | 236 | 0.5 | 82 | 102 | 416 |
| | | 1.5 | 72 | 105 | 234 |
| | | 2.5 | 83 | 108 | 362 |
| | | 3.5 | 76 | 121 | 205 |
| | | 5.5 | 89 | 127 | 292 |
| | | 7.5 | 89 | 123 | 319 |
| | | 9.5 | 84 | 106 | 416 |
| **Water column particles** | | | | | |
| 582 CTD 24 | 233 | 10 | 139 ± 24 | 298 ± 27 | 264 ± 63 |
| 582 CTD 24 | 233 | 20 | 201 ± 51 | 600 ± 140 | 376 ± 302 |
| 582 CTD 24 | 233 | 50 | 167 ± 6 | 471 ± 30 | 250 ± 14 |
| 582 CTD 24 | 233 | 100 | 135 ± 7 | 287 ± 2 | 257 ± 25 |
| 582 CTD 24 | 233 | 150 | 140 ± 0 | 224 ± 7 | 375 ± 17 |
| 582 CTD 24 | 233 | 200 | 132 ± 12 | 339 ± 30 | 225 ± 48 |
| **582 CTD 24** | **233** | **BW** | **138 ± 7** | **376 ± 71** | **222 ± 7** |
| **Sediments** | | | | | |
| 554 MUC 5 | 412 | 0.5 | 81 | 115 | 271 |
| | | 1.5 | 77 | 87 | 682 |
| | | 3.5 | 89 | 123 | 322 |
| | | 5.5 | 86 | 121 | 297 |
| | | 7.5 | 95 | 135 | 324 |
| | | 9.5 | 90 | 126 | 317 |
| 534 MUC 3 | 786 | 0.25 | 90 | 119 | 364 |
| | | 0.75 | 82 | 111 | 309 |
| | | 2.25 | 95 | 144 | 278 |
| | | 3.75 | 99 | 154 | 281 |
| | | 5.5 | 108 | 154 | 359 |
| | | 7.5 | 127 | 161 | 603 |
| | | 8 | 122 | 185 | 357 |
| 524 MUC 1 | 1108 | 0.25 | 83 | 120 | 271 |
| | | 0.75 | 89 | 127 | 299 |
| | | 2.25 | 96 | 144 | 286 |
| | | 3.75 | 112 | 168 | 338 |
| | | 5.5 | 117 | 181 | 332 |
| | | 7.5 | 127 | 200 | 349 |
| **Average water column particles** | | | **134 ± 12** | **310 ± 40** | **309 ± 87** |
| **Average sediments** | | | **81** | **110** | **400** |

### 3.4.4 Benthic chamber fluxes (sediment-water interface)

The total benthic chamber $TPO_4^{3-}$ fluxes off Mauretania are directed into the water column (positive values) at all stations (Fig. 3.7 A, Table 3.3). The highest $TPO_4^{3-}$ flux of 0.2 ± 0.07 mmol $m^{-2}$ $d^{-1}$ was found at 47 m water depth (St. I) where a bottom water oxygen concentration of 50 µM was measured. With an exception at 91 m water depth (St. III), the phosphate release rates decreased smoothly with increasing water depth to values of 0.05 ± 0.005 at the deepest stations. A comparatively low P release of 0.09 ± 0.045 mmol $m^{-2}$ $d^{-1}$ at was measured at station III (90 m water depth) coinciding with the lowest bottom water oxygen concentration of 25µM found along the depth transect (Fig. 3.7 A).

**Table 3.3** Benthic chamber $TPO_4^{3-}$ and DIC fluxes and diffusive $TPO_4^{3-}$ and $Fe^{2+}$ fluxes from cruise M107 and MSM17/4. The error given for the benthic chamber fluxes comes from the determination of the fluxes using two benthic chambers. Diffusive fluxes were calculated according to Fick's first law using the uppermost porewater and the bottom water concentration.

| No. | Station | Gear | Benthic chamber $TPO_4^{3-}$ flux [mmol $m^{-2}$ $d^{-1}$] | Diffusive $TPO_4^{3-}$ flux [mmol $m^{-2}$ $d^{-1}$] | Diffusive $Fe^{2+}$ flux [mmol $m^{-2}$ $d^{-1}$] | Benthic chamber DIC flux [mmol $m^{-2}$ $d^{-1}$] |
|---|---|---|---|---|---|---|
| I | 658 | MUC13 | | 0.02 | 0.02 | |
| | 665 | BIGO2-4 | 0.2 ± 0.07 | | | 20.06 ± 0.69 |
| II | 686 | MUC19 | | 0.04 | 0.03 | |
| | 688 | BIGO2-5 | 0.17 ± 0.03 | | | 15.34 ± 2.67 |
| III | 628 | MUC10 | | 0.01 | 0.01 | |
| | 630 | BIGO1-3 | 0.09 ± 0.05 | | | 10.75 ± 2.15 |
| IV | 672 | MUC17 | | 0.03 | 0.03 | |
| | | BIGO1-4 | 0.16 ± 0.01 | | | 9.52 ± 1.03 |
| V | 697 | MUC20 | | 0.04 | 0.02 | |
| | 617 | BIGO2-3 | 0.14 ± 0.03 | | | 7.93 ± 0.69 |
| VI | 612 | MUC8 | | 0.02 | 0.01 | |
| | 598 | BIGO1-2 | 0.11 ± 0.05 | | | 8.64 ± 0.07 |
| VII | 554 | MUC5 | | 0.01 | 0 | |
| | 557 | BIGO2-2 | 0.08 ± 0.02 | | | 5.64 ± 2.5 |
| VIII | 534 | MUC3 | | 0.03 | 0.01 | |
| | 547 | BIGO1-1 | 0.05 ± 0.01 | | | 5.8 ± 1.2 |
| IX | 527 | BIGO2-1 | 0.06 ± 0.01 | | | 5.86 ± 2.3 |
| | 669 | MUC15 | | 0.02 | 0 | |
| | 524 | MUC1 | | 0.02 | 0 | |

### 3.4.5 Diffusive Iron fluxes

The diffusive $Fe^{2+}$ fluxes along the depth transect ranged from 0.08 to 0 mmol $m^{-2}$ $d^{-1}$ detected at 47 m (St. I) and 1108 m (St. IX) water depth (Fig. 3.7B, Table 3.3). At station III (91 m water depth), Fe fluxes decreased to a local minimum similar as described for the $TPO_4^{3-}$ fluxes. Below, the $Fe^{2+}$ fluxes increased again, before they decreased slightly with greater water depth. An

exception was found at 786 m water depth (St. VIII), where the $Fe^{2+}$ flux increased to a relatively high value of 0.05 mmol $m^{-2}$ $d^{-1}$.

### 3.4.6 Water column particles

The measured concentrations of TPP, PIP, POP and POC are reported in supplement, Table S3.2. The TPP concentrations of the analyzed water column particles were much higher at St. I (47 m water depth) compared to St. VI (236 m water depth).

PIP concentrations in the sampled particulate matter was highest in the surface waters at St. I (0.3 µM) and lowest (0.014 µM) in 225 m water depth at St. VI. On average PIP comprised 49 % of TPP. As POP is the result of the difference of the TPP and the PIP concentration, the trends described before are also valid for POP concentrations in the water column particles.

Very high POC concentrations of 51 and 27 µM were measured at 10 and 20 m water depth at St. I. Lowest concentrations of ~ 4 µM were found in 150 m water depth at St. XI.

The mean POC/TPP, POC/PIP and POC/POP ratios were 134 ± 12, 310 ± 40 and 309 ± 87, respectively (Table 3.2).

### 3.4.7 Oxygen manipulation experiments

Three MUCs from 237 m water depth were retrieved to conduct ex situ oxygen manipulation experiments (Fig. 3.5). The initial $Fe^{2+}$ and $PO_4^{3-}$ concentrations before oxygen draw down were ~ 0.04 µM in core and 0.08 µM in core B and C. These values were measured about 8 hours after the first measurement allowing the system to rebalance the disturbances from core retrieval. The initial nitrate concentrations were very robust at 1.6 µM in all three cores. The drawdown of oxygen started after one day and lasted for another day until anoxic bottom water conditions were established. The release of $Fe^{2+}$ into the bottom waters was delayed by approximately 5 days and for $PO_4^{3-}$ around 2.5 days after that point. The sharp increase in P release occurs slightly after the point when $NO_3^-$ was completely consumed and coincides with the beginning of a strong $NH_4^-$ release (Fig. 3.5). $NO_2^-$ concentrations were relatively constant throughout the experiment, only at the beginning of the experiment concentrations peaked at 17 µM in core A and 13 µM in core B due to the addition of 16.12 µmol $NO_3^-$ $L^{-1}$ for testing purposes.

The $Fe^{2+}$ and $PO_4^{3-}$ concentrations were still increasing when the experimental set up for core A was stopped reaching 6.7 µM $Fe^{2+}$ and 8.9 µM $PO_4^{3-}$ in the bottom waters. $NH_4^-$ concentrations increased to values of 77.7 µM.

Core B was oxygenated again after ~ 10 days of anoxia. The initial $O_2$ bottom water concentrations were reached after less than one day of oxygenation. P concentrations remained on a plateau for ~ 1 day and started to slightly decrease thereafter, but were still enhanced to 3.3 µM after ~ 3 days of oxygenation compared to the initial bottom water concentrations. $Fe^{2+}$

concentrations started to decrease after about half a day and ended at 0.7 µM at the experiment end. Although, these concentrations are still one order of magnitude larger than in the initial bottom water concentrations, the draw down is faster than compared to $PO_4^{3-}$ indicating more $O_2$ sensitivity of Fe.

$NO_3^-$ concentrations increased coincidentally with the addition of oxygen whereas the $NH_4^-$ release persisted until the end of the experiment.

In the oxygenated control core C, Fe and P concentrations stayed rather constant during the entire experiment duration. $NO_3^-$ concentrations decreased in the second half of the experiment to ~ 7.7 µM whereas $NH_4^-$ increases coincidentally to ~ 8.9 µM. Both constitutes remained at this concentration levels for the rest of the experiment. There was no $NO_2^-$ detected in the control core C during the entire experiment.

The diffusive $Fe^{2+}$ and $TPO_4^{3-}$ fluxes were calculated from the slope of the increasing solute concentrations (Fig. 3.5, Table 3.6). In the following, these fluxes are named 'potential' fluxes as they do not reflect measurements at naturally occurring environmental conditions during the cruise.

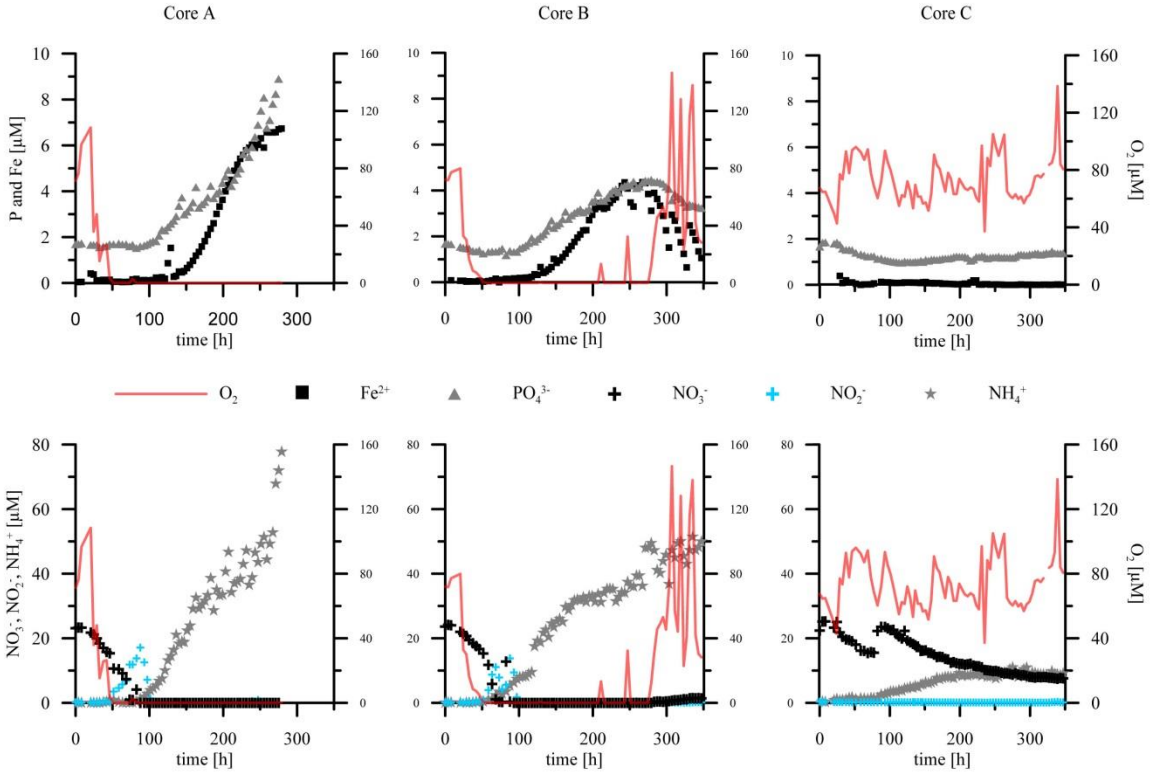


**Fig. 3.5** Bottom water concentrations of $PO_4^{3-}$, $Fe^{2+}$, $NO_3^-$, $NO_2^-$ and $NH_4$ [µM] during ex situ oxygen manipulation experiments in three multiple-cores (A, B and C). Core A was kept anoxic for the entire experiment duration whereas core B was oxygenated again after ~12.5 days with anoxic overlying bottom waters. Core C was run as a control core with more or less constant bottom water $O_2$ concentrations.

**Table 3.6.** Evolution of nutrient concentrations of $PO_4^{3-}$, $Fe^{2+}$, $NO_3^-$, $NO_2^-$ and $NH_4$ in the overlying waters of three multiple-corers during ex situ $O_2$ manipulation experiment. Core A was kept anoxic until the end of the experiment, whereas Core B was oxygenated again before slicing. Core C was the control core kept at more or less stable oxygen concentrations.

| No. | Station | Gear | Incubation time ($FTPO_4^{3-}$) [h] | **Diffusive $TPO_4^{3-}$ flux [mmol $m^{-2}$ $d^{-1}$]** | Average **$TPO_4^{3}$ flux** | Incubation time ($FFe^{2+}$) [h] | **Diffusive $Fe^{2+}$ flux [mmol $m^{-2}$ $d^{-1}$]** | Average **$Fe^{2+}$ flux** |
|---|---|---|---|---|---|---|---|---|
| VI | 583 | MUC7A | 162.08 | 0.19 | 0.15 ± 0.04 | 126.08 | 0.35 | 0.27 ± 0.08 |
| | | MUC7B | 170.08 | 0.11 | | 116.08 | 0.19 | |

## 3.5 Discussion

### 3.5.1 P and Fe release

**Phosphate turnover**

Benthic chamber P release is mainly driven by organic matter remineralization in sediments and further enhanced by low oxygen concentrations in overlying bottom waters (Ingall and Jahnke, 1994).

The degradation of organic matter can be estimated from the dissolved inorganic carbon (DIC) fluxes measured with our lander system. Both, DIC and P fluxes decrease exponentially with water depth (Fig. 3.7A and C) indicating a strong coupling. If P release would be driven by POC degradation alone, one would expect a relation of the DIC and the P fluxes according to Redfield (1963) with a C/P ratio of 106. However, the correlation of both fluxes shown in Fig. 3.6 indicates higher P release than expected from Redfield. Surprisingly, our in-situ flux data show that P is preferentially released even though oxygen concentrations in ambient bottom water are higher than the threshold for enhanced P release (20 µM) observed in previous studies (Wallmann 2010).

The measured total benthic chamber P fluxes exceed the diffusive fluxes by one order of magnitude implying that the P release is dominated by non-diffusive processes (Table 3.3). The high permeability of sandy sediments off Mauritania (Fig. 3.7E) likely allows bottom water to flow through surface sediments along horizontal pressure gradients induced by bottom currents and topography (Huettel et al., 2003). Hence, a large portion of the measured total P flux may have been induced by this process. Sandy sediments are an indicator for strong bottom water currents causing fast POC degradation and erosive loss of the fine grained material which was observed in water depth down to 240 m along the depth transect (Sokoll et al., 2016). As reported by Dale et al. (2014), the seafloor of the Mauritanian shelf is densely populated by macrofauna and speckled by burrow holes indicating that the P fluxes may have been further enhanced by bioirrigation. The impact of bioirrigation on solute exchange is frequently described in literature, e.g. Aller (1980, 2001), Canfield and Des Marais (1993), Thamdrup et al. (1994), Berelson et al. (2003), Meysman et al. (2006), Kristensen et al. (2012), Dale et al. (2013) and others. Bioirrigating organisms exchange bottom and porewater by ventilating their burrows for feeding purposes. The shape of the burrow is thereby very important for the microniche that is created and how the exchange of porewater solutes to the bottom waters is directed (Meysman et al, 2006, Kristensen et al., 2012). Along the depth transect, distinct varieties of the traces of benthic organisms were observed indicating that the organisms are sensitive to changes in sediment characteristics and bottom water oxygen concentrations. Numerous traces of organisms were found in the sediments with higher sand content and vice versa. Furthermore, the lowest bottom water oxygen concentrations were found concurrently with a decrease of the bioirrigation

coefficients and a sharp drop in P release (Fig. 3.7A and D). In contrast, in other oxygen deficient areas e.g. off Peru the highest release rates typically coincided with lowest bottom water oxygen concentrations. The good correlation between bioirrigation intensity and benthic chamber P flux suggests that bioirrigation has a strong effect on benthic P release along the depth transect.

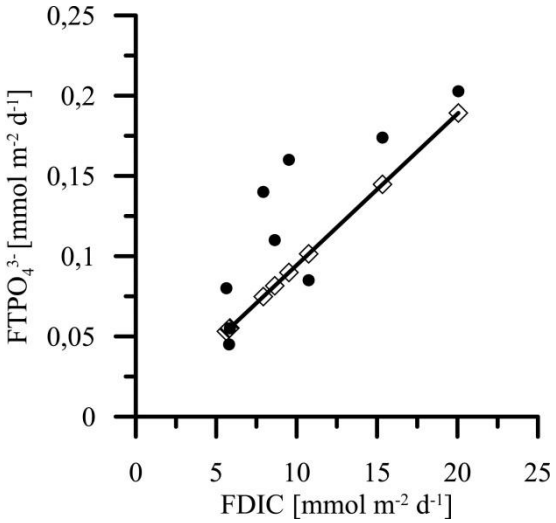


**Fig. 3.6** Measured benthic chamber $TPO_4^{3-}$ fluxes vs. DIC fluxes (closed circles) and the theoretical $TPO_4^{3-}$ fluxes that would derive from organic matter degradation according to Redfield composition (open rectangles connected with the black line). The deviation from the measured and the theoretical fluxes indicates that further P sources than particulate organic phosphorus (POP) are needed to maintain the measured release rates.

The inorganic P fraction (PIP) contributes significantly to the total P inventory of sediments along the depth transect off Mauritania. Our analyses revealed a mean PIP fraction of 75 % of the total sedimentary P inventory. The sedimentary PIP inventory can be enhanced by the conversion of POP into PIP while TPP remains constant, a process that is called sink-switching (Ruttenberg and Berner, 1993, Faul et al., 2005). Most of the PIP formed in marine sediments is composed of carbonate fluoride apatite (Ruttenberg and Berner, 1993). This authigenic mineral phase precipitates from ambient pore fluids that are enriched in dissolved phosphate due to POP degradation. Our water column particle and sediment composition data suggest that sink-switching occured off Mauritania. We found that sediments were enriched in PIP and depleted in POP compared to water column particles (Table 3.2). Furthermore, our down-core data suggest that POP to PIP conversion takes place already at the sediment/water interface and intensifies with sediment depth (Table 3.2).

A P mass balance was set up for two selected stations in our study area considering the rain rate of TPP to the sediment, the benthic chamber release of dissolved P, and TPP burial below the bioturbated zone (Table 3.4). At the shallow station where sediments are not accumulating because of strong bottom currents, the mass balance was closed within the error range. This

means that the rain rate of TPP to the seabed derived from the POC/ DIC data and the TPP/POC ratio in water column particles was as high as the benthic chamber P flux into the water column. At the deep station where sediments accumulated at a high rate, the balance was not closed, because the TPP rain rate was smaller than the sum of the benthic dissolved P release and TPP burial flux (Table. 3.4). This observation indicates that down-slope transport of TPP contributed significantly to the burial flux. The deficit may also be explained by a lower POC/TPP ratio in sinking particles reaching the seabed compared to the suspended particles that were sampled and analyzed in this study. Finally, it is possible that the high benthic fluxes measured during our cruise induces a decline in the TPP stock of surface sediments reflecting non-steady state conditions in P supply/release as postulated for the Peruvian OMZ (Lomnitz et al. 2016).

**Table 3.4** P mass-balance estimates on the P sources to maintain the measured P release at St. I (47 m) and VI (236 m).

| **Parameter** | **Calculation / Source** | **St. I** | **St. II** |
|---|---|---|---|
| Total benthic chamber P release **$FTPO_4^{3-}$** (mmol $m^{-2}$ $d^{-1}$) | measured | 0.2 ± 0.07 | 0.11 ± 0.05 |
| P release form POP degradation **$F_{P(POP)}$** (mmol $m^{-2}$ $d^{-1}$) | $F_{P(POP)} = F_{DIC} / (\frac{POC}{POP})$ <br> $\frac{POC}{POP}$ is the ratio of particles collected in the bottom water (lowest sample in water column) | 0.09 ± 0.003 | 0.04 ± 0 |
| P release form TPP degradation **$F_{TPP(WC)}$** (mmol $m^{-2}$ $d^{-1}$) | $F_{TPP,(WC)} = F_{DIC} / (\frac{POC}{TPP})$ <br> $\frac{POC}{TPP}$ is the ratio of particles collected in the bottom water (lowest sample in water column) | 0.15 ± 0.006 | 0.08 ± 0.001 |
| Sedimentation rate **SR** (cm $yr^{-1}$) | Dale et al., 2013 | 0 | 0.35 |
| Mass accumulation rate **MAR** (g $cm^{-2}$ $yr^{-1}$) | $MAR = \varphi (1-\phi) SR$ with: <br> $\varphi$ = 1.8 (dry bulk density (g $cm^{-3}$) from Förster, 2011) <br> $\phi$ = 0.49 (porosity a the lower core end) | 0 | 0.32 |
| P burial **$P_{tot}$** (mmol $m^{-2}$ $d^{-1}$) | $P_{tot} = MAR * [P_{10}]$ <br> $P_{10}$ = (P concentration in 10 cm depth, supplement Table S.3.1) | 0 | 0.08 |
| P release from the dissolution of Fe (oxyhydr)oxides **$F_{P(Fe)e}$** (mmol $m^{-2}$ $d^{-1}$) | $F_{P(Fe)} = F_{Fe2+} / \left(\frac{Fe}{P}\right)$ <br> ($\frac{Fe}{P}$= 10, Slomp et al., 1996) | 0.0083 | 0.0037 |
| P from terrigenous input $F_{P(terr)}$ (mmol $m^{-2}$ $d^{-1}$) | $F_{P(terr)} = MAR * [Al_{0-1}] * \frac{P}{Al}$ <br> $Al_{0-1}$ = 0.84 mmol $g^{-1}$ (Al concentration of surface sediment, supplement Table S.3.1) <br> $\frac{P}{Al}$ = 0.01 (ratio of P and Al in the surface sediment, supplement Table S.3.1) | 0 | 7.4 x $10^{-6}$ |
| P deficit **$F_{P(def)}$** (mmol $m^{-2}$ $d^{-1}$) | $F_{P(\mathrm{def})} = F_{P(TPP,WC)} + F_{P(Fe)} + F_{P(terr)} - (FTPO_4^{3-} + P_{tot})$ | **0.04** | **0.1** |

**Iron fluxes ($FFe^{2+}$)**

Benthic diffusive Fe fluxes are mainly controlled by the availability of reactive Fe (oxyhydr)oxides that are reductively dissolved during organic matter degradation (Scholz et al., 2011 and references therein). Bottom water oxygen concentrations of less than 20 µM favor benthic Fe release (Dale et al., 2015). Even though bottom waters of Mauritania are more oxic than this apparent threshold value, Fe release across the sediment water interface was measured.
Fe release was induced by a shallow Fe reduction zone due to intense organic matter degradation in the surface sediments at St. I (47 m) to VI (236 m). Hydrogen sulfide accumulation produced by sulfate reduction started within ~ 9 to 11 cm sediment depth (Fig. 3.2). In the transition zone between hydrogen sulfide and Fe-release above iron sulfides precipitated. Below 250 m water depth, bottom water oxygen levels rose and organic carbon degradation decreased leading to a shift of the Fe reduction zone deeper into the sediments (~ 5 – 15 cm), and a decrease in Fe release (Fig. 3.2, 3.7B and C).

Fe release across the sediment water interface in the oxygenated bottom waters off the Mauritanian upwelling could likely be controlled by two effects described in literature before. On the one hand, a recent study of Klar et al. (2017) showed that dissolved Fe released from the sediments could be stabilized by complexation to organic ligands in oxic waters. One the other hand, Severmann et al. (2010) proposed a mechanism where burrow-dwelling organisms create niches in their burrows where oxygen is rapidly consumed leading to the disappearance of the thin oxidized layer of the surface sediment. In turn, the barrier that prevented the exchange of $Fe^{2+}$ from the porewater with the bottom water is broken and $Fe^{2+}$ concentrations increase in the burrow and can be exchanged with the bottom waters by pumping organisms. In addition, it was reported for suboxic sediments that burrow-dwelling organisms may increase benthic $Fe^{2+}$ fluxes (Berelson et al., 2003, Elrod et al., 2004). This scenario could also happen off Mauritania as the Fe fluxes increased with high bioirrigation intensity and vice versa (Fig. 3.7 B and D).

The flux peak observed at St. VIII (786 m water depth) was likely not an artifact. Independent data of dissolved Fe in the water column revealed a dFe plume and high turbidity values in the bottom waters of St. VIII (Raap, personal communication). Hence, in this case it is likely that sediment resuspension favored the release of Fe. Again, rapid Fe complexation to organic ligands may stabilized the dissolved Fe from the pore waters.

The mean Fe/Al ratio of all cores along the depth transect was 0.55 which is in the range of the reported background ratio of 0.4 to 0.8 (Table 3.5). The large range of the Fe/Al background ratio is a result of the various rock and sediment types in the Saharan dessert – the source area for the Fe supply. However, the sedimentary Fe/Al ratios are enriched in Fe compared to the average upper continental crust with a Fe/Al ratio of 0.44 (McLennan, 2001).

Increased ratios of 0.61 on average were found at stations III to V although dissolved Fe was released from the sediments. This indicates an intense detrital Fe supply exceeding the Fe release. Therefore, Fe redistribution due to dissolution, transport and re-precipitation cannot be determined from the Fe/Al ratios. The shifts in solid phase concentrations were likely an effect of grain size changes induced by strong bottom water currents. Elevated Fe/Al ratios were found to be concurrent to enhanced Ti/Al ratios at St. III to V (Fig. 3.4).

**Table 3.5** Average sedimentary Fe/Al ratios of the multiple-corers from each station along the depth transect.

| **Station** | **Bottom water depth** | **Fe/Al** |
|---|---|---|
| 659 MUC 14 | 47 | 0.47 |
| 686 MUC 19 | 66 | 0.51 |
| 628 MUC 10 | 90 | 0.63 |
| 672 MUC 17 | 129 | 0.62 |
| 697 MUC 20 | 169 | 0.61 |
| 583 MUC 7C | 236 | 0.57 |
| 554 MUC 5 | 412 | 0.5 |
| 534 MUC 3 | 786 | 0.5 |
| 524 MUC 1 | 1108 | 0.51 |
| **Average Fe/Al** | | **0.55** |

**Fig. 3.7**

(A) Benthic chamber $TPO_4^{3-}$ in mmol $m^{-2}$ $d^{-1}$ along the depth transect at 18°N.
(B) Diffusive $Fe^{2+}$ fluxes in mmol $m^{-2}$ $d^{-1}$ along the depth transect at 18°N.
(C) FDIC fluxes in mmol $m^{-2}$ $d^{-1}$ along the depth transect at 18°N (Clemens et al., 2014).
(D) Depth-integrated bioirrigation coefficient (dimensionless) along the 18°N depth transect, normalized to the deepest station (Gier et al., submitted).
(E) Permeability in $m^2$ determined during MSM17-4 at the same sites along the 18°N depth transect as visited during M107 (Sokoll et al., 2016).
(F) Sand / Mud distribution in % described by Dale et al. (2014), derived from samples taken during MSM17-4 at the same stations as sampled during M107 along the 18°N depth transect.

The Roman numbers on top denote the station numbers that are also given in Table 3.1.

The grey lines at 90 and 412 m water depths depict the two bottom water oxygen minima that were observed during cruise M107.

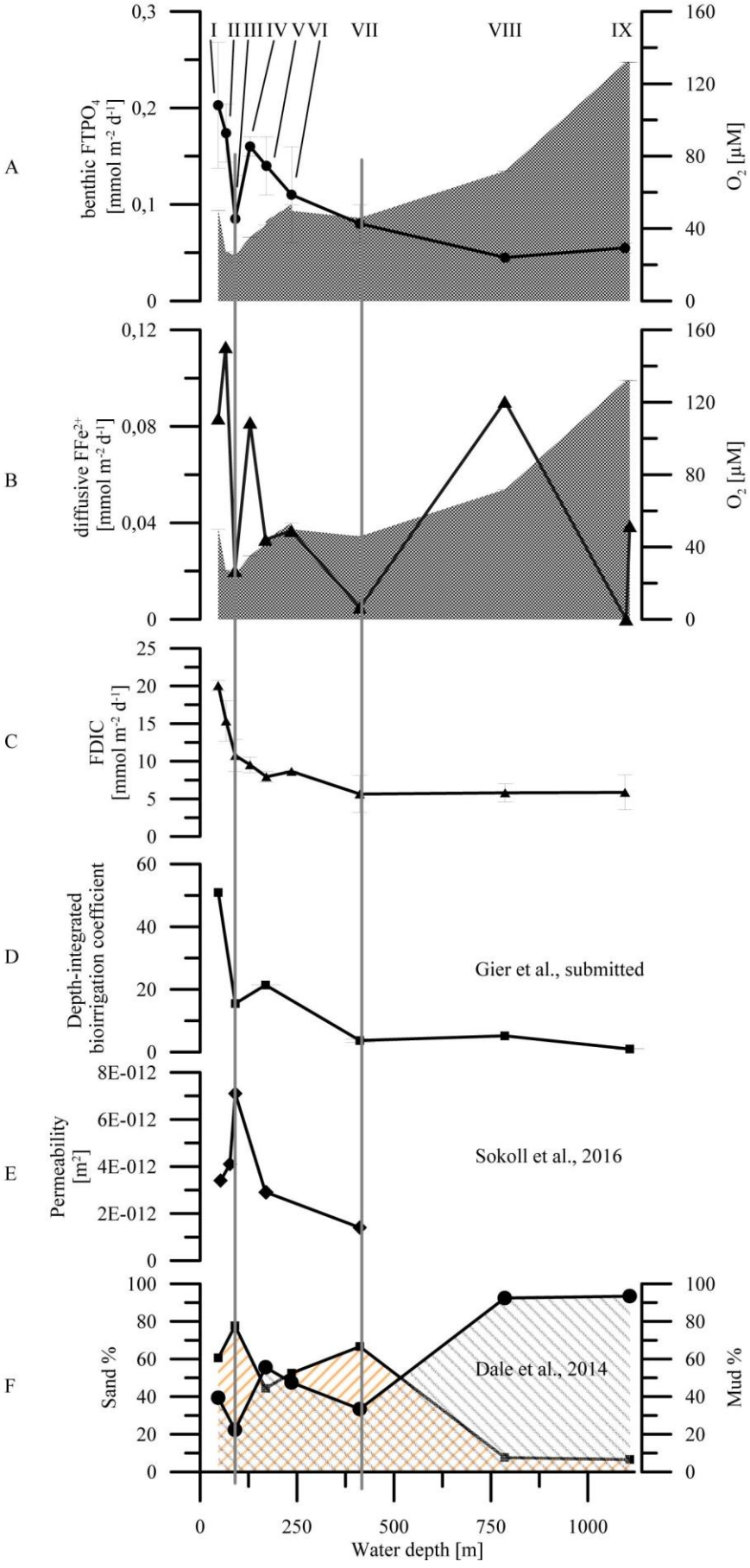
A
B
C
D
E
F
I II III IV V VI VII VIII IX
benthic FTPO4 [mmol m-2 d-1]
diffusive FFe2+ [mmol m-2 d-1]
FDIC [mmol m-2 d-1]
Depth-integrated bioirrigation coefficient
Permeability [m2]
Sand %
Mud %
O2 [µM]
Gier et al., submitted
Sokoll et al., 2016
Dale et al., 2014
Water depth [m]
0
250
500
750
1000

**Comparison of P and Fe fluxes from two cruises**

P and Fe fluxes were measured during spring in the upwelling season in 2011 (MSM17/4) and at the end of spring in 2014 (M107). The same stations were visited during these cruises.

Overall, the data sets of the P and Fe fluxes at 18° N are in the same order of magnitude (Fig. 3.8 and 3.9). However, the P and Fe release rates were continuously lower in water depths between 40 and 240 m during MSM17-4. This could be an effect of overall higher bottom water oxygen concentrations ($\geq$ 50 µM $O_2$) compared to the conditions during M107 (Table 3.1) inhibiting benthic nutrient exchange to the overlying bottom waters.

Only at 98 and 236 m water depth the Fe release was higher than during cruise M107. During M107 cores from 66, 90 and 129 m water depth were sliced in 2 cm intervals due to the use of rhizones, whereas all other cores from M107 and MSM17-4 were sliced in 1cm intervals. However, as diffusive fluxes are usually calculated from the very surface sediment, the magnitudes of the $Fe^{2+}$ fluxes determined from MSM17-4 cores are more realistic. Nevertheless, both datasets include the sharp decline of the Fe flux at ~ 90 m water depth consolidating this feature and indicating long time persistence. Furthermore, the unusual high $Fe^{2+}$ flux found at 789 m water depth was even higher during the previous cruise.

Overall, it remains puzzling if the decreased bottom water oxygen concentration in shallow waters and the slightly enhanced P and Fe release are a consequence of ongoing oxygen loss in the Mauritanian upwelling as we only compare two data sets.

### 3.5.2 Comparison of Fe and P fluxes in the Mauritanian and the Peruvian Oxygen Minimum Zone

In this section, we compare comprehensive data sets of P and Fe fluxes of two prominent eastern boundary upwelling systems, the Mauritanian and Peruvian Upwelling (Noffke et al, 2012, Lomnitz et al., 2016, Scholz et al, 2016). The most prominent difference between the two areas is the bottom water oxygen concentration. Mauritanian bottom waters were not reaching $O_2$ concentrations below 20 µM (a threshold for the definition of an OMZ; Helly and Levin, 2004) at any time during our measuring campaigns. Even during the intense upwelling periods in spring, when the sampling campaigns took place, the lowest $O_2$ levels detected at ~ 90 m water depth were around 27 µM (M107 cruise in 2014). In contrast, the Peruvian Upwelling is highly dynamic where long-lasting periods of anoxic and nitrate-reducing (nitrogenous) conditions are interrupted by short-lived oxic and sulfidic events (Gutiérrez et al., 2008, Noffke et al., 2012, Schunk et al., 2013, Scholz et al., 2016, Graco et al., 2016 in discussion).

Furthermore, the primary production rates of the Mauritanian Upwelling are slightly lower (0.3-2.3 g C $m^{-2}$ $d^{-1}$ (Morel et al., 1996)) than reported for the Peruvian Upwelling area (1.8-3.6 g C $m^{-2}$ $d^{-1}$ (Dale et al., 2015 and references therein). However, $PO_4^{3-}$ and $Fe^{2+}$ fluxes are ultimately

driven by POC degradation in the sediment. In the present context, it is therefore more meaningful to compare DIC fluxes rather than primary production rates in the two upwelling areas.

Overall, the DIC fluxes indicate much higher organic matter degradation at shallow water depths of about 70 m off Peru (65.9 ± 21 mmol $m^{-2}d^{-1}$) compared to Mauritania (15.34 ± 2.67 mmol $m^{-2}d^{-1}$). Hence, the amount of carbon reaching the sea floor has to be much lower off Mauritania than off Peru. Furthermore, the microbial community degrading organic matter in the sediments is likely different, e.g. dense mats of sulfide-oxidizing bacteria are absent off Mauritania due to high bottom water $O_2$ concentrations.

**Phosphate release rates**

Mauritanian and Peruvian P release rates diverge mainly in water depth between 50 to 420 m (Fig. 3.8, Noffke et al., 2012, Lomnitz et al., 2016, this study). P release measured off Peru is up to 2 times higher than off Mauretania. Accordingly, the porewater phosphate concentrations reported off Peru were in general at least twice as high as off Mauretania (Noffke et al., 2012, this study).

As mentioned above, high POC degradation rates and low bottom water oxygen concentrations favor a strong P release. However, also local features modulate the magnitude of the fluxes significantly. Off Peru, sulfide oxidizing bacteria have been suggested to play a key role in benthic P cycling (Lomnitz et al., 2016). They were found in dense bacterial mats in water depth between 70 and 300 m and are adapted to the oscillating redox conditions prevailing there. It was described that such organisms store intracellular polyphosphates during oxic conditions and degrade these to gain energy when anoxic conditions occur (Schulz and Schulz, 2005). While polyphosphates are degraded phosphate is released to the bottom water enhancing the benthic phosphate release. Such organisms are absent in the Mauritanian Upwelling, but instead burrow dwelling macrofauna is present modulating P release rates (see section 6.2.).

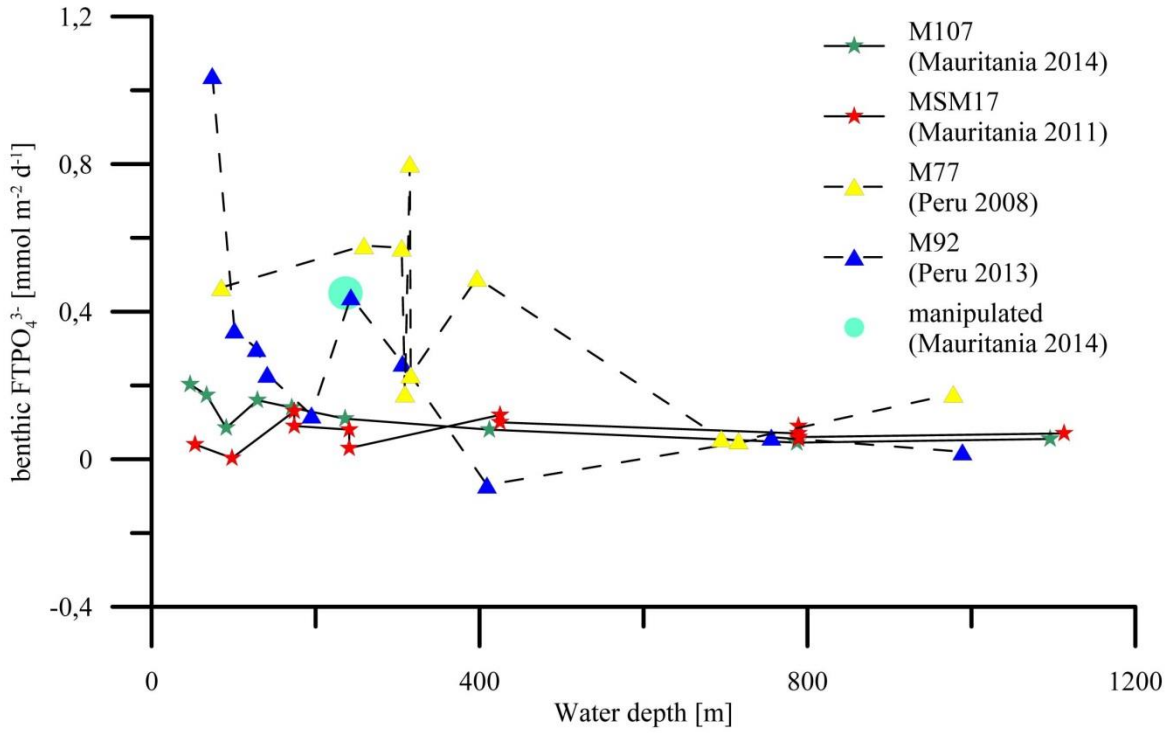


**Fig. 3.8** Datasets of benthic chamber $TPO_4^{3-}$ (mmol $m^{-2}$ $d^{-1}$) from the Mauritanian Upwelling (MSM17/4 and M107) along the 18°N depth transect and from the Peruvian Upwelling (M77 and M92) along 11 and 12°S depth transects. The single blue dot denotes the P release determined from the $O_2$ manipulation experiments.

**Iron release**

Despite considerable differences in the bottom water oxygen concentrations, the Fe fluxes of the Mauritanian and Peruvian Upwelling are in overall good accordance (Fig. 3.9). At first sight, the similarity of Fe fluxes off Mauretania and Peru is remarkable. The porewater $Fe^{2+}$ concentrations found off Mauritania were of the same magnitude or slightly lower as found in the porewaters of the Peruvian Upwelling region (Noffke et al., 2012). Especially $Fe^{2+}$ fluxes measured during the M92 cruise are more or less of the same order of magnitude as off Mauritania, but during that sampling campaign weakly sulfidic waters and high porewater sulfide concentrations (Scholz et al., 2016) reduced $Fe^{2+}$ fluxes on the shallow shelf. In contrast, some stations from the M77 cruise (Noffke et al., 2012, 11° S, similar water depths) had exceptional high $Fe^{2+}$ fluxes at ~ 80 m water depth. As suggested by Noffke et al., 2012 this was due to an oxygenation event that took place shortly before the sampling campaign. During this event dissolved Fe was reoxidized and deposited at the seafloor thereby replenishing the reactive Fe inventory of the sediments. During the following anoxic period, the precipitated Fe (oxyhydr)oxides were dissolved and released to the bottom water. Low Fe fluxes in the Peruvian core OMZ measured during both cruises M77 and M92 were attributed to persistent anoxic bottom waters causing a depletion of the available Fe pool over time (Noffke et al., 2012, Scholz et al., 2011, 2014). Overall, numerous

environmental characteristics of both areas lead to comparable benthic Fe fluxes although major control parameters, like the degradation rates of organic matter and the bottom water oxygen level were largely different. In conclusion, this means that the prediction of benthic Fe fluxes is a complex problem and requires the consideration of various environmental parameters.

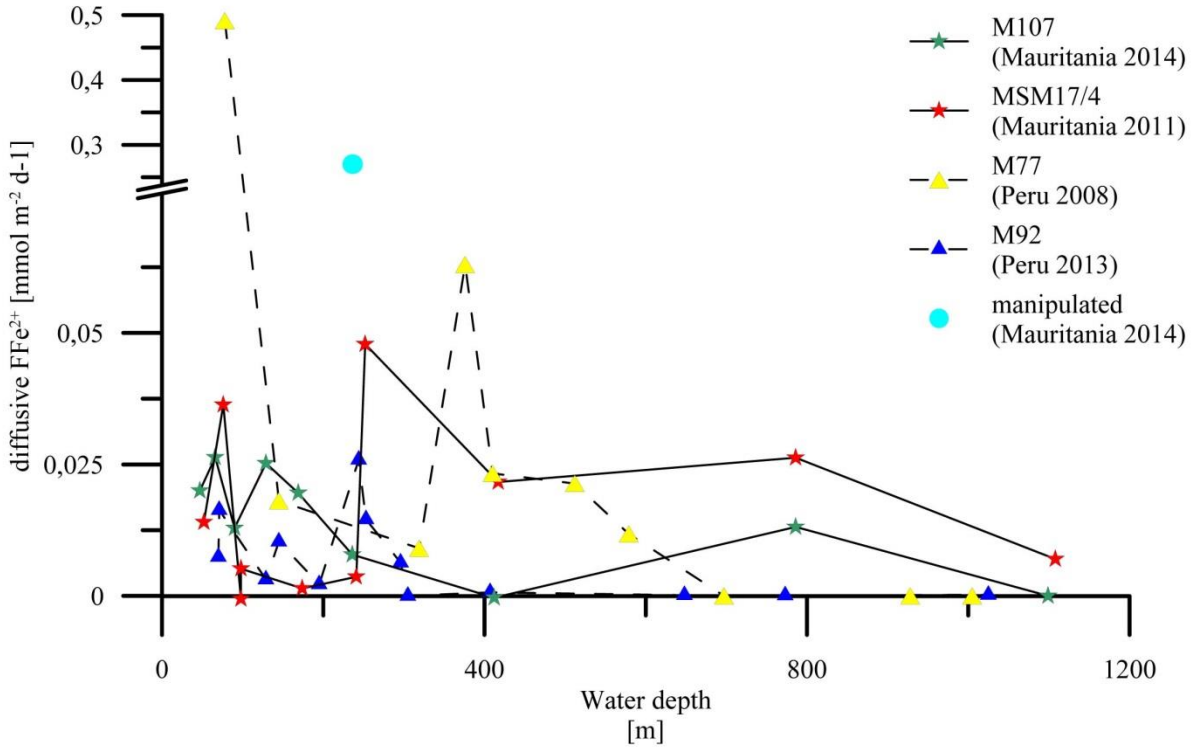


**Fig. 3.9** Datasets of diffusive $Fe^{2+}$ fluxes (mmol $m^{-2}$ $d^{-1}$) from the Mauritanian Upwelling (MSM17/4 and M107) along the 18°N depth transect and from the Peruvian Upwelling (M77 and M92) along 11 and 12°S depths transects. The single blue dot denotes the Fe release determined from the $O_2$ manipulation experiments.

### 3.5.3 Ex situ deoxygenation experiments

In order to estimate the P and Fe release potential of the Mauritanian sediments under anoxic conditions, we conducted ex situ deoxygenation experiments. The resulting P release into the bottom water after less than 9 days without oxygen reached 0.15 ± 0.04 mmol $m^{-2}$ $d^{-1}$, which is in the same order of magnitude as found in the OMZ off Peru (Fig. 3.5 and Table 3.6, Noffke et al., 2012, Lomnitz et al., 2016). Similarly, the Fe release increased to 0.27 mmol $m^{-2}$ $d^{-1}$ which is only slightly lower than the fluxes measured off Peru after bottom water oxygenation (Fig. 3.5, Table 3.6). This result implies a significant release potential of dissolved Fe and P from the sediment off the Mauritanian Upwelling upon increasing deoxygenation. However, it remains unknown how indicative the experimental results are for natural P release when $O_2$ concentrations would decrease in the future. Due to the seasonality of the upwelling it is likely that nutrients are released in a pulse after reloading the nutrient inventories during less reducing periods. Similar mechanisms were described for the Peruvian Upwelling where nutrient capacities reload during oxygenation events and unload during strong anoxic phases (Noffke et al., 2012).

## 3.6 Conclusions

Benthic P and Fe release within the Mauritanian Upwelling area is largely controlled by the rate of organic matter degradation in the surface sediment. In addition, sediment characteristics seem to have a certain impact on benthic fluxes while the effect of bottom water oxygenation is low. Both, intense bioirrigation as well as bottom water percolation through permeable surface sediments along horizontal pressure gradients induced by bottom currents and topography enhance the nutrient release across the sediment bottom water interface. Dissolved Fe escapes to the water column through anoxic microniches build by burrowing organisms and is likely stabilized by complexation with organic ligands in the bottom waters. P mass balance calculations reveal a P deficit at 240 m water depth that could be a result of intense downslope transport of P containing particles contributing to the P burial flux at this station or a lower TPP/POC ratio of the sinking particles compared to the suspended particles that we analyzed.

Moreover, comparing P and Fe fluxes from 2011 and 2014 revealed only slight differences that are likely induced by higher bottom water oxygen concentrations during the first sampling campaign. Ex situ deoxygenation experiments resulted in P and Fe fluxes comparable in magnitude to naturally occurring benthic fluxes in the OMZ offshore Peru where anoxic conditions in the water column prevail. Although these results indicate enhanced nutrient release from sediments underneath the Mauritanian OMZ in case of progressive deoxygenation, it remains somehow unclear how sediments will react on longer time scales and how the overall upwelling system will be affected.

## Acknowledgements

We are very grateful to the crew of RV *Meteor* during cruise M107 and the crew of RV *Maria S. Merian* during cruise MSM17/4 for the support. Our thanks also go to A. Petersen, M. Türk, and S. Cherednichenko for their assistance in deploying the landers. For their enthusiastic help and cooperation during biogeochemical analyses on board and in the home laboratory, we thank B. Domeyer, V. Thönissen, S. Trinkler, S. Kriwanek, A. Bleyer, R. Suhrberg. This work is a contribution to the Sonderforschungsbereich 754 “Climate – Biogeochemistry Interactions in the Tropical Ocean” (www.sfb754.de), which is supported by the Deutsche Forschungsgemeinschaft.

## Author contributions

U. Lomnitz, A. W. Dale, S. Sommer and D. Clemens conducted the shipboard work and geochemical analysis, and contributed to the manuscript. C. Hensen, K. Wallmann, F.Scholz and A. Noffke contributed to the interpretation and discussion of the data and helped with the manuscript preparation.

## 3.7 References

Aspila, K. I., H. Agemian, and A. S. Y. Chau (1976), A semi-automated Method for the Determination of Inorganic, Organic and Total Phosphate in Sediments, Analyst, 101, 187-197.

Baker, A. R., T. D. Jickells, M. Witt, and K. L. Linge (2006), Trends in the solubility of iron, aluminium, manganese and phosphorus in aerosol collected over the Atlantic Ocean, Marine Chemistry, 98(1), 43-58.

Behrenfeld, M. J., and P. G. Falkowski (1997), Photosynthetic rates derived from satellite-based chlorophyll concentration, Limnology and Oceanography, 42(1), 1-20.

Berelson, W., J. McManus, K. Coale, K. Johnson, D. Burdige, T. Kilgore, D. Colodner, F. Chavez, R. Kudela, and J. Boucher (2003), A time series of benthic flux measurements from Monterey Bay, CA, Continental Shelf Research, 23(5), 457-481.

Berghuis, E. M., G. C. A. Duineveld, and J. Hegeman (1993), Primary production and distribution of phytopigments in the water column and sediments on the upwelling shelf off the Mauritanian coast (Northwest Africa), Hydrobiologia, 258(1), 81-93.

Broecker, W. S. (1982), Glacial to interglacial changes in ocean chemistry, Progress in Oceanography, 11(2), 151-197.

Carr, M.-E. (2001), Estimation of potential productivity in Eastern Boundary Currents using remote sensing, Deep Sea Research Part II: Topical Studies in Oceanography, 49(1–3), 59-80.

Clemens, D. (2014), Quantifying benthic organic matter decomposition in the Mauritanian oxygen minimum zone (18° N). Bachelor Thesis, Christian-Albrechts-Universität zu Kiel. 31 pages, Kiel.

Cropper, T. E., E. Hanna, and G. R. Bigg (2014), Spatial and temporal seasonal trends in coastal upwelling off Northwest Africa, 1981–2012, Deep Sea Research Part I: Oceanographic Research Papers, 86, 94-111.

Dale, A. W., V. J. Bertics, T. Treude, S. Sommer, and K. Wallmann (2013), Modeling benthic–pelagic nutrient exchange processes and porewater distributions in a seasonally hypoxic sediment: evidence for massive phosphate release by *Beggiatoa*?, Biogeosciences, 10(2), 629-651.

Dale, A. W., S. Sommer, E. Ryabenko, A. Noffke, L. Bohlen, K. Wallmann, K. Stolpovsky, J. Greinert, and O. Pfannkuche (2014), Benthic nitrogen fluxes and fractionation of nitrate in the Mauritanian oxygen minimum zone (Eastern Tropical North Atlantic), Geochimica et Cosmochimica Acta, 134(0), 234-256.

Dale, A. W., et al. (2015), Organic carbon production, mineralisation and preservation on the Peruvian margin, Biogeosciences, 12(5), 1537-1559.

Emerson, D. (2015), The Irony of Iron – Biogenic Iron Oxides as an Iron Source to the Ocean, Frontiers in Microbiology, 6, 1502.

Elrod, V. A., W. M. Berelson, K. H. Coale, and K. S. Johnson (2004), The flux of iron from continental shelf sediments: A missing source for global budgets, Geophysical Research Letters, 31(12).

Faul, K. L., A. Paytan, and M. L. Delaney (2005), Phosphorus distribution in sinking oceanic particulate matter, Marine Chemistry, 97(3–4), 307-333.

Fischer, G., C. Reuter, G. Karakas, N. Nowald, and G. Wefer (2009), Offshore advection of particles within the Cape Blanc filament, Mauritania: Results from observational and modelling studies, Progress in Oceanography, 83(1–4), 322-330.

Förster, A.: Geotechnical measurements to characterise slope sediments and to identify landslide mechanisms and their impact on ecosystems, PhD dissertation, Bremen University, Bremen, 2011.

Glud, R. N. (2008), Oxygen dynamics of marine sediments, Marine Biology Research, 4(4), 243-289.

Graco, M., S. Purca, B. Dewitte, O. Morón, J. Ledesma, G. Flores, C. Castro, and D. Gutiérrez (2016), The OMZ and nutrients features as a signature of interannual and low frequency variability off the peruvian upwelling system, Biogeosciences Discuss., 2016, 1-36.

Gutiérrez, D., E. Enríquez, S. Purca, L. Quipúzcoa, R. Marquina, G. Flores, and M. Graco (2008), Oxygenation episodes on the continental shelf of central Peru: Remote forcing and benthic ecosystem response, Progress in Oceanography, 79(2–4), 177-189.

Hartmann, M., P. J. Müller, E. Suess, and C. H. van der Weijden (1976), Chemistry of Late Quaternary sediments and their interstitial waters of sediment cores from the Nort-West African continental margin, in Supplement to: Hartmann, M et al. (1976): Chemistry of Late Quaternary sediments and their interstitial waters from the northwest African continental margin. Meteor Forschungsergebnisse, Deutsche Forschungsgemeinschaft, Reihe C Geologie und Geophysik, Gebrüder Bornträger, Berlin, Stuttgart, C24, 1-67, edited, PANGAEA.

Helly, J. J., and L. A. Levin (2004), Global distribution of naturally occurring marine hypoxia on continental margins, Deep Sea Research Part I: Oceanographic Research Papers, 51(9), 1159-1168.

Ingall, E., and R. Jahnke (1994), Evidence for enhanced phosphorus regeneration from marine sediments overlain by oxygen depleted waters, Geochimica et Cosmochimica Acta, 58(11), 2571-2575.

Ingall, E., and R. Jahnke (1997), Influence of water-column anoxia on the elemental fractionation of carbon and phosphorus during sediment diagenesis, Marine Geology, 139(1–4), 219-229.

Klar, J. K., et al. (2017), Stability of dissolved and soluble Fe(II) in shelf sediment pore waters and release to an oxic water column, Biogeochemistry, 1-19.

Kristensen, E., G. Penha-Lopes, M. Delefosse, T. Valdemarsen, C. O. Quintana, and G. T. Banta (2012), What is bioturbation? The need for a precise definition for fauna in aquatic sciences, Marine Ecology Progress Series, 446, 285-302.

Li, Y.-H., and S. Gregory (1974), Diffusion of ions in sea water and in deep-sea sediments, Geochimica et Cosmochimica Acta, 38(5), 703-714.

Lomnitz, U., S. Sommer, A. W. Dale, C. R. Löscher, A. Noffke, K. Wallmann, and C. Hensen (2016), Benthic phosphorus cycling in the Peruvian oxygen minimum zone, Biogeosciences, 13(5), 1367-1386.

Martin, J. H. (1990), Glacial-interglacial CO2 change: The Iron Hypothesis, Paleoceanography, 5(1), 1-13.

McLennan, S. M. (2001), Relationships between the trace element composition of sedimentary rocks and upper continental crust, Geochemistry, Geophysics, Geosystems, 2(4).

McManus, J., W. M. Berelson, K. H. Coale, K. S. Johnson, and T. E. Kilgore (1997), Phosphorus regeneration in continental margin sediments, Geochimica et Cosmochimica Acta, 61(14), 2891-2907.

Mittelstaedt, E. (1983), The upwelling area off Northwest Africa—A description of phenomena related to coastal upwelling, Progress in Oceanography, 12(3), 307-331.

Morel, A., D. Antoine, M. Babin, and Y. Dandonneau (1996), Measured and modeled primary production in the northeast Atlantic (EUMELI JGOFS program): the impact of natural variations in photosynthetic parameters on model predictive skill, Deep Sea Research Part I: Oceanographic Research Papers, 43(8), 1273-1304.

Noffke A., Hensen C., Sommer S., S. F., Bohlen L., Mosch T., Graco M., and Wallmann K. (2012), Title Benthic iron and phosphorus fluxes across the Peruvian oxygen minimum zone, Limnology and Oceanography, 57(3), 851-867.

Ohnemus, D. C., and P. J. Lam (2015), Cycling of lithogenic marine particles in the US GEOTRACES North Atlantic transect, Deep Sea Research Part II: Topical Studies in Oceanography, 116, 283-302.

Oschlies, A., K. G. Schulz, U. Riebesell, and A. Schmittner (2008), Simulated 21st century's increase in oceanic suboxia by CO2-enhanced biotic carbon export, Global Biogeochemical Cycles, 22(4), GB4008.

Pauly, D., and V. Christensen (1995), Primary production required to sustain global fisheries, Nature, 374(6519), 255-257.

Paytan, A., and K. McLaughlin (2007), The Oceanic Phosphorus Cycle, Chemical Reviews, 107(2), 563-576.

Redfield, A. C., B. H. Ketchum, and F. A. Richards (1963), The influence of organisms on the composition of seawater, in The Sea, edited by N. M. Hill, pp. 26-77, Academic Press, London.

Ruttenberg, K. C., and R. A. Berner (1993), Authigenic apatite formation and burial in sediments from non-upwelling, continental margin environments, Geochimica et Cosmochimica Acta, 57(5), 991-1007.

Scheuvens, D., L. Schütz, K. Kandler, M. Ebert, and S. Weinbruch (2013), Bulk composition of northern African dust and its source sediments — A compilation, Earth-Science Reviews, 116, 170-194.

Schmidtko, S., L. Stramma, and M. Visbeck (2017), Decline in global oceanic oxygen content during the past five decades, Nature, 542(7641), 335-339.

Scholz, F., J. McManus, A. C. Mix, C. Hensen, and R. R. Schneider (2014), The impact of ocean deoxygenation on iron release from continental margin sediments, Nature Geosci, 7(6), 433-437.

Scholz, F., C. Hensen, A. Noffke, A. Rohde, V. Liebetrau, and K. Wallmann (2011), Early diagenesis of redox-sensitive trace metals in the Peru upwelling area – response to ENSO-related oxygen fluctuations in the water column, Geochimica et Cosmochimica Acta, 75(22), 7257-7276.

Scholz, F., et al. (2016), Nitrate-dependent iron oxidation limits iron transport in anoxic ocean regions, Earth and Planetary Science Letters, 454, 272-281.

Schulz, H. N., and H. D. Schulz (2005), Large Sulfur Bacteria and the Formation of Phosphorite, Science, 307(5708), 416-418.

Schunck, H., et al. (2013), Giant Hydrogen Sulfide Plume in the Oxygen Minimum Zone off Peru Supports Chemolithoautotrophy, PLOS ONE, 8(8).

Severmann, S., J. McManus, W. M. Berelson, and D. E. Hammond (2010), The continental shelf benthic iron flux and its isotope composition, Geochimica et Cosmochimica Acta, 74(14), 3984-4004.

Sokoll, S., G. Lavik, S. Sommer, T. Goldhammer, M. M. M. Kuypers, and M. Holtappels (2016), Extensive nitrogen loss from permeable sediments off North-West Africa, Journal of Geophysical Research: Biogeosciences, 121(4), 1144-1157.

Sommer, S., P. Linke, O. Pfannkuche, T. Schleicher, S. v. Deimling, A. Reitz, M. Haeckel, and C. Hensen (2009), Seabed methane emissions and the habitat of frenulate tubeworms on the Captain Arutyunov mud volcano (Gulf of Cadiz), Marine Ecology Progress Series, 382, 69-86.

Stookey, L. L. (1970), Ferrozine---a new spectrophotometric reagent for iron, Analytical Chemistry, 42(7), 779-781.

Stramma, L., G. C. Johnson, J. Sprintall, and V. Mohrholz (2008), Expanding Oxygen-Minimum Zones in the Tropical Oceans, Science, 320(5876), 655-658.

Sundby, B., L. G. Anderson, P. O. J. Hall, Å. Iverfeldt, M. M. R. van der Loeff, and S. F. G. Westerlund (1986), The effect of oxygen on release and uptake of cobalt, manganese, iron and phosphate at the sediment-water interface, Geochimica et Cosmochimica Acta, 50(6), 1281-1288.

Wallmann, K. (2010), Phosphorus imbalance in the global ocean?, Global Biogeochemical Cycles, 24(4).

# 4 Widespread iron enrichment below oxygen deficient waters along the South American Coast from 3 to 33 °S

U. Lomnitz[1], F. Scholz[1], C. Hensen[1], and K. Wallmann[1]

[1]GEOMAR Helmholtz-Centre for Ocean Research Kiel, Wischhofstr. 1-3, 24148 Kiel

Correspondence to: Ulrike Lomnitz (ulomnitz@geomar.de)

In preparation for submission

## Abstract

Sediment cores retrieved from the lower boundary of oxygen deficient water bodies (700 – 1100 m water depth) offshore South America between 3 to 33°S were analyzed for evidence of diagenetic iron enrichments caused by the offshore export of dissolved iron from the core of the oxygen minimum zone (OMZ). Previous studies off Peru (Scholz et al., 2014 and 2016) suggested that Fe released by dissimilatory Fe-reduction in permanently oxygen deficient areas of the OMZ can be transported over large distances and re-precipitated at the lower boundary where sufficient oxygen is available. Essentially, our results confirm this hypothesis: Fe/Al ratios of sediments from within the OMZ (11 and 12 °S) were lower than the lithogenic background supporting strong benthic Fe loss due to low bottom water oxygen concentrations and Fe/Al ratios of sediments from the lower boundary of the OMZ (3 – 33°S) are enhanced compared to the lithogenic background. Fe extractions were carried out to differentiate between reactive, pyrite-, and silicate-bound Fe. The results show that silicate Fe is the dominating phase in sediments at the lower boundary of the OMZ. XRD analyses indicate that iron is mainly bound to the authigenic clay mineral glauconite. Although it is known that glauconitization is a widespread phenomenon in deep sea sediments, so far there was no direct evidence that it occurs over an area of more than 3000 km along the South American coast and that there is a clear relation to Fe release within the OMZ. Moreover, due to the fixation of Fe in form of glauconite, Fe is not available for short-term benthic Fe cycling, e.g. caused by the expected global expansion of OMZs. However, the precise effects of deoxygenation on this Fe reservoir are not well constrained and remain subject to further investigations.

## 4.1 Introduction

A large part of the ocean's primary production is limited by micro-nutrients such as iron and other trace elements (Martin, 1990, Boyd and Ellwood, 2010). Organisms require for example bioavailable iron for metabolic processes e.g. to form metalloenzymes for photosynthesis (Raiswell and Canfield, 2012). Due to its sensitivity to oxygen, concentrations of dissolved iron in seawater are very low. Most of the bioavailable Fe in surface waters has been considered to be derived from eolian dust input, however, more recently sediment derived iron has also been considered as important source for the oceanic iron inventory (Lam and Bishop, 2008, Scholz et al., 2014a, Dale et al., 2015, Scholz et al, 2016). The Fe release into the bottom water was found to be strongly enhanced in sediments overlain by anoxic bottom waters as prevailing in oxygen minimum zones (OMZs) (Severmann et al., 2010, Noffke et al., 2012). Reductive dissolution of Fe (oxyhydr)oxides to dissolved ferrous Fe is induced by Fe-reducing bacteria (Scholz et al., 2016 and references therein) and diminishes the reactive Fe pool of the sediments, while the absence of an oxidized surface layer in the sediments favors $Fe^{2+}$ release into bottom waters (Noffke et al., 2012). This Fe loss in the core OMZ can be derived from solid phase Fe/Al ratios which are

below the lithogenic background ($Fe/Al_{lithback}$) of 0.47 (Scholz et al., 2011). In contrast, Fe/Al ratios of sediments at the lower boundary of the OMZ are higher than the lithogenic background, depicting a diagenetic Fe re-precipitation due to higher bottom water oxygen and nitrate concentrations (Scholz et al., 2016). A large fraction of the diagenetically released Fe is trapped here and not available for fueling primary productivity in the surface ocean. It is therefore crucial to investigate the regional expansion and the geochemical signature of such Fe enrichments.

Here, we present a comprehensive collection of sediment cores retrieved between 3 and 33°S that were geochemically analyzed in order to identify Fe enrichments and characterize Fe species and minerals. Cores were mainly taken in water depth between 700 and 1100 m at bottom water $O_2$ concentrations > 20 µM. For comparison, we investigated also a few cores from the core OMZ.

## 4.2 Study Area

The Eastern South Pacific OMZ is one of the largest open marine water masses being depleted in oxygen. OMZs establish due to upwelling of cold, nutrient rich waters inducing high rates of export production and oxygen respiration. Coast parallel winds are the driver for offshore Ekman transport of surface waters whereas seasonal changes in wind intensity modulate the OMZ intensity. Additionally, the El Niño Southern Oscillation (ENSO) and internal waves lead to interannual water geochemistry variations on short time scales (Gutiérrez et al., 2008). OMZ sediments are dominated by diatomaceous muds with a total organic carbon content of up to 20 % in the core OMZ and 5 to 10 % in water depth > 600 m (Böning et al., 2004). The supply of detrital material is low due to the very small number of rivers discharging on the west side of the Andes into the Pacific Ocean. OMZs are hotspots for benthic biogeochemical cycling due to the redox-sensitivity of numerus marco- and micronutrient fluxes. Due to intense organic matter degradation in sediments of the core OMZ, nutrients such as phosphate and iron were reported to be released into the water column (Noffke et al., 2012, Scholz et al., 2011). However, only a small fraction of the released nutrients is recycled to the photic zone further fueling primary production. Large parts of the released nutrients are subject to fast re-oxidation in the bottom waters and / or offshore transport

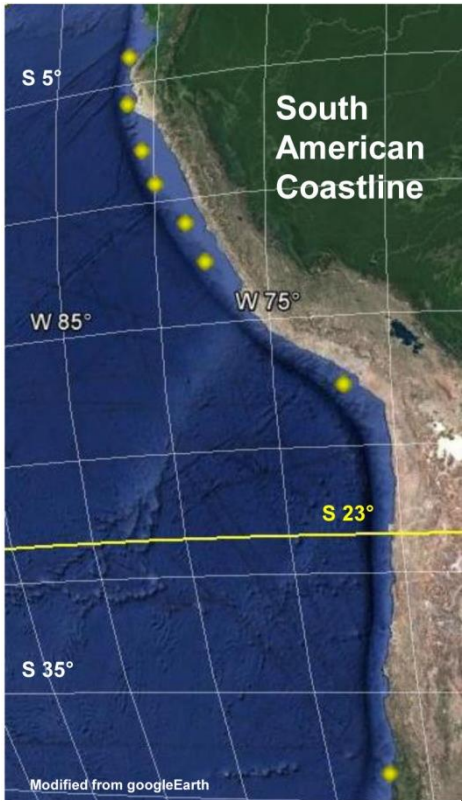


**Fig. 4.1** Map of the core locations (yellow dots) with sedimentatry Fe enrichments ranging from 3 to 33°S.

close to the seabed (Scholz et al., 2014). Hence, it is crucial to investigate the sediment geochemistry of sediments below the OMZ along the entire South American Coast.

## 4.3 Methods

Sediment cores were analyzed using total digestion, sequential Fe extraction and X-ray diffraction analysis (XRD) in order to investigate whether Fe enrichments that were previously described for sediments below the OMZ at 11°S (Scholz et al., 2011, 2014, 2016) are a local finding or widespread along the South American Coast.

We investigated surface sediments retrieved with a multiple-corer at 6 stations within the core OMZ ($O_2$ < 20 µM) and 11 stations located below the lower oxycline of the OMZ between 3 and 33°S (Fig. 4.1). Corers were taken during 4 different cruises in 2008, 2010 and 2013 along the South American Coast (Table 4.1).

**Table 4.1** Station list including the cruise of core recovery, geographical coordinates, water depth, date of sampling, bottom water $O_2$ concentrations at sampling time. The sedimentation rates were taken from previously published data: [a]Scholz et al., 2011, [b]Dale et al., 2015, [c]Lomnitz, 2012 (Master thesis).

| Cruise | Station | Lat. °S | Long. °W | Date | Water depth (m) | Bottom water $O_2$ (µM) | Sediment-ation rate (cm $yr^{-1}$) |
|---|---|---|---|---|---|---|---|
| M77/2 | 060-1MUC | 3°51'5.4'' | 81° 15'29.52'' | 12/12/2008 | 701 | 34 | |
| M77/2 | 059-2MUC | 3°56'57.12'' | 81°19'9.48'' | 12/12/2008 | 995 | 66 | |
| M77/2 | 052-3MUC | 5°29'0.6'' | 81°27'0.72'' | 12/09/2008 | 1252 | 69 | |
| M77/2 | 047-3MUC | 7°52'0.48'' | 80°31'21.72'' | 12/07/2008 | 625 | 3 | |
| M77/2 | 028-2MUC | 09°17'41.4'' | 79°53'51.6'' | 12/03/2008 | 1107 | 53 | |
| M77/1 | 455MUC21 | 11°0'0.72'' | 78°19'14.16'' | 11/04/2008 | 465 | 3 | |
| M77/1 | 445MUC15 | 10°59'58.92'' | 78°30'1.08'' | 11/03/2008 | 928 | 27 | |
| M77/1 | 549MUC53 | 10°59'48.48'' | 78°31'15.6'' | 11/13/2008 | 1008 | 44 | 0.058[a] |
| M92 | 107MUC23 | 12°27'11.88'' | 77°29'29.76'' | 01/15/2008 | 407 | bdl | |
| M92 | 86MUC17 | 12°31'23.88'' | 77°35'12.84'' | 01/13/2013 | 774 | 32 | 0.035[b] |
| M92 | 155MUC28 | 12°35'23.64'' | 77°40'59.88'' | 01/19/2013 | 1025 | 46 | 0.06[b] |
| M77/1 | 623MUC87 | 12°38'9.6'' | 77°34'34.68'' | 11/20/2008 | 1085 | 28 | |
| M77/1 | 407MUC07 | 17°34'22.08'' | 71°55'59.88'' | 10/29/2008 | 790 | 46 | |
| M77/1 | 409MUC09 | 17°38'21.48 | 71°58'14.88'' | 10/30/2008 | 920 | 59 | |
| SO210 | 124MUC12 | 33°23'25.44'' | 71°51'0.72'' | 10/28/2010 | 165 | 10 | |
| SO210 | 113-2MUC09 | 33°23'59.28'' | 71°51'59.4'' | 10/26/2010 | 232 | 6 | 0.18[c] |
| SO210 | 104MUC06 | 33°23'21.48'' | 73°52'44.4'' | 10/25/2010 | 337 | 19 | |

Total Al, Fe and potassium (K) concentrations were determined by ICP-OES after complete sediment dissolution using HCl, $HNO_3$ and HF (Scholz et al., 2011). The average standard deviations were 0.64 % RDS for Al, 0.69 % RSD for Fe and 0.73 % RSD for K. To ensure

reproducibility of our measurements we included the referenced sediment standards SDO-1 and MESS-3 to our measurements.

The sequential Fe extractions were performed according to the following protocol:
In a first step, **easily HCl-extractable Fe ($Fe_{0.5M\text{-}HCl}$)** (Fe bound to amorphous Fe(III)oxides, carbonates, Fe monosulfides, and some silicate minerals (Kostka and Luther, 1994)). was leached by adding 20 ml of 0.5 M HCl to 0.5 g of freeze dried and ground sediment. Samples were shaken for 1 h and afterwards centrifuged to separate sample solution from the remaining sediment. After decantation and filtration of the overlying solution, the remaining sediments was washed with 10 ml MilliQ, centrifuged and decanted. Both solutions were mixed and analyzed using ICP-OES VARIAN 720-ES.

Secondly, we extracted **silicate Fe ($Fe_{Si}$)** comprising Fe bound in clay minerals (Huerta-Diaz and Morse, 1990). Therefore, 10 ml of 10M HF were added to the remaining sediments from the first step and shaken for 1 h and decanted afterwards. Another 10 ml of 10 M HF were added and shaken for 16 h. Addition of 2 g of boric acid for 8 h induced dissolution of fluoride minerals that may have precipitated. After centrifugation and decantation, this solution was added to the previously decanted sample solution. The remaining sediments were washed with 10 ml boiling deionized water and the sample solution was added to the combined solutions. The combined solutions were measured using ICP-OES.

In the last extraction step **pyrite Fe ($Fe_{Py}$)** was separated from the remaining sediment from the last extraction step by shaking for 2 h in 10 ml concentrated $HNO_3$ (Huerta-Diaz and Morse, 1990). Afterwards the solution was filtered through a cellulose filter to separate the solution from low-density organic aggregates (Scholz and Neumann, 2007), then it was washed with 10 ml deionized water and filtered again. The combined solutions were measured using ICP-OES.

A notable disadvantage of the HCl-based extraction is that it does not fully dissolve crystalline Fe (oxyhydr)oxides such as goethite and hematite, although these are considered reactive on early diagenetic time scales (Canfield et al., 1992). However, Scholz et al. (2014) showed that the extraction efficiency for Fe minerals leached by 0.5 M HCl and by sodium dithionite are in quite good agreement ($R^2 = 0.72$) for sediments from 11°S.

We monitored the long-term precision of the extraction protocol by including an in-house standard into each extraction run. This in-house standard consists of a homogenized mixture of sediments from the Peruvian continental margin at 11°S. We calculated an average precision of 8% relative standard deviation (RSD) for $Fe_{0.5M\text{-}HCl}$, 4% RSD for $Fe_{sil}$ and 2% for $Fe_{py}$. Only samples where the total recovery is within this error range are reported in the following sections. The average recovery (±1 SD) for these samples was 97 ± 12%.

XRD analysis and quantification of mineral phases, especially glauconite, was carried out using the full-pattern method QUAX at the Central Laboratory for Crystallography and Applied Material Science at the University of Bremen (Vogt et al., 2002). The relative error for glauconite is 5-10 %.

## 4.4 Results and Discussion

In this study, sediments originating from and below the OMZ along the South American continental margin were investigated in order to find out, if similar depletion/enrichment patterns as described along 11°S off Peru (Scholz et al., 2011) exist elsewhere along the margin. We assume the same lithogenic background ratio for all latitudes due to a more or less homogenous rock composition in the source regions of the hinterland in the Andes.

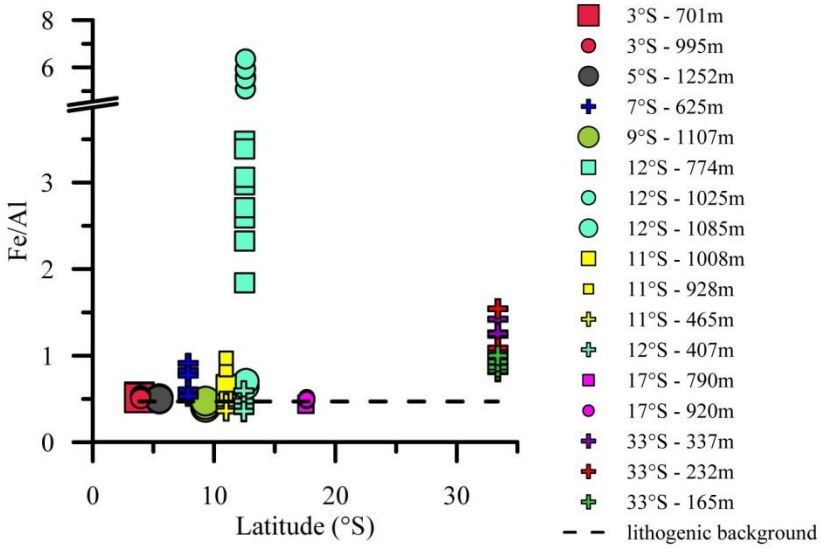


**Fig. 4.2** Fe/Al ratios against the latitude for all investigated cores. The dashed line represents the lithogenic background Fe/Al ratio of 0.47. The legend is valid for all following figures where the same symbols were used.

As expected, the Fe/Al ratios of sediments recovered from within the OMZ ($O_2$ < 20 µM) at 11 and 12°S were slightly below the lithogenic background ratio (Fig. 4.2). In contrast, sediments of cores from 33°S had distinctly higher Fe/Al ratios compared to the lithogenic background (Fig. 4.2), although originating form oxygen deficient waters indicating transient shifts of the OMZ boundaries. The Fe/Al ratios of the sediments from below the OMZ were all elevated compared to the lithogenic background, except in sediments of one core from 17°S (790 m water depth, Fig. 4.2). The overall elevated Fe/Al ratios of sediments from below the OMZ indicate that the Fe enrichment in those sediments is a widespread phenomenon off South America.

Sequential Fe extractions were carried out to identify the Fe speciations in surface sediments (Fig. 4.3). Within the OMZ, Fe is bound in silicate minerals ($Fe_{Sil}$, 67 %), pyrite (26%), and reactive Fe (7%). Below the OMZ, the fractions of reactive Fe and Fe bound in pyrite are strongly diminished and Fe is almost exclusively bound in silicates (94%). The speciation data seem to suggest that

pyrite and reactive Fe phases are transformed into authigenic Fe-bearing silicates at the lower rim of the OMZ. However, the low Fe/Al ratios within the OMZ and the strong Fe/Al increase at the lower rim (Fig. 4.2) point to an additional down-slope Fe transport process that leads to iron depletion in the OMZ and iron enrichment below. Considering the speciation data, it may be concluded that Fe is either transferred in dissolved form or as iron-rich authigenic silicate phase that is preferentially eroded at the upper slope and redeposited at the lower rim of the OMZ.

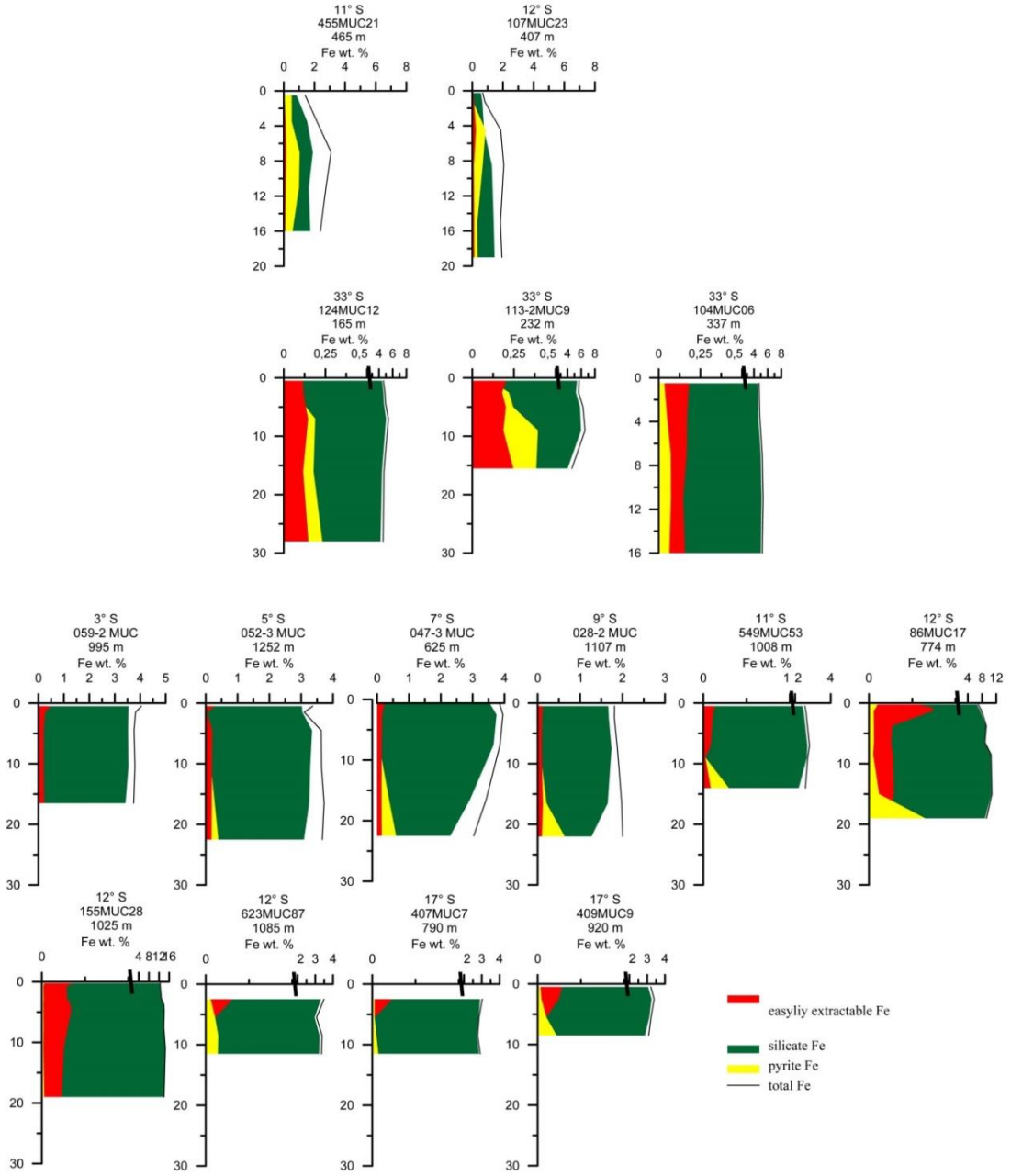


**Fig. 4.3** Distribution of sedimentary Fe species (easily extractable Fe, silicate Fe and pyrite Fe) and total Fe with sediment depth. The upper two rows show Fe species in sediments retrieved within the OMZ ($O_2$ ranging from 0 to 18 µM) at 11, 12 and 33°S. The lower rows show selected cores between 3 and 33°S retrieved below the lower oxycline of the OMZ at bottom water oxygen concentrations $O_2 > 20$ µM.

In order to identify the Fe containing minerals, XRD analyses were conducted. Based on these results, large parts of the Fe accumulating below the OMZ are transformed into the authigenic clay mineral glauconite (Fig 4.4). Glauconite is an authigenic clay mineral containing Fe (II) and Fe (III). It exists mainly in the form of green grains, but occurs also as coatings. During glauconite formation, $Al^{3+}$ is replaced by $Fe^{2+}$ and Mg in the octahedral layers and alkali ions such as potassium (K) are taken up in the exchangeable interlayers to balance the crystal lattice's charge (Scholz et al., 2014 and references therein). For this "layer lattice theory" a detrital smectite precursor is needed (Odin and Matter et al., 1981, Odom, 1984) that evolves from a K-poor glauconitic smectite to a K-rich glauconitic mica (Amorosi et al., 2007).

Numerous studies reported previously, that glauconitization is a widely found process in deep sea sediments favored by slightly reducing conditions and low sedimentation rates and reworking around to world (Odin and Matter et al. 1981). Suits and Arthur (2000) described sediments from the Peruvian margin composed nearly entirely of glauconite with a Fe content of over 18 wt. %. However, the results of the XRD analysis of the sediments show that glauconite occurs in nearly all investigated cores from 3 to 33°S, except 409MUC09 from 17°S (Fig. 4.4). Most glauconite (up to 59 wt. %) was found at 12° S in a core from 1025 m water depth. On average, glauconite comprised 38 wt. % of the sediment at this station, similar as found in a core at 12°S at 774 m water depth. In contrast, a core retrieved during another cruise, but in close vicinity to these stations (623MUC87), contained low glauconite content in the analyzed sediments.

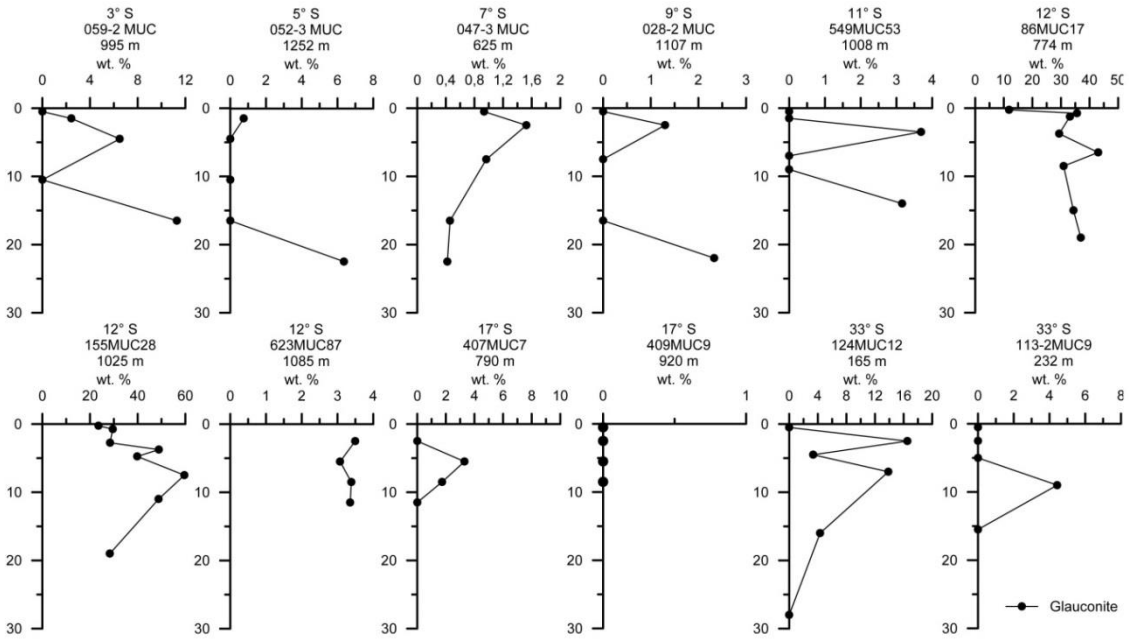


**Fig. 4.4** Sedimentary glauconite content (wt. %) determined by XRD analyses for selected sediment cores from 3 to 33°S. Note that the scales are adapted to the glauconite content for better visualization.

Sediments retrieved from within the OMZ at 11 and 12 were not expected to contain glauconite because prevailing anoxic conditions lead to increased sulfidation of the sediments inhibiting glauconitization. However, this assumption was only validated for sediments from 465 m at 11°S.

At the other station at 12°S (407 m water depth), the sediments contained more than 3 wt. % glauconite. Sediments retrieved from hypoxic waters (33°S) contained up to 16 wt. % glauconite (165 m water depth, 33°S). In some cores, the glauconite content shows zick-zack patterns that are likely depicting changes in the formation conditions of glauconite over time.

Further implications for authigenic glauconite formation are depicted in a plot of K/Al and Fe/Al showing linear trends (Fig. 4.5). During glauconite formation, $Al^{3+}$ is replaced by $Fe^{2+}$ and Mg in the octahedral layers and alkali ions such as potassium (K) are taken up in the exchangeable interlayers to balance the crystal lattice's charge (Scholz et al., 2014 and references therein). For this "layer lattice theory" a detrital smectite precursor is needed (Odin and Matter et al., 1981, Odom, 1984) that evolves from a K-poor glauconitic smectite to a K-rich glauconitic mica (Amorosi et al., 2007). The range of the K/Al ratios observed in our data likely depicts variations in formation kinetics, reaction stoichiometry, and environmental conditions (Baldermann et al., 2017).

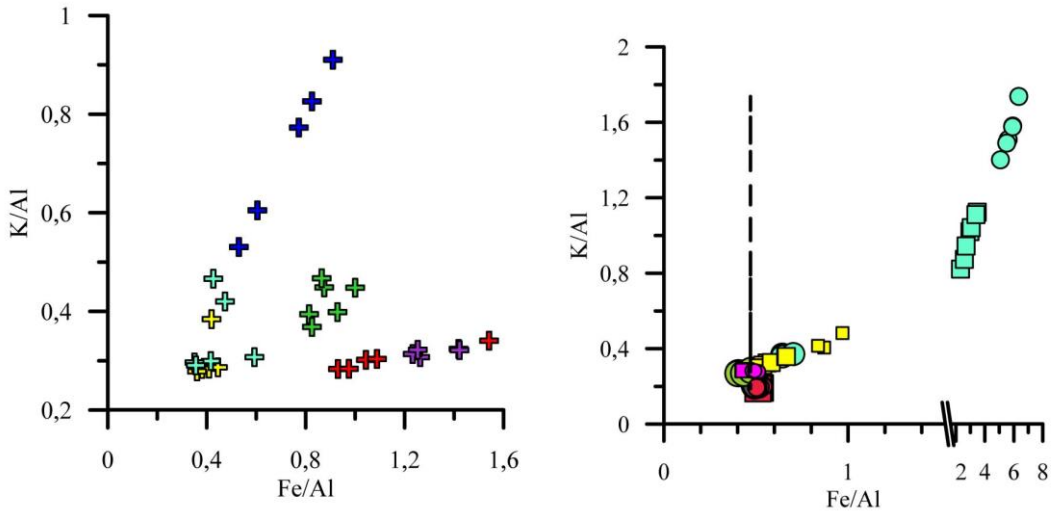


**Fig. 4.5** K/Al vs. Fe/Al plot for cores retrieved in oxygen depleted waters (left panel) and cores retrieved below the lower oxycline of the OMZ (right panel). The dashed line represents the lithogenic background of the Fe/Al ratio (Legend, see Fig. 4.2).

It was previously suggested that low sedimentation rates and a slightly reducing, non-sulfidic milieu with enhanced dissolved Fe concentrations are required for the precipitation of glauconite (Odin and Matter, 1981). Additionally, Si, K, and Mg have to be available in the pore water, which is typically the case in marine subsurface environments. Sediments below oxygen deficient waters off South America are typically fulfilling these requirements. The sedimentation rates are lower than those on the shelf due to a diminished input of terrigenous material (Scholz et al., 2011, Dale et al., 2015) and slightly reducing conditions in the porewater are maintained by low organic matter supply from the water column in such water depth (POC rain rate 5.2 ± 5 – 3.4 ± 1

mmol $m^{-2}$ $d^{-1}$, Dale et al., 2015). As reactive Fe (Fe (oxyhydr)oxides, carbonates, Fe-monosulfides and pyrite) could be transformed to pyrite by sulfidation and is thus no longer available for incorporation into other minerals e.g. glauconite, it is useful to characterize the degree of pyritization (DOP). This parameter was introdcuced by Berner (1970) and is defined as the $Fe_{pyr}/Fe_{react}$ ratio. However, due to varying extraction methods applied, we employ the ratio ($Fe_{py}$ / ($Fe_{0.5M\ HCl}$ + $Fe_{py}$)) that is closely related to DOP (Scholz et al., 2014).

Mean $Fe_{py}$ / ($Fe_{0.5M\ HCl}$ + $Fe_{py}$) ratios range from 0.3 to 0.9 in sediments retrieved from within the OMZ (Fig. 4.6A). The highest ratios occurred in a core from 11°S, 465 m water depth. Concurrently, to the highest $Fe_{py}$ / ($Fe_{0.5M\ HCl}$ + $Fe_{py}$) ratios in the sediments, the glauconite content is lowest (Fig. 4.6B). In sediments retrieved from below the OMZ the mean $Fe_{py}$ / ($Fe_{0.5M\ HCl}$ + $Fe_{py}$) ratios vary from 0.1 to 0.5 (Fig. 4.6A). Highest glauconite contents occurred coincidently with mean $Fe_{py}$ / ($Fe_{0.5M\ HCl}$ + $Fe_{py}$) <0.3 (Fig. 4.6B). At higher ratios, the glauconite content is diminished. Nonetheless, low glauconite contents were also found in sediments with mean $Fe_{py}$ / ($Fe_{0.5M\ HCl}$ + $Fe_{py}$) ratios > 0.5.

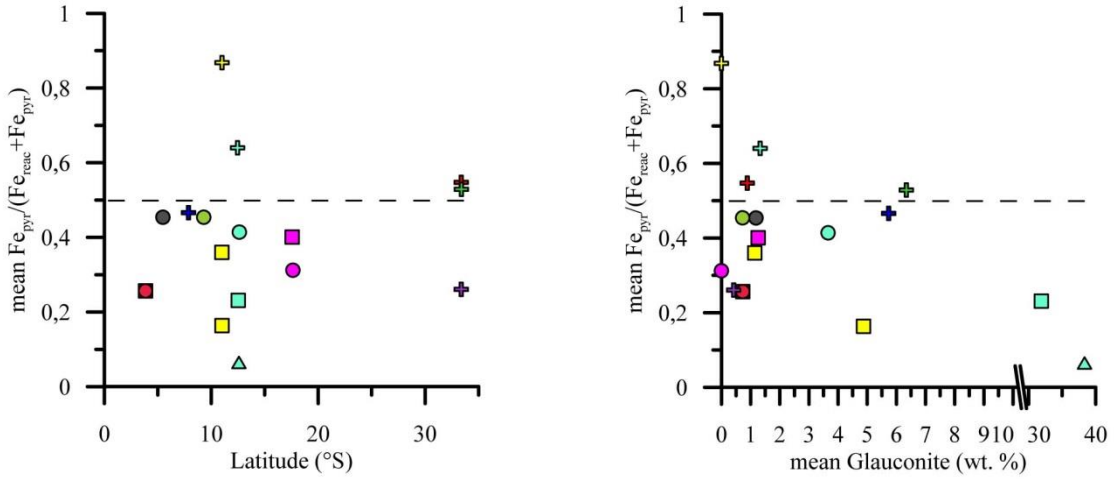


**Fig. 4.6 A** Mean $Fe_{py}$ / ($Fe_{0.5M\ HCl}$ + $Fe_{py}$) ratios against the Latitude for all cores. **4.6B** Mean $Fe_{py}$ / ($Fe_{0.5M\ HCl}$ + $Fe_{py}$) ratios against the average glauconite content of the investigated cores. Crosses mark cores retrieved at bottom water $O_2$ < 20 µM. The dashed line indicates a mean $Fe_{py}$ / ($Fe_{0.5M\ HCl}$ + $Fe_{py}$) ratio of 0.5 below which all cores from below the OMZ plot.

The porewater Fe concentrations in the sediments with highest glauconite content were between 0 and ~ 35 µM (Fig. 4.7). The bottom water oxygen concentrations were generally above 20 µM, but glauconite was also found in sediments overlain by low oxygen waters ($O_2$ < 20 µM) during sampling, e.g. 104MUC06 and 113-2MUC09. Here, $Fe^{2+}$ concentrations reached up to 86 µM.

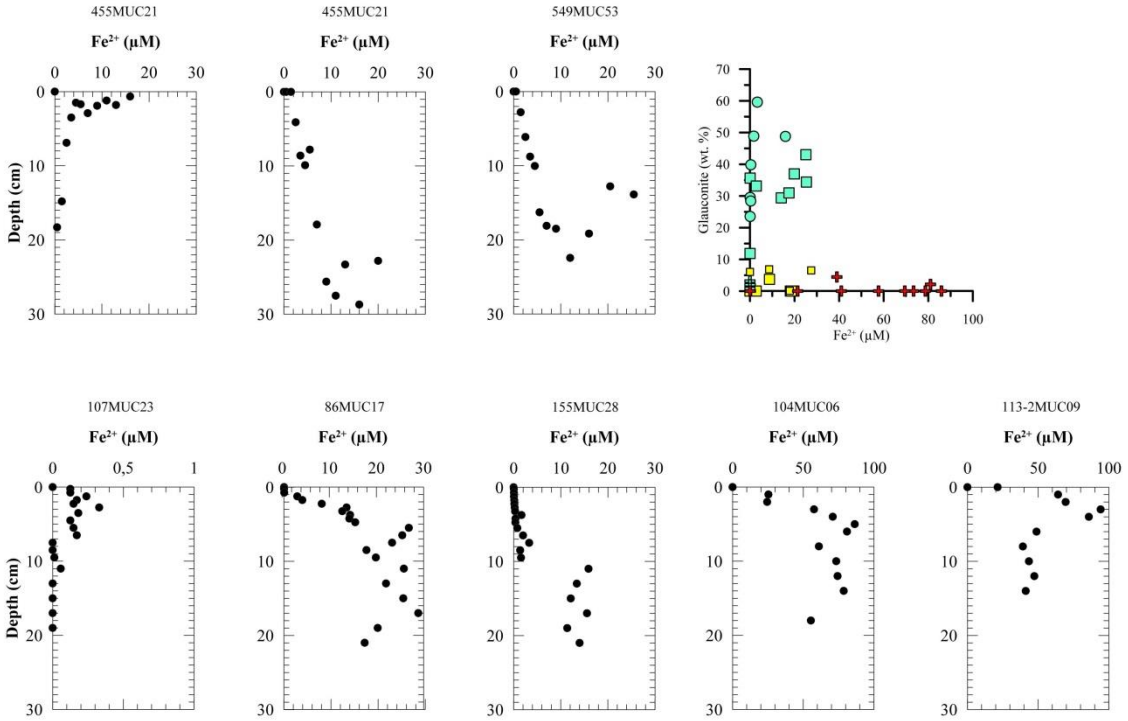


**Fig. 4.7** Porewater concentrations of Fe2+ with sediment depth for all cores where data were available. The panel in the upper right shows a plot of the sedimentary glauconite content versus the Fe2+ porewater concentration.

Some cores showed special features, i.e. no glauconite although expected or vice versa. These results are discussed in more detail below.

The highest glauconite content that was found at 33°S occurred in a core retrieved from oxygen deficient waters ($O_2$ ~ 10 µM) at 165 m water depth. Its mean $Fe_{py}$ / ($Fe_{0.5M\ HCl}$ + $Fe_{py}$) ratio of 0.5 indicate moderately sulfidic conditions. The findings at 33°S likely indicate non-steady state of the upper OMZ oxycline, i.e. short term changes of the water column oxygenation. As the process of sulfidation lasts only hours to a few days in contrast to the formation of glauconite that occurs on time scales of years (Scholz et al., 2014 and references therein) it is likely, that the sedimentary conditions during sampling display unfavorable glauconite formation conditions, but are not reflecting the main prevailing conditions at this station. At the other stations along the 33°S transect glauconite was sparsely occurring. This could be a result of more stable, but unfavorable conditions for glauconite formation. Note that the sedimentation rates reported for these stations are one order of magnitude larger than found off Peru at 11 and 12°S (Table 4.1) were highest glauconite contents were detected.

The only core investigated that contained no glauconite was found at 17°S at 920 m water depth. At the same latitude, a core retrieved in 790 m water depth contained some glauconite. Geochemical parameters e.g. the ratios of Fe/Al or $Fe_{py}$ / ($Fe_{0.5M\ HCl}$ + $Fe_{py}$) and the $Fe_{sil}$ content of the sediments of both cores are comparable. The bottom water oxygen concentrations ranged around 50 µM at both sites. However, the lower OMZ boundary shoals in southward direction.

Oxygen measurements indicate that the lower OMZ boundary (20 µM $O_2$) occurs at ~ 450 m at 17°S, whereas it was found between 750 and 800 m at 11 and 12°S. Hence, the deposition zone for reactive Fe from the core OMZ and therewith glauconitization shifts to shallower water depth.

Distinct heterogeneity concerning the total iron and glauconite content was found in cores retrieved at 12°S. The intense Fe enrichment and high glauconite content found in cores from the M92 cruise, was absent in a core from the M77/1 cruise. However, the distance between the sampling positions of core 623MUC87 and 155MUC28 is about 13 km and shows that the intensity of Fe enrichment below the OMZ seems to be extremely variable along the 12°S depth transect. Erdem et al. (2016) showed that the slope of the sea floor is critical at our sampling stations. Therefore, we suppose that landslides are likely affecting the sediment composition in this area (Lam et al. 2012) leading to distinct varieties of the investigated sediments.

In summary, our observations reveal that the sediments with the highest glauconite contents (on average 35 wt. %) were found below the OMZ at 12° S. The background conditions for glauconitization can be described with low sedimentation rates and the highest solid phase Fe content in all investigated samples of this study. Coincidently, the mean $Fe_{py}$ / ($Fe_{0.5M\ HCl}$ + $Fe_{py}$) ratio, indicating the degree of sulfidation of the sediment, was lowest and porewater $Fe^{2+}$ concentrations ranged between 0.03 and 25 µM and are not correlated with the glauconite content at these stations (Fig. 4.7). Our data confirm that low sedimentation rates and a slightly reducing, non-sulfidic milieu are required for the precipitation of glauconite (Odin and Matter, 1981). Interestingly, we found the highest glauconite contents in sediments with low concentrations of dissolved iron (Fig. 4.7). Hence, our data do not support the hypothesis that glauconite formation is favored by high dissolved Fe concentrations in ambient pore fluids (Odin and Matter, 1981).

In conclusion, the formation of widespread glauconite deposits below OMZ waters represent a long-term Fe sink for Fe mobilized from the core OMZ. Fe captured in authigenic clay minerals is reactive on time scales of thousands of years and is thus largely excluded from short-term benthic biogeochemical cycling. The fact that Fe is not fixed to more reactive Fe-oxide phases makes it unavailable for recycling, e.g. due to large-scale reductive events like the expansion of OMZs. Nonetheless, persistent vertical expansion of oxygen deficient waters could still lead to remobilization of the ferrous and ferric Fe pool below the recent OMZ along the South American Coast on millennial time scales. In such a long-term scenario, the today's negative feedback of Fe accumulation could reverse into a positive feedback by additionally fueling the bioavailable nutrient reservoir of the water column. Future work will have to be conducted to evaluate the potential Fe release from such reservoirs.

## Acknowledgements

We thank the captains and crew of RV *Sonne* cruise 210 and of RV *Meteor* cruises M77 and M92 for their assistance during the fieldwork. Special thank goes to the chief scientists of the named cruises for giving us excess to conduct geochemical analysis on achieved sediments cores. Sedimentary analyses were performed on board and in the land based laboratories with the invaluable assistance of L. Bohlen, A. Bleyer, B. Domeyer, M. Dibbern, R. Ebbinghaus, T. Mosch, A. Noffke, R. Suhrberg, S. Trinkler and V. Thoenissen. Multi-corer deployments were smoothly achieved with the wizardry of A. Petersen, M. Türk and S. Cherednichenko. This work is a contribution of the Sonderforschungsbereich 754 "Climate – Biogeochemistry Interactions in the Tropical Ocean" (www.sfb754.de) which is supported by the Deutsche Forschungsgemeinschaft.

## Author contributions

In cooperation with the technician A. Beck, U. Lomnitz carried out geochemical analysis of the archived sediment cores. U. Lomnitz prepared the manuscript with contributions of all co-authors.

## 4.5 References

Amorosi, A., I. Sammartino, and F. Tateo (2007), Evolution patterns of glaucony maturity: A mineralogical and geochemical approach, Deep Sea Research Part II: Topical Studies in Oceanography, 54(11–13), 1364-1374.

Baldermann, A., M. Dietzel, V. Mavromatis, F. Mittermayr, L. N. Warr, and K. Wemmer (2017), The role of Fe on the formation and diagenesis of interstratified glauconite-smectite and illite-smectite: A case study of Upper Cretaceous shallow-water carbonates, Chemical Geology, 453, 21-34.

Berner, R. A. (1970), Sedimentary pyrite formation, American Journal of Science, 268(1), 1-23.

Böning, P., H.-J. Brumsack, M. E. Böttcher, B. Schnetger, C. Kriete, J. Kallmeyer, and S. L. Borchers (2004), Geochemistry of Peruvian near-surface sediments, Geochimica et Cosmochimica Acta, 68(21), 4429-4451.

Boyd, P. W., and M. J. Ellwood (2010), The biogeochemical cycle of iron in the ocean, Nature Geosci, 3(10), 675-682.

Canfield, D. E., R. Raiswell, and S. H. Bottrell (1992), The reactivity of sedimentary iron minerals toward sulfide, American Journal of Science, 292(9), 659-683.

Dale, A. W., L. Nickelsen, F. Scholz, C. Hensen, A. Oschlies, and K. Wallmann (2015), A revised global estimate of dissolved iron fluxes from marine sediments, Global Biogeochemical Cycles, 29(5), 691-707.

Erdem, Z., J. Schönfeld, N. Glock, M. Dengler, T. Mosch, S. Sommer, J. Elger, and A. Eisenhauer (2016), Peruvian sediments as recorders of an evolving hiatus for the last 22 thousand years, Quaternary Science Reviews, 137, 1-14.

Gutiérrez, D., E. Enríquez, S. Purca, L. Quipúzcoa, R. Marquina, G. Flores, and M. Graco (2008), Oxygenation episodes on the continental shelf of central Peru: Remote forcing and benthic ecosystem response, Progress in Oceanography, 79(2–4), 177-189.

Huerta-Diaz, M. A., and J. W. Morse (1990), A quantitative method for determination of trace metal concentrations in sedimentary pyrite, Marine Chemistry, 29(0), 119-144.

Kostka, J. E., and G. W. Luther Iii (1994), Partitioning and speciation of solid phase iron in saltmarsh sediments, Geochimica et Cosmochimica Acta, 58(7), 1701-1710.

Lam, P. J., and J. K. B. Bishop (2008), The continental margin is a key source of iron to the HNLC North Pacific Ocean, Geophysical Research Letters, 35(7).

Lam, P. J., D. C. Ohnemus, and M. A. Marcus (2012), The speciation of marine particulate iron adjacent to active and passive continental margins, Geochimica et Cosmochimica Acta, 80, 108-124.

Martin, J. H. (1990), Glacial-interglacial CO2 change: The Iron Hypothesis, Paleoceanography, 5(1), 1-13.

Noffke A., Hensen C., Sommer S., S. F., Bohlen L., Mosch T., Graco M., and Wallmann K. (2012), Title Benthic iron and phosphorus fluxes across the Peruvian oxygen minimum zone, Limnology and Oceanography, 57(3), 851-867.

Odin, G. S., and A. Matter (1981), De glauconiarum origine, Sedimentology, 28(5), 611-641.

Odom, I. E. (1984), Glauconite and celadonite minerals, Reviews in Mineralogy and Geochemistry, 13(1), 545-584.

Raiswell, R., and D. E. Canfield (2012), The iron biogeochemical cycle Past and Present, Geochemical Perspectives, 1(1), 1-232.

Scholz, F., and T. Neumann (2007), Trace element diagenesis in pyrite-rich sediments of the Achterwasser lagoon, SW Baltic Sea, Marine Chemistry, 107(4), 516-532.

Scholz, F., C. Hensen, A. Noffke, A. Rohde, V. Liebetrau, and K. Wallmann (2011), Early diagenesis of redox-sensitive trace metals in the Peru upwelling area – response to ENSO-related oxygen fluctuations in the water column, Geochimica et Cosmochimica Acta, 75(22), 7257-7276.

Scholz, F., S. Severmann, J. McManus, A. Noffke, U. Lomnitz, and C. Hensen (2014), On the isotope composition of reactive iron in marine sediments: Redox shuttle versus early diagenesis, Chemical Geology, 389, 48-59.

Scholz, F., Löscher, C., Fiskal, A., Sommer, S., Hensen, C., Lomnitz, U., Wuttig, K., Goettlicher, J., Kossel, E., Steininger, R. and Canfield, D. E. (2016), Nitrate-dependent iron oxidation limits iron transport in anoxic ocean regions, Earth and Planetary Science Letters, 454, 272-281.

Severmann, S., J. McManus, W. M. Berelson, and D. E. Hammond (2010), The continental shelf benthic iron flux and its isotope composition, Geochimica et Cosmochimica Acta, 74(14), 3984-4004.

Suits, N. S., and M. A. Arthur (2000), Sulfur diagenesis and partitioning in Holocene Peru shelf and upper slope sediments, Chemical Geology, 163(1–4), 219-234.

Vogt, C., J. Lauterjung, and R. X. Fischer (2002), Investigation of the clay fraction (<2 μm) of the clay minerals society reference clays, Clays and Clay Minerals, 50(3), 388-400.

# 5 Synthesis and Outlook

The three studies that were presented in this work are an important contribution towards the understanding of P and Fe turnover in oxygen-deficient waters.

The first study focused on the Peruvian OMZ validated the previously reported extremely high P release form anoxic sediments. Our study quantifies the P sources for the release including the rain rates of P from water column particles that were until then unknown. Surprisingly, the P sources could not account for the P release in the core OMZ from ~150 to 300 m water depth. We attribute the excess P release to the occurrence of large sulfide-oxidizing bacteria at the seafloor. However, if such bacteria maintain the P mass balance for the missing P highly variable bottom water conditions have to prevail. Those bacteria were described, e.g. off Namibia, to store internally polyphosphates during less reducing or even oxygenation events and degrade the internal P reservoir at times when no other electron acceptors are available anymore to gain energy. While metabolizing the polyphosphates, the organisms release phosphate to the surrounding water. However, this process has to be verified for the species occurring off Peru. From that perspective, new open research questions evolve:

- How is P cycling of mat-forming sulfide-oxidizing bacteria affected by changing bottom water concentrations of $O_2$, $NO_3^-$ and $NO_2^-$? What is their contribution to the total benthic P release?

Furthermore, the studies on water column particles should be extended to find out:

- What is the fraction of authigenic P phases in water column particles and is the dissolved benthic P load related to the formation of such P phases? Is authigenic P formation affecting the potential link between benthic P release and the enhancement of the biological pump?

In the second study of the thesis the first benthic Fe and P fluxes from the moderate Mauritanian OMZ are presented. Although the recent release rates were found to be low, compared to the Peruvian OMZ, it is crucial to further investigate the region with regard to the ongoing deoxygenation. Especially the role of strong Fe input from Saharan dust particles to the water column and sediments has to be investigated in the light of decreasing water column and bottom water oxygen concentrations. Hence, the first and the second study of the thesis emphasize the need to better constrain the circumstances for Fe and P release at varying bottom water conditions to predict future scenarios. Therefore the following questions should be intensively investigated:

- What are the threshold values of $O_2$, $NO_3^-$and $NO_2^-$ for Fe and P release from sediments and how do these depend on sedimentary Fe and P speciation and binding forms?

In the third study, we show that Fe enrichments below the lower oxycline of the OMZ off South America occur from 3 to 33°S. Such a large enrichment zone leads to the question:

- What is the potential for Fe and P release from Fe enriched sediments at the lower rim of the OMZ with regard to spreading OMZs in the future? Which Fe species are controlling the benthic flux?

The mentioned open research questions are likely to be answered by further field work programs and experimental work on limited timespans. However, to fully understand oceanic systems and its changes, times series data would be the most promising method to reliably answer questions and predict the ocean's future evolution. Of course, such time series have to be conducted over long time spans and would need to be extended to benthic work as well to link the coupled water column processes and sediment reactions.

# 6 Acknowlegdements

Ich möchte mich herzlich bei Christian Hensen und Klaus Wallmann bedanken. Ihr habt mich immer bestens unterstützt und mir durch unzählige interessante Disskusionen und die Möglichkeit zur Teilnahme an diversen Seereisen sehr viel Wissen vermittelt und meinen Erfahrungsschatz bereichert. Durch euch habe ich einen Einstieg in die Wissenschaft erhalten und für dieses Vertrauen danke ich euch sehr!
Außerdem danke ich Stefan Sommer, Andy Dale und Florian Scholz dafür, dass ihr immer für Diskussionen bereit wart und mich ergänzend durch die Doktorandenzeit begleitet und betreut habt. Florian, du hast meine Art und Weise im Labor zu arbeiten maßgeblich geschult. Danke, dass du mir bei meiner ersten Seereise soviel gezeigt und beigebracht hast. Stefan, danke dass du stets ein offenes Ohr für mich hattest und die vielen kleinen Auszeiten beim gemeinsamen Mittagessen. Außerdem möchte ich Anna Noffke für ihre Kooperation danken. Anna, du hast auf Grund deiner Doktorarbeit den Grundstein zu dieser Arbeit gelegt und viele deiner fortführenden Gedanken mit mir geteilt und diskutiert.

Ein weiterer besonderer Dank gilt den Technikerinnnen und Technikern unserer Arbeitsgruppe. Liebe Bettina Domeyer, Anke Bleyer, Regina Surberg, Antje Beck und Sven Trinkler, ihr habt mich großartig bei der Durchführung aller Laborarbeiten unterstützt. Unser freundschaftlicher Umgang hat so manche Fleißarbeit und Spätschicht zu einem lustigen Ereignis werden lassen. Ihr seid das Rückrad der Arbeitsgruppe, danke, dass ihr so tolle Arbeit macht! Außerdem sind Sonja Kriwanek, Asmus Petersen, Sergey Cherednichenko und Matthias Türk zu nennen, die tolle Arbeit während der Einsätze der Großgeräte auf den Seereisen geleistet haben.

Weiterhin möchte ich Chris Schelten und der gesamten Doktorandenkohorte des SFB 754 danken. Wir hatten, vor allem maßgeblich durch Chris‘ unermüdliche Arbeit, viele sehr interessante Veranstaltungen zusammen und haben gelernt uns zu vernetzen.

Liebe Verena Thönissen, mit dir habe ich über die Arbeit eine Freundin dazugewonnen, die ich sehr schätze. Im Labor warst du mir stets eine große Hilfe und im Privatleben immer wieder eine Stütze. Du hast mir mit deinen Babysitterdiensten den Rücken für die Arbeit freigehalten, danke!

Nicht zu letzt möchte ich meiner Familie danken. Ihr habt meine Hochs und Tiefs ausgehalten und immer an mich geglaubt. Ihr habt mich nach euren verfügbaren Kräften unterstützt und mir geholfen fokussiert zu bleiben. Ihr habt mir mit eurer Zeit für Thies maßgeblich geholfen, Famile und Beruf unter einen Hut zu bekommen. Meine Dankbarkeit dafür ist nicht in Worte zu fassen. Dirk, du bist das Beste, was mir passieren konnte. Ich würde jederzeit alles genauso wieder machen. Danke, dass du da bist!

# 7 Supplement

## 7.1 Additonal material relating to chapter 2 : Benthic phosphorus cycling in the Peruvian oxygen minimum zone

**Table S2.1:** TPP, PIP, POP and POC concentrations of water column particles [µmol $L^{-1}$] and sediments [µmol $mg^{-1}$]. The standard deviation for TPP (RSD = 10%), PIP (RSD = 7%) and POP (RSD = 10%) of the water column particles was calculated from the duplicate measurements of the stations I, IV and V. The standard deviation for sedimentary TPP (RDS = 4%) and PIP (RSD = 6%) concentrations was derived from repeated measurements of the sediment standards MESS-3 and SDO-1. The POC measurements have a standard deviation of 2%. The POC/xP (where xP = TPP, PIP or POP) ratios were calculated from these concentrations.

| Station | | Water depth (m) / sediment depth (cm) | TPP [µmol $L^{-1}$] / [µmol $mg^{-1}$] | PIP [µmol $L^{-1}$] / [µmol $mg^{-1}$] | POP [µmol $L^{-1}$] / [µmol $mg^{-1}$] | POC [µmol $L^{-1}$] / [µmol $mg^{-1}$] | POC/TPP | POC/PIP | POC/POP |
|---|---|---|---|---|---|---|---|---|---|
| **Water column** | | | | | | | | | |
| I | 98CTD26 | 10 | 0.146 | 0.097 | 0.049 | 12.88 | 89 | 133 | 277 |
| | | 20 | 0.127 | 0.071 | 0.056 | 10.37 | 82 | 147 | 185 |
| | | 50 | 0.134 | 0.058 | 0.075 | 10.40 | 78 | 178 | 141 |
| | | 65 | 0.152 | 0.077 | 0.074 | 14.55 | 96 | 189 | 195 |
| | | 70 | 0.202 | 0.078 | 0.123 | 15.31 | 76 | 197 | 126 |
| **Sediment** | | | | | | | | | |
| I | 220MUC39 | 0.25 | 0.063 | 0.036 | 0.027 | 5.056 | 81 | 140 | 191 |
| | | 0.75 | 0.065 | 0.039 | 0.026 | 4.970 | 77 | 128 | 194 |
| | | 1.25 | 0.044 | 0.031 | 0.013 | 3.111 | 71 | 100 | 245 |
| | | 2.25 | 0.041 | 0.030 | 0.011 | 2.773 | 68 | 91 | 264 |
| | | 3.25 | 0.040 | 0.027 | 0.013 | 2.908 | 73 | 109 | 226 |
| | | 4.25 | 0.042 | 0.033 | 0.010 | 2.826 | 67 | 86 | 291 |
| | | 5.5 | 0.052 | 0.041 | 0.011 | 2.590 | 50 | 63 | 246 |

| | | | | | | | | | |
|---|---|---|---|---|---|---|---|---|---|
| **Water column** | | | | | | | | | |
| III | 269CTD70 | 20 | 0.105 | 0.054 | 0.051 | 8.94 | 85 | 165 | 174 |
| | | 50 | 0.070 | 0.037 | 0.033 | 7.43 | 107 | 202 | 227 |
| | | 125 | 0.118 | 0.064 | 0.054 | 8.03 | 68 | 125 | 149 |
| **Sediment** | | | | | | | | | |
| III | 248MUC46 | 0.25 | 0.082 | 0.077 | 0.005 | 5.650 | 69 | 73 | - |
| | | 0.75 | 0.046 | 0.024 | 0.022 | 5.745 | 124 | 235 | 262 |
| | | 1.25 | 0.049 | 0.030 | 0.019 | 6.664 | 137 | 225 | 351 |
| | | 1.75 | 0.052 | 0.031 | 0.021 | 7.012 | 136 | 229 | 335 |
| | | 2.25 | 0.051 | 0.030 | 0.021 | 6.997 | 137 | 231 | 336 |
| | | 3.25 | 0.052 | 0.031 | 0.021 | 5.883 | 114 | 188 | 287 |
| | | 4.25 | 0.052 | 0.031 | 0.021 | 6.863 | 132 | 221 | 328 |
| | | 4.75 | 0.050 | 0.029 | 0.021 | 6.940 | 139 | 237 | 337 |
| **Water column** | | | | | | | | | |
| IV | 111CTD29 | 10 | 0.171 | 0.088 | 0.083 | 17.59 | 103 | 200 | 220 |
| | | 20 | 0.069 | 0.038 | 0.031 | 6.31 | 93 | 165 | 219 |
| | | 50 | 0.061 | 0.028 | 0.033 | 7.66 | 125 | 274 | 234 |
| | | 100 | 0.090 | 0.038 | 0.052 | 7.39 | 82 | 199 | 143 |
| | | 141 | 0.075 | 0.025 | 0.050 | 7.09 | 94 | 291 | 142 |

| | | | | | | | | | |
|---|---|---|---|---|---|---|---|---|---|
| **Sediment** | | | | | | | | | |
| IV | 36MUC10 | 0.25 | 0.080 | 0.048 | 0.032 | 6.455 | 81 | 134 | 205 |
| | | 0.75 | 0.065 | 0.038 | 0.027 | 7.749 | 119 | 204 | 283 |
| | | 1.25 | 0.065 | 0.042 | 0.023 | 7.919 | 122 | 189 | 343 |
| | | 2.75 | 0.051 | 0.031 | 0.020 | 7.182 | 142 | 232 | 364 |
| | | 3.25 | 0.053 | 0.032 | 0.020 | 7.391 | 140 | 228 | 361 |
| | | 4.25 | 0.060 | 0.040 | 0.020 | 7.592 | 127 | 192 | 376 |
| | | 5.5 | 0.062 | 0.044 | 0.019 | 7.972 | 128 | 183 | 430 |
| **Water column** | | | | | | | | | |
| V | 279CTD81 | 50 | 0.058 | 0.013 | 0.045 | 6.93 | 119 | 548 | 174 |
| | | 100 | 0.069 | 0.017 | 0.053 | 7.08 | 106 | 451 | 138 |
| | | 190 | 0.072 | 0.023 | 0.049 | 8.90 | 132 | 385 | 213 |
| **Sediment** | | | | | | | | | |
| V | 247MUC45 | 0.25 | 0.092 | 0.038 | 0.054 | 12.881 | 140 | 340 | 238 |
| | | 0.75 | 0.076 | 0.034 | 0.042 | 9.286 | 122 | 270 | 222 |
| | | 1.25 | 0.068 | 0.027 | 0.040 | 11.027 | 163 | 405 | 273 |
| | | 1.75 | 0.075 | 0.056 | 0.019 | 13.730 | 182 | 245 | - |
| | | 2.25 | 0.078 | 0.036 | 0.042 | 11.188 | 143 | 314 | 264 |
| | | 3.25 | 0.079 | 0.035 | 0.044 | 10.890 | 138 | 314 | 245 |
| | | 4.25 | 0.072 | 0.032 | 0.040 | 10.009 | 140 | 314 | 252 |
| | | 5.5 | 0.071 | 0.033 | 0.038 | 11.080 | 156 | 341 | 289 |

| | | | | | | | | | |
|---|---|---|---|---|---|---|---|---|---|
| **Water column** | | | | | | | | | |
| VI | 92CTD24 | 10 | 0.986 | 0.579 | 0.407 | 89.09 | 91 | 155 | 234 |
| | | 50 | 0.045 | 0.020 | 0.025 | 3.98 | 88 | 197 | 158 |
| | | 100 | 0.028 | 0.015 | 0.013 | 5.05 | 179 | 335 | 384 |
| | | 150 | 0.049 | 0.025 | 0.025 | 4.65 | 95 | 189 | 190 |
| | | 200 | 0.041 | 0.017 | 0.024 | 5.44 | 133 | 326 | 225 |
| | | 240 | | 0.020 | 0.051 | 4.45 | 62 | 217 | 87 |
| **Sediment** | | | | | | | | | |
| VI | 198MUC34 | 0.25 | 0.102 | 0.059 | 0.043 | 8.666 | 85 | 146 | 201 |
| | | 0.75 | 0.086 | 0.041 | 0.045 | 10.164 | 118 | 250 | 225 |
| | | 1.25 | 0.091 | 0.047 | 0.044 | 12.334 | 136 | 263 | 282 |
| | | 1.75 | 0.093 | 0.046 | 0.047 | 12.072 | 130 | 263 | 258 |
| | | 2.25 | 0.091 | 0.051 | 0.040 | 11.360 | 125 | 225 | 282 |
| | | 3.25 | 0.084 | 0.040 | 0.044 | 12.342 | 147 | 309 | 280 |
| | | 3.75 | 0.093 | 0.059 | 0.034 | 13.184 | 141 | 222 | 388 |
| | | 5.5 | 0.093 | 0.047 | 0.046 | 13.439 | 144 | 288 | 289 |
| **Water column** | | | | | | | | | |
| VIII | 66CTD16 | 30 | 0.135 | 0.096 | 0.039 | 16.16 | 120 | 169 | 414 |
| | | 50 | 0.043 | 0.024 | 0.019 | 5.96 | 138 | 244 | 318 |
| | | 150 | 0.030 | 0.012 | 0.018 | 2.98 | 99 | 258 | 161 |
| | | 250 | 0.021 | 0.006 | 0.014 | 2.23 | 108 | 363 | 155 |
| | | 350 | 0.020 | 0.007 | 0.013 | 2.83 | 143 | 420 | 217 |
| | | 407 | 0.037 | 0.017 | 0.020 | 3.55 | 96 | 209 | 178 |

| | | | | | | | | | |
|---|---|---|---|---|---|---|---|---|---|
| **Sediment** | | | | | | | | | |
| VIII | 107MUC23 | 0.25 | 0.730 | 0.712 | 0.019 | 5.504 | 8 | 8 | 296 |
| | | 0.75 | 1.346 | 1.321 | 0.025 | 5.062 | 4 | 4 | 201 |
| | | 1.25 | 1.580 | 1.551 | 0.029 | 4.114 | 3 | 3 | 141 |
| | | 2.25 | 2.372 | 2.327 | 0.045 | 3.676 | 2 | 2 | 81 |
| | | 3.5 | 1.027 | 1.017 | 0.010 | 6.219 | 6 | 6 | 653 |
| | | 4.5 | 0.622 | 0.611 | 0.011 | 7.251 | 12 | 12 | 653 |
| | | 5.5 | 0.480 | 0.470 | 0.010 | 7.788 | 16 | 17 | 791 |

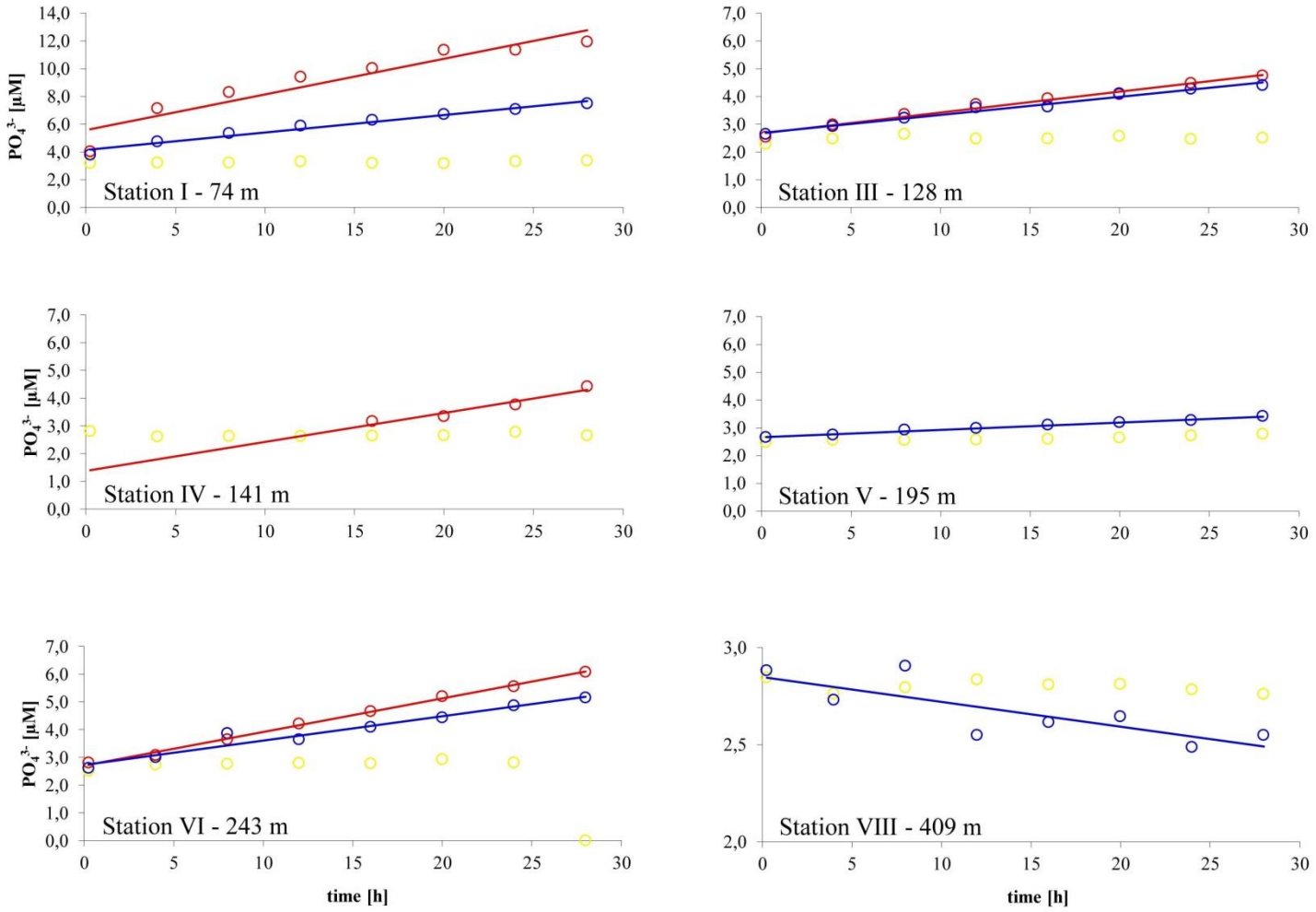


**Figure S2.1:** Phosphate ($PO_4^{3-}$) concentrations of the benthic lander chambers BIGO I (red) and BIGO II (blue) from cruise M92. The yellow dots show the $PO_4^{3-}$-concentration of the ambient bottom water. At stations IV, V and VII concentrations were only measued in one chamber.

## 7.2 Additonal material relating to chapter 3: Benthic phosphate and iron fluxes in the Mauritanian upwelling

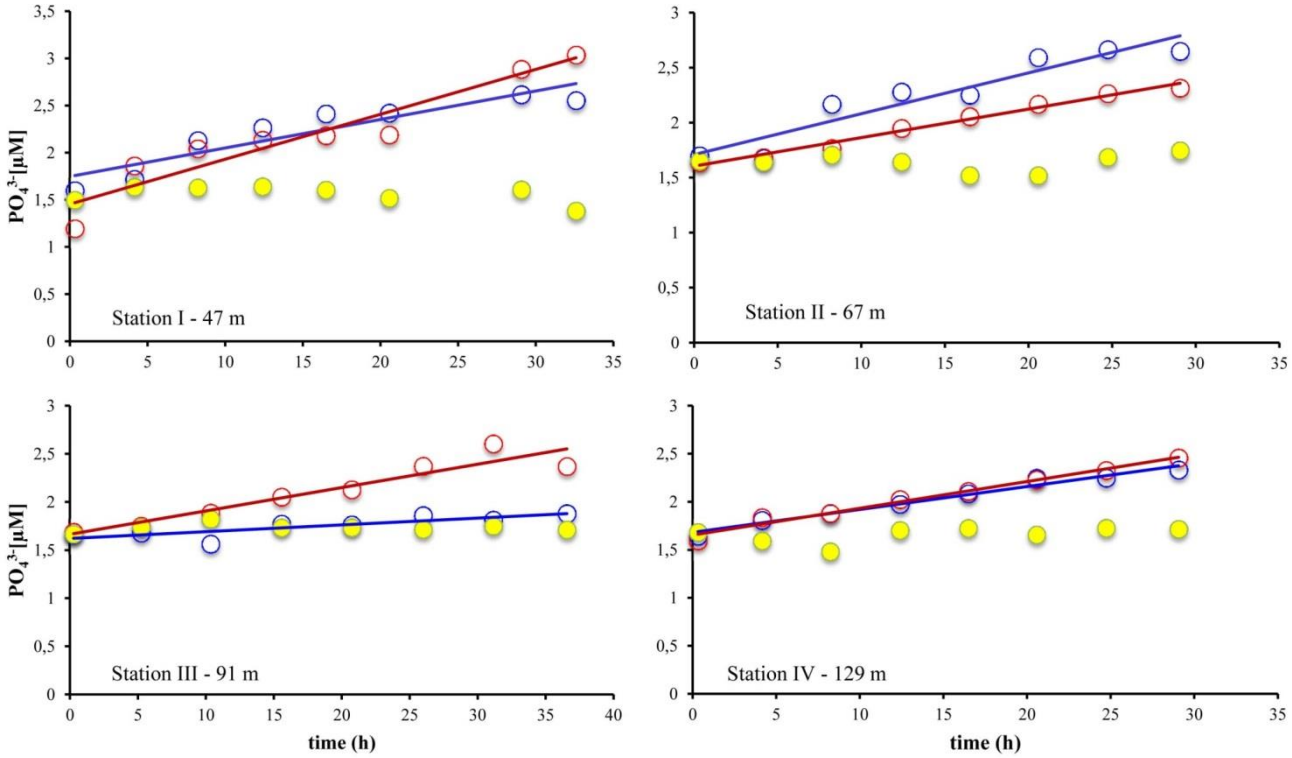

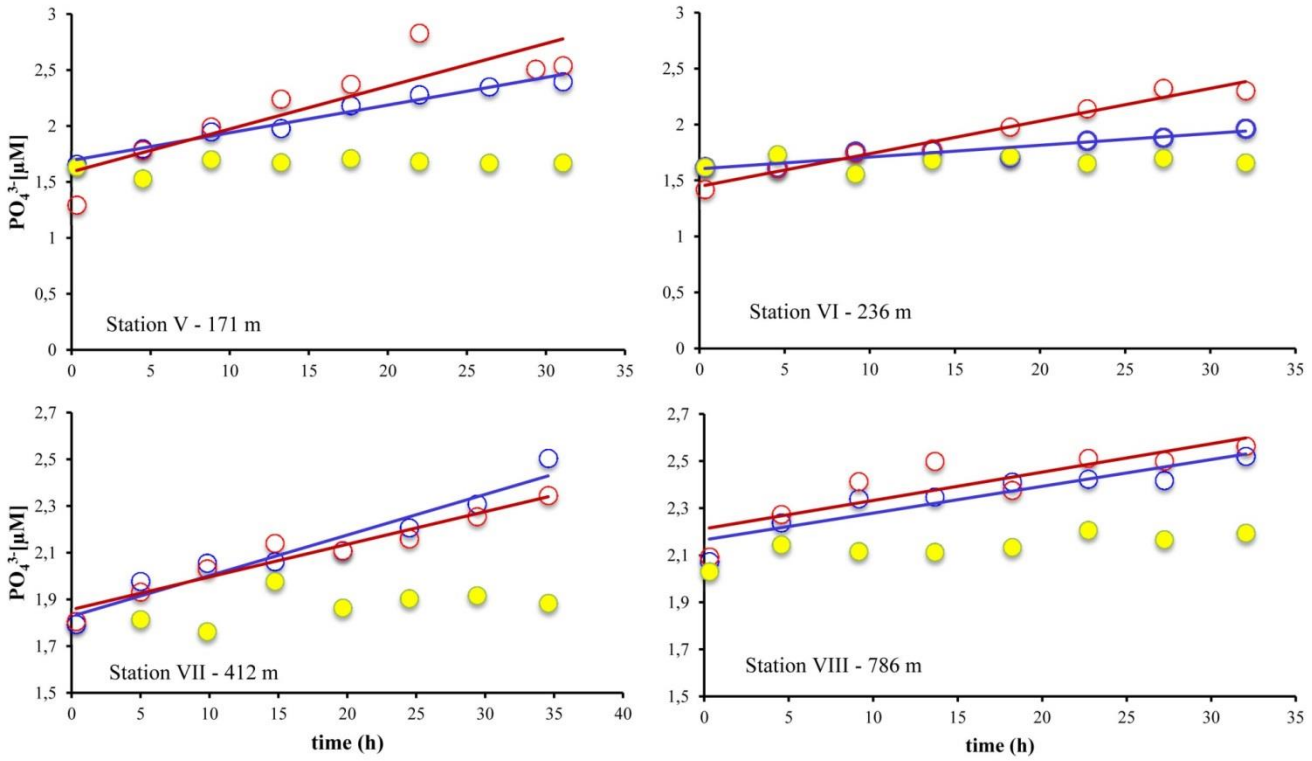
Station V - 171 m
Station VI - 236 m
Station VII - 412 m
Station VIII - 786 m
$PO_4^{3-}$[µM]
time (h)

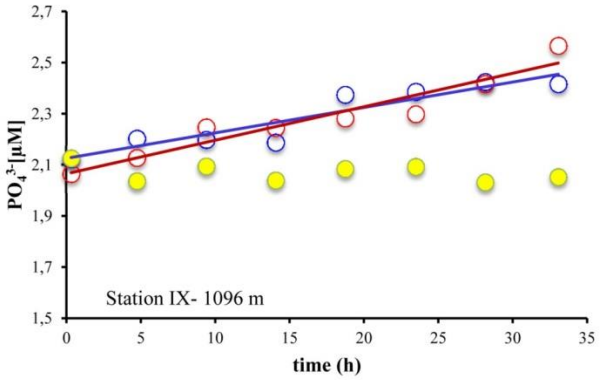


**Figure S3.1:** Phosphate ($PO_4^{3-}$) concentrations of the benthic lander chambers BIGO I (red) and BIGO II (blue) from cruise M107. The yellow dots show the $PO_4^{3-}$-concentration of the ambient bottom water.

**Table S3.1** Solid phase concentrations of Al, Fe and P in mg $g^{-1}$ and POC in wt. % of all analyzed cores from cruise M107.

| Cruise M107 - Core | Water depht | Sed depth | Al | Fe | P | POC |
|---|---|---|---|---|---|---|
| | m | cm | mg $g^{-1}$ | mg $g^{-1}$ | mg $g^{-1}$ | wt. % |
| 659 MUC 14 | 46 | 0.5 | 16.54 | 7.37 | 0.31 | 1.07 |
| 659 MUC 14 | 46 | 1.5 | 14.26 | 6.63 | 0.30 | 1.10 |
| 659 MUC 14 | 46 | 2.5 | 18.07 | 8.35 | 0.36 | 0.73 |
| 659 MUC 14 | 46 | 3.5 | 16.67 | 8.27 | 0.35 | 0.69 |
| 659 MUC 14 | 46 | 3.5 | 16.71 | 8.24 | 0.35 | |
| 659 MUC 14 | 46 | 5.5 | 19.46 | 8.97 | 0.33 | 1.07 |
| 659 MUC 14 | 46 | 7.5 | 17.96 | 8.29 | 0.31 | 1.06 |
| 659 MUC 14 | 46 | 9.5 | 20.20 | 9.28 | 0.33 | 0.81 |
| 659 MUC 14 | 46 | 13 | 18.52 | 8.47 | 0.37 | 0.67 |
| 659 MUC 14 | 46 | 17 | 18.74 | 8.65 | 0.31 | 0.80 |
| 659 MUC 14 | 46 | 23 | 15.44 | 7.01 | 0.24 | 0.55 |
| | | | | | | |
| 686 MUC 19 | 66 | 0.5 | 19.88 | 10.07 | 0.34 | 0.73 |
| 686 MUC 19 | 66 | 1.5 | 17.57 | 9.09 | 0.28 | 0.66 |
| 686 MUC 19 | 66 | 2.5 | 18.44 | 9.37 | 0.30 | 0.71 |
| 686 MUC 19 | 66 | 3.5 | 19.44 | 9.92 | 0.32 | 0.72 |
| 686 MUC 19 | 66 | 5.5 | 20.65 | 10.27 | 0.32 | 0.83 |
| 686 MUC 19 | 66 | 7.5 | 18.94 | 9.75 | 0.30 | 0.74 |
| 686 MUC 19 | 66 | 9.5 | 18.32 | 9.77 | 0.32 | 0.70 |
| 686 MUC 19 | 66 | 9.5 | 17.66 | 9.29 | 0.32 | |
| 686 MUC 19 | 66 | 13 | 16.06 | 8.18 | 0.28 | 0.59 |
| 686 MUC 19 | 66 | 16 | 19.09 | 9.60 | 0.30 | 0.65 |
| 686 MUC 19 | 66 | 21 | 17.11 | 8.18 | 0.25 | 0.63 |

| | | | | | | |
|---|---|---|---|---|---|---|
| 628 MUC 10 | 90 | 1 | 11.54 | 8.00 | 0.31 | 0.55 |
| 628 MUC 10 | 90 | 3 | 11.96 | 8.04 | 0.32 | 0.64 |
| 628 MUC 10 | 90 | 5 | 14.62 | 8.84 | 0.32 | 0.75 |
| 628 MUC 10 | 90 | 5 | 13.97 | 8.34 | 0.30 | |
| 628 MUC 10 | 90 | 9 | 16.87 | 10.14 | 0.38 | 0.84 |
| 628 MUC 10 | 90 | 13 | 14.58 | 8.60 | 0.28 | 0.62 |
| 628 MUC 10 | 90 | 17 | 15.35 | 9.16 | 0.28 | 0.73 |
| 628 MUC 10 | 90 | 21 | 14.78 | 8.89 | 0.43 | 0.73 |
| 628 MUC 10 | 90 | 21 | 14.36 | 8.68 | 0.45 | |
| | | | | | | |
| 697 MUC 20 | 169 | 0.5 | 27.98 | 16.41 | 0.48 | 1.28 |
| 697 MUC 20 | 169 | 1.5 | 27.11 | 16.44 | 0.47 | 1.16 |
| 697 MUC 20 | 169 | 1.5 | 27.24 | 16.58 | 0.46 | |
| 697 MUC 20 | 169 | 2.5 | 26.92 | 16.12 | 0.44 | 1.18 |
| 697 MUC 20 | 169 | 3.5 | 26.69 | 15.90 | 0.39 | 1.13 |
| 697 MUC 20 | 169 | 5.5 | 26.42 | 15.68 | 0.38 | 1.04 |
| 697 MUC 20 | 169 | 7.5 | 25.98 | 15.66 | 0.36 | 1.03 |
| 697 MUC 20 | 169 | 9.5 | 26.56 | 15.95 | 0.38 | 1.08 |
| 697 MUC 20 | 169 | 13 | 26.50 | 16.35 | 0.36 | 1.19 |
| 697 MUC 20 | 169 | 17 | 25.99 | 16.13 | 0.37 | 1.19 |
| 697 MUC 20 | 169 | 23 | 25.85 | 16.13 | 0.36 | 1.18 |
| 697 MUC 20 | 169 | 27 | 24.96 | 15.62 | 0.34 | 1.15 |

| | | | | | | |
|---|---|---|---|---|---|---|
| 672 MUC 17 | 129 | 0.5 | 20.31 | 12.70 | 0.45 | 0.75 |
| 672 MUC 17 | 129 | 1.5 | 21.47 | 13.26 | 0.41 | 0.77 |
| 672 MUC 17 | 129 | 2.5 | 21.03 | 12.75 | 0.39 | 1.01 |
| 672 MUC 17 | 129 | 3.5 | 16.77 | 10.13 | 0.36 | 0.86 |
| 672 MUC 17 | 129 | 3.5 | 20.48 | 12.34 | 0.37 | |
| 672 MUC 17 | 129 | 5.5 | 23.15 | 13.46 | 0.41 | 0.01 |
| 672 MUC 17 | 129 | 7.5 | 21.46 | 12.76 | 0.39 | 0.78 |
| 672 MUC 17 | 129 | 9.5 | 21.08 | 12.79 | 0.42 | 0.81 |
| 672 MUC 17 | 129 | 13 | 20.37 | 13.01 | 0.38 | 1.08 |
| 672 MUC 17 | 129 | 17 | 16.92 | 11.89 | 0.38 | 1.01 |
| 672 MUC 17 | 129 | 21 | 19.98 | 12.44 | 0.34 | 1.18 |
| | | | | | | |
| 583 MUC 7A | 236 | 0.5 | 20.36 | 12.07 | 0.30 | 0.74 |
| 583 MUC 7A | 236 | 1.5 | 19.64 | 12.57 | 0.31 | 0.66 |
| 583 MUC 7A | 236 | 2.5 | 20.42 | 13.57 | 0.31 | 0.72 |
| 583 MUC 7A | 236 | 3.5 | 22.63 | 14.07 | 0.33 | 0.85 |
| 583 MUC 7A | 236 | 5.5 | 22.12 | 13.61 | 0.29 | 0.81 |
| 583 MUC 7A | 236 | 5.5 | 22.38 | 13.67 | 0.30 | |
| 583 MUC 7A | 236 | 7.5 | 22.74 | 13.17 | 0.27 | 0.83 |
| 583 MUC 7A | 236 | 9.5 | 22.71 | 13.11 | 0.28 | 0.78 |
| 583 MUC 7A | 236 | 13 | 24.62 | 13.69 | 0.30 | 0.84 |
| 583 MUC 7A | 236 | 17 | 23.24 | 13.28 | 0.28 | 0.88 |
| 583 MUC 7A | 236 | 23 | 23.17 | 14.01 | 0.27 | 0.93 |
| 583 MUC 7A | 236 | 27 | 20.22 | 12.42 | 0.24 | 0.72 |

| | | | | | | |
|---|---|---|---|---|---|---|
| 583 MUC 7B | 236 | 0.25 | 21.90 | 12.37 | 0.32 | 0.80 |
| 583 MUC 7B | 236 | 1.5 | 23.37 | 15.49 | 0.36 | 0.96 |
| 583 MUC 7B | 236 | 2.5 | 23.31 | 13.93 | 0.33 | 0.89 |
| 583 MUC 7B | 236 | 3.5 | 22.30 | 13.11 | 0.34 | 0.84 |
| 583 MUC 7B | 236 | 5.5 | 21.99 | 12.76 | 0.28 | 0.76 |
| 583 MUC 7B | 236 | 7.5 | 22.90 | 13.14 | 0.28 | 0.76 |
| 583 MUC 7B | 236 | 9.5 | 22.58 | 13.31 | 0.29 | 0.76 |
| 583 MUC 7B | 236 | 13 | 23.87 | 13.96 | 0.29 | 0.80 |
| 583 MUC 7B | 236 | 13 | 23.77 | 13.84 | 0.29 | |
| 583 MUC 7B | 236 | 17 | 23.87 | 14.03 | 0.29 | 0.90 |
| 583 MUC 7B | 236 | 23 | 20.99 | 12.72 | 0.25 | 0.74 |
| | | | | | | |
| 583 MUC 7C | 236 | 0.5 | 22.97 | 13.50 | 0.34 | 0.90 |
| 583 MUC 7C | 236 | 1.5 | 22.33 | 13.04 | 0.29 | 0.82 |
| 583 MUC 7C | 236 | 2.5 | 22.71 | 12.93 | 0.31 | 0.87 |
| 583 MUC 7C | 236 | 3.5 | 22.36 | 12.59 | 0.28 | 0.80 |
| 583 MUC 7C | 236 | 5.5 | 26.57 | 14.83 | 0.35 | 1.11 |
| 583 MUC 7C | 236 | 5.5 | 26.38 | 14.68 | 0.34 | |
| 583 MUC 7C | 236 | 7.5 | 22.45 | 12.92 | 0.27 | 0.94 |
| 583 MUC 7C | 236 | 7.5 | 22.62 | 13.16 | 0.28 | |
| 583 MUC 7C | 236 | 9.5 | 22.16 | 12.89 | 0.27 | 0.86 |
| 583 MUC 7C | 236 | 13 | 23.76 | 13.24 | 0.32 | 0.79 |
| 583 MUC 7C | 236 | 17 | 23.41 | 13.40 | 0.29 | 0.71 |

| | | | | | | |
|---|---|---|---|---|---|---|
| 554 MUC 5 | 412 | 0.5 | 28.15 | 12.94 | 0.30 | 0.79 |
| 554 MUC 5 | 412 | 1.5 | 29.67 | 14.19 | 0.33 | 0.87 |
| 554 MUC 5 | 412 | 2.5 | 34.83 | 18.00 | 0.41 | 1.32 |
| 554 MUC 5 | 412 | 3.5 | 36.02 | 18.48 | 0.44 | 1.40 |
| 554 MUC 5 | 412 | 5.5 | 37.20 | 19.22 | 0.46 | 1.45 |
| 554 MUC 5 | 412 | 5.5 | 37.19 | 19.24 | 0.47 | |
| 554 MUC 5 | 412 | 7.5 | 38.36 | 19.27 | 0.46 | 1.48 |
| 554 MUC 5 | 412 | 9.5 | 38.03 | 19.07 | 0.44 | 1.34 |
| 554 MUC 5 | 412 | 13 | 36.84 | 17.50 | 0.39 | 1.29 |
| 554 MUC 5 | 412 | 17 | 35.84 | 17.38 | 0.39 | 1.31 |
| 554 MUC 5 | 412 | 23 | 35.55 | 17.56 | 0.36 | 1.37 |
| 554 MUC 5 | 412 | 23 | 35.75 | 17.39 | 0.36 | |
| 554 MUC 5 | 412 | 27 | 34.98 | 17.08 | 0.34 | 1.31 |
| | | | | | | |
| 534 MUC 3 | 786 | 0.25 | 53.10 | 28.00 | 0.88 | 2.68 |
| 534 MUC 3 | 786 | 1.25 | 54.66 | 27.84 | 0.82 | 2.67 |
| 534 MUC 3 | 786 | 2.25 | 55.03 | 27.28 | 0.75 | 2.63 |
| 534 MUC 3 | 786 | 3.25 | 55.53 | 26.98 | 0.70 | 2.53 |
| 534 MUC 3 | 786 | 4.25 | 55.53 | 26.50 | 0.66 | 2.46 |
| 534 MUC 3 | 786 | 5.5 | 55.65 | 26.50 | 0.65 | 2.41 |
| 534 MUC 3 | 786 | 7.5 | 56.00 | 27.44 | 0.66 | 2.79 |
| 534 MUC 3 | 786 | 7.5 | 56.03 | 27.38 | 0.67 | |
| 534 MUC 3 | 786 | 9.5 | 53.26 | 26.83 | 0.63 | 2.80 |
| 534 MUC 3 | 786 | 13 | 53.87 | 26.87 | 0.64 | 2.77 |
| 534 MUC 3 | 786 | 17 | 57.38 | 29.09 | 0.65 | 2.94 |
| 534 MUC 3 | 786 | 23 | 57.57 | 29.63 | 0.64 | 2.96 |

| | | | | | | |
|---|---|---|---|---|---|---|
| 524 MUC 1 | 1108 | 0.25 | 57.35 | 30.44 | 0.87 | 2.56 |
| 524 MUC 1 | 1108 | 1.25 | 58.46 | 29.72 | 0.77 | 2.52 |
| 524 MUC 1 | 1108 | 2.25 | 60.17 | 29.75 | 0.79 | 2.59 |
| 524 MUC 1 | 1108 | 3.25 | 58.72 | 28.70 | 0.71 | 2.53 |
| 524 MUC 1 | 1108 | 4.25 | 61.73 | 30.17 | 0.71 | 2.89 |
| 524 MUC 1 | 1108 | 5.5 | 62.21 | 30.91 | 0.71 | 2.97 |
| 524 MUC 1 | 1108 | 7.5 | 62.50 | 31.20 | 0.71 | 3.11 |
| 524 MUC 1 | 1108 | 9.5 | 63.05 | 31.98 | 0.72 | 3.19 |
| 524 MUC 1 | 1108 | 13 | 64.32 | 33.02 | 0.73 | |
| 524 MUC 1 | 1108 | 13 | 63.94 | 32.79 | 0.71 | 3.18 |
| 524 MUC 1 | 1108 | 17 | 64.64 | 33.40 | 0.69 | 3.21 |
| 524 MUC 1 | 1108 | 22 | 65.39 | 34.33 | 0.68 | 3.22 |
| 524 MUC 1 | 1108 | 26 | 66.21 | 34.43 | 0.67 | 3.33 |

**Table S3.2** Concentrations of TPP, PIP, POP and POC (µmol $L^{-1}$) of water column particles sampled during cruise M107.

| **Cruise M107** | **Water depth** | **Sample depth** | **TPP** | **PIP** | **POP** | **POC** |
|---|---|---|---|---|---|---|
| **Station** | **(m)** | **(m)** | **(µmol $L^{-1}$)** | **(µmol $L^{-1}$)** | **(µmol $L^{-1}$)** | **(µmol $L^{-1}$)** |
| 582 CTD 24 | 233 | 225 | 3.77 | 0.01 | 0.02 | 4.95 |
| 582 CTD 24 | 233 | 200 | 0.04 | 0.02 | 0.02 | 4.69 |
| 582 CTD 24 | 233 | 150 | 4.13 | 0.02 | 0.01 | 3.94 |
| 582 CTD 24 | 233 | 100 | 0.03 | 0.01 | 0.02 | 4.47 |
| 582 CTD 24 | 233 | 50 | 6.20 | 0.02 | 0.04 | 9.76 |
| 582 CTD 24 | 233 | 20 | 0.06 | 0.02 | 0.04 | 12.29 |
| 582 CTD 24 | 233 | 10 | 10.89 | 0.04 | 0.04 | 10.85 |
| 645 CTD 46 | 46 | 40 | 0.11 | 0.06 | 0.03 | 11.59 |
| 645 CTD 46 | 46 | 20 | 34.63 | 0.20 | 0.12 | 27.09 |
| 645 CTD 46 | 46 | 10 | 0.48 | 0.29 | 0.23 | 47.14 |

# Ulrike Lomnitz

**M.Sc. Geowissenschaften**

Flensburger Str. 65, 24106 Kiel
+49 431 530 500 44
ulomnitz88@gmail.com


# Curriculum Vitae

## Personal Information

| | |
|---|---|
| Date of birth | 05.02.1988 |
| Place of birth | Kyritz |
| Nationality | German |

## Education

| | |
|---|---|
| since Okt. 2012 | PhD candidate<br>GEOMAR Helmholtz Centre for Ocean Research Kiel<br>Thesis topic: Benthic cycling of phosphate and iron under low oxygen conditions<br>Supervisor: Prof. Dr. Klaus Wallmann |
| Sep. 2012 | Msc. Geowisschaften<br>Christian-Albrechts Universität zu Kiel<br>Thesis topic: *Contrasting studies of redox-sensitive trace metals in the oxygen minimum zone off the Chilean and Peruvian coasts*<br>Supervisors: Prof. Dr. Klaus Wallmann and Dr. Christian Hensen |
| Okt. 2010 | Bsc. Geowissenschaften<br>Christian-Albrechts Universität zu Kiel<br>Thesis topic: *Paläozeanografische Rekonstruktionsansätze für das Holozän an den Küsten von Ecuador und Peru*<br>Supervisors: Prof. Dr. Ralph Schneider and Dr. Guillaume Leduc |

## Research Experience

| | |
|---|---|
| 2010 – 2012 | Research Assistant, SFB 754 |
| | online available data base for sedimentation rates |
| 2010 | Research cruise SO 210 |
| 2011 | Research cruise M84/2 |
| 2012 | Research cruise M86/5 |
| 2013 | Research cruise M92 |
| 2014 | Research cruise M107 |

## Conference

| | |
|---|---|
| 2013 | Ocean Science Meeting in Honolulu, Hawaii |
| | Poster with the title: *Drivers and mechanisms for high $TPO_4$ release rates in the oxygen minimum zone off Peru* |

## Summer school

| | |
|---|---|
| 2011 | ECORD Summer school entitled *Subseafloor fluid flow and gas hydrates* |

## Publications

Dale, A. W., Sommer, S., **Lomnitz, U.**, Montes, I., Treude, T., Liebetrau, V., Gier, J., Hensen, C., Dengler, M., Stolpovsky, K., Bryant, L. and Wallmann, K.: (2015), Organic carbon production, mineralisation and preservation on the Peruvian margin, Biogeosciences, 12(5), 1537-1559.

Dale, A. W., Sommer, S., **Lomnitz, U.**, Bourbonnais, A., and K. Wallmann (2016), Biological nitrate transport in sediments on the Peruvian margin mitigates benthic sulfide emissions and drives pelagic N loss during stagnation events, Deep Sea Research Part I: Oceanographic Research Papers, 112, 123-136.

**Lomnitz, U**., Sommer, S., Dale A. W., Löscher C. R., Noffke A., Wallmann K., and Hensen C. (2016), Benthic phosphorus cycling in the Peruvian oxygen minimum zone, Biogeosciences, 13(5), 1367-1386.

Scholz, F., Severmann S., McManus J., Noffke A., **Lomnitz U.**, and Hensen C.. 2014. On the isotope composition of reactive iron in marine sediments: Redox shuttle versus early diagenesis. Chemical Geology 389: 48-59.

Scholz, F., Löscher, C., Fiskal, A., Sommer, S., Hensen, C., **Lomnitz, U.**, Wuttig, K., Goettlicher, J., Kossel, E., Steininger, R. and Canfield, D. E. (2016), Nitrate-dependent iron oxidation limits iron transport in anoxic ocean regions, Earth and Planetary Science Letters, 454, 272-281.

Sommer, S., Gier, J., Treude, T., **Lomnitz, U.**, Dengler, M., Cardich, J. and Dale, A.: Depletion of oxygen, nitrate and nitrite in the Peruvian oxygen minimum zone cause an imbalance of benthic nitrogen fluxes. Deep-Sea Research Part I, 113-122, 2016.